ISSN 0038-531X

Russian Original Vol. 53, No. 2, August, 1982

February, 1983

SATEAZ 53(2) 515-576 (1982)

SOVIET ATOMIC ENERGY

АТОМНАЯ ЭНЕРГИЯ
(ATOMNAYA ÉNERGIYA)

TRANSLATED FROM RUSSIAN

PEEL HERE

CONSULTANTS BUREAU, NEW YORK

SOVIET ATOMIC ENERGY

Soviet Atomic Energy is abstracted or indexed in *Chemical Abstracts, Chemical Titles, Pollution Abstracts, Science Research Abstracts, Parts A and B, Safety Science Abstracts Journal, Current Contents, Energy Research Abstracts,* and *Engineering Index.*

Mailed in the USA by Publications Expediting, Inc., 200 Meacham Avenue, Elmont, NY 11003.

POSTMASTER: Send address changes to *Soviet Atomic Energy,* Plenum Publishing Corporation, 233 Spring Street, New York, NY 10013.

Soviet Atomic Energy is a translation of *Atomnaya Energiya,* a publication of the Academy of Sciences of the USSR.

An agreement with the Copyright Agency of the USSR (VAAP) makes available both advance copies of the Russian journal and original glossy photographs and artwork. This serves to decrease the necessary time lag between publication of the original and publication of the translation and helps to improve the quality of the latter. The translation began with the first issue of the Russian journal.

Consultants Bureau journals appear about six months after the publication of the original Russian issue. For bibliographic accuracy, the English issue published by Consultants Bureau carries the same number and date as the original Russian from which it was translated. For example, a Russian issue published in December will appear in a Consultants Bureau English translation about the following June, but the translation issue will carry the December date. When ordering any volume or particular issue of a Consultants Bureau journal, please specify the date and, where applicable, the volume and issue numbers of the original Russian. The material you will receive will be a translation of that Russian volume or issue.

Subscription (2 volumes per year)
Vols. 52 & 53: $440 (domestic); $489 (foreign)
Vols. 54 & 55: $500 (domestic); $555 (foreign)

Single Issue: $50
Single Article: $7.50

CONSULTANTS BUREAU, NEW YORK AND LONDON

c/b
233 Spring Street
New York, New York 10013

Published monthly. Second-class postage paid at Jamaica, New York 11431.

SOVIET ATOMIC ENERGY

A translation of *Atomnaya Énergiya*

February, 1983

Volume 53, Number 2 August, 1982

CONTENTS

CONTENTS

(continued)

ARTICLES

COMPARISON ANALYSIS OF THE RELIABILITY AND EFFICIENCY OF NUCLEAR POWER STATION UNITS WITH ONE AND TWO TURBOGENERATOR SETS

I. Ya. Emel'yanov, A. I. Klemin, Yu. I. Koryakin,
V. S. Emel'yanov, and N. A. Trekhova

UDC 621.311.2:621.039

The large-scale nuclear-power construction developed and planned in the Soviet Union demands that, for its technologicoeconomic analysis, certain new factors which in previous stages did not have special importance must be taken into consideration. In the first place, today the operating reliability of nuclear power station generating units should be related to these factors.

It is well known that in the Soviet Union the power generation capacities will be built up on the basis of nuclear power generating units with reactors with a capacity of 1000 MW or more, for which two grouping concepts are assumed: double-modular (reactor + two turbines) and single-modular (reactor + one turbine). The first concept has been achieved in practice, in the form of units with RBMK-1000 and VVÉR-440, while the second is marked for achievement in units with VVÉR-1000 (except for the fifth unit of the Novovoronezh Nuclear Power Station). The VVÉR-1000 reactors in single-module execution occupy a large fraction (more than 50%) of the planned structure of the forthcoming buildup of nuclear power station capacities through 1990. It is well known that there is no experience in the operation of large-scale nuclear single-modules in the Soviet Union; however, there is experience abroad.

In [1], an attempt was undertaken to analyze the efficiency of nuclear power station units of equal capacity with one (single-module) and two (double-module) turbogenerator sets, taking account only of the reliability aspects. It was supposed, firstly, that the units are equal with respect to nominal power; secondly, that they operate in identical load conditions (in particular, in base-load conditions); and, thirdly, that they have identical reactor facilities and other equipment, with the exception of the turbogenerator units differing in capacity uniformly by one-half. For this, the simplest structural–functional nuclear power station layouts were considered in order to calculate the reliability (Fig. 1), including the layouts of the reactor facility (all equipment of the reactor building: reactor, main circulation pumps, separators, pipelines, accessories, etc.) and of the turbogenerator set or sets (all equipment of the machine hall: the turbogenerator set itself, pipelines, accessories, etc.).

Within the scope of these assumptions, we shall continue the investigation of the possibilities of using single- and double-modules in nuclear power generation with the inclusion of efficiency assessments based on the plant reliability characteristics achieved at the present time, the closing costs of electric power generation in the European part of the Soviet Union, the specific gas consumption in thermal power stations, and the calculated capital investment values.

The reliability of single- and double-modules will be compared with respect to the power generation of nuclear power stations over a quite prolonged interval of calendar time with the established operating conditions. This index is the most suitable for the economic analysis of these facilities.

As the quantitative characteristic of reliability of both turbogenerator sets and reactor facilities we shall use a complex index, equal to the ratio of the average output at failure (the reciprocal quantity is the average rate of failure λ)* to the average time of emergency repair of the plant being considered (the reciprocal quantity is the average rate of recovery μ). The index is suitable for this investigation in that it compositely defines the dependability and repairability of the plant – the principal components of its operating reliability. It is obvious that the higher the index, the more reliable the plant.

Within the scope of the assumptions concerning the exponential laws of the distribution of output at failure and the time of recovery for a plant of single- or double-modules, i.e., for the condition of constancy in time of the rates of failure λ and recovery μ of a plant (λ_r, μ_r, λ_M, μ_M, λ_D, and μ_D), the functioning of the modules in this problem can be described by a homogeneous Markoff process [2]. Here and in the future, the suffixes "r", "M" and "D" will be used for denoting the individual characteristics of the reactor facility and the turbogenerator sets of single- and double-modules, respectively.

*For an exponential reliability model, the average rate of failure coincides with the average parameter of a stream of failures in the interval of time being considered.

Translated from Atomnaya Énergiya, Vol. 53, No. 2, pp. 67-70, August, 1982. Original article submitted December 1, 1981.

0038-531X/82/5302- 0515$07.50

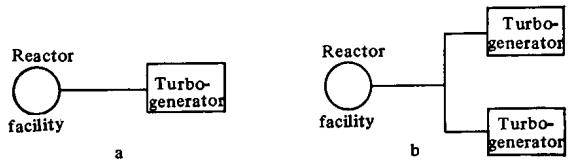

Fig. 1

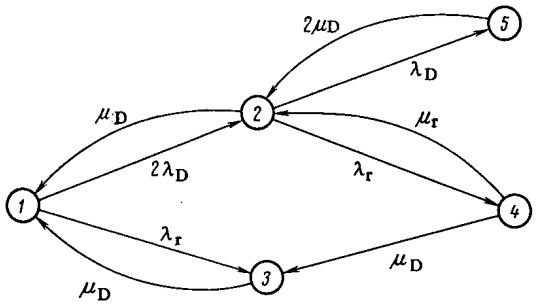

Fig. 2

Fig. 1. Simplest structural-functional layouts for calculating the reliability of single- (a) and double-modules (b).

Fig. 2. Graph of states of the Markoff process used in the problem of reliability assessment to describe the functioning of a double-module.

As we are interested in the power generation of the modules over a quite long interval of time, then, in view of the ergodicity of homogeneous Markoff processes, this index is determined by the final probabilities of states (for $t \to \infty$). These probabilities are found as the result of solving the so-called steady-state problem [2].

The number of states of the Markoff process describing the functioning of the double-module is equal to five: First, all of the plant operating efficiently and the unit is able to provide nominal power; second, one turbogenerator set operating inefficiently and the unit is able to provide one-half of nominal power; third, inefficient operation of the reactor facility and the power of the unit is 0; fourth, inefficient operation of the reactor facility and of one turbogenerator set and the power of the unit is 0; and fifth, inefficient operation of both turbogenerator sets and the power of the unit is 0. These states and possible transitions between them (i.e., the graph of states of the Markoff process) are shown in Fig. 2. When constructing the graph it was supposed that the repair of a failed plant is begun immediately after its failure.

For the double-module, the final probabilities of efficient states (states with a power different from 0) are equal to

$$P_1 = \frac{\rho r^2 (\gamma+\rho+1)}{(\rho+\gamma)[\rho(r+1)^2+r(r+2)]+(\rho+1)r^2};$$
$$P_2 = \frac{2\rho r(\gamma+\rho)}{(\rho+\gamma)[\rho(r+1)^2+r(r+2)]+(\rho+1)r^2}, \quad (1)$$

where

$$r = \frac{\mu_D}{\lambda_D}, \quad \rho = \frac{\mu_r}{\lambda_r}, \quad \gamma = \frac{\mu_D}{\lambda_r}.$$

The number of states of the Markoff process describing the functioning of the single-module is equal to three: First, all of the plant operating efficiently and the unit is able to provide nominal power; second, inefficient operation of the turbogenerator set and the power of the unit is 0; and third, inefficient operation of the reactor facility and the power of the unit is 0. The graph of states of this Markoff process is shown in Fig. 3.

The final probability of an efficient operating state (the state in which the unit can provide nominal power) is

$$P_1^* = \frac{R\rho}{(1+R)\rho+R}, \quad (2)$$

where

$$R = \frac{\mu_M}{\lambda_M}.$$

The power outputs of the single- and double-modules over a time T are calculated, respectively, by the formulas

$$E_1 = \frac{R\rho N_{nom} T}{(1+R)\rho+R};$$
$$E_2 = \frac{\rho r[(\gamma+\rho)(r+1)+r]N_{nom}T}{(\gamma+p)[\rho(r+1)^2+r(r+2)]+(\rho+1)r^2}. \quad (3)$$

As the numerical investigations of [1] showed, if the quantity r exceeds the quantity R by not more than a factor of 1.5 with $10 \leqslant r \leqslant 100$, and the reactor facility reliability, which is also the reliability of the separate turbogenerator set, is of the same order, the gain in power output of the double-module in comparison to the single-module amounts to 1-5%.

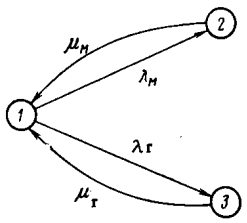

Fig. 3. Graph of states of the Markoff process used in the problem of reliability assessment to describe the functioning of a single-module.

Now we shall calculate the power generation of single- and double-modules based on the following starting data: As the starting data for the reactor facility and the double-module turbogenerator set we shall use the reliability indexes obtained as the result of statistical processing of the operating data of nuclear power station units with RBMK-1000 reactors, and for the single-module turbogenerator set, we shall use the appraised estimates of the rates of failure λ_M and recovery μ_M. For a high confidence, we shall conduct the calculation for several values of the complex reliability index of the single-module turbogenerator set covering the expected range, with constant reliability indexes of the reactor facility and of the double-module turbogenerator set. In the calculations of the reliability characteristics of the reactor facility we shall use the existing data for the RBMK-1000. It can be expected that the operating reliability indexes of the VVÉR-1000 will not be significantly different from them. The starting data for the plant reliability assumed in the calculations are shown in Table 1. Attention should be paid to the fact that the current level of reactor construction ensures a reactor facility reliability in excess of the reliability of the turbogenerator set.

The steady-state values of the power generation of the single- and double-modules (E_1 and E_2, respectively) over the time T amount to $0.778 \cdot T \cdot N_{nom}$ and $0.805 \cdot T \cdot N_{nom}$ for the single-module, and $0.835 \cdot T \cdot N_{nom}$ for the double-module. The corresponding ratios of E_2/E_1 are equal to 1.07 and 1.04. Thus, the gain in power generation of the double-module by comparison with the single-module is estimated as 4-7%.

Let us determine the possible efficiency losses from the underproduction of this amount of electric power in a nuclear power station with single-modules. For this we shall use the following as starting data:

the station is used 6500 h/yr (the design value for nuclear power stations introduced); in the calculation, it has also been assumed that this number is achieved in the second year after startup of the power generation unit;

the closed costs on power in the European part of the Soviet Union amount to 3? – 39 rubles/(MW·h) for peak stations [3];

the specific gas consumption in a thermal power station is equal to 308 g arb.ton/(kW·h).

The underproduction of power by a single-module with a capacity of 10^6 kW, calculated on the basis of these considerations, amounts to $260\text{-}445 \cdot 10^6$ kW·h/yr (for 4-7% respectively).

Taking account of the closed costs, we estimate the national economical expenditure in making up for the underproduction of electric power. As in the case of emergency shutdown of a nuclear power station, the underproduction of electric power must be made up by peak closed thermal power stations operating on coal or gas–petroleum residue fuel; the economic losses in a single reactor with a power generation capacity of 10^6 kW (single-module) are estimated as $10\text{-}17 \cdot 10^6$ rubles/yr. At the same time, it must be taken into account that, theoretically, transition from a double-module to a single-module, because of the smaller capital investment, can reduce the calculated costs by approximately $2.2 \cdot 10^6$ rubles/yr (with a reduction of the capital costs by $10 \cdot 10^6$ rubles). This can be related to a reduction of the number of heat-exchange plant units, accessories, pipelines, and also structural bodies. Moreover, the additional gain for the single-module, because of the reduced specific heat expenditure of the K-1000-65/1500 turbines in comparison to the K-500-65/3000, will be on the order of $2 \cdot 10^6$ rubles.

Thus, the total additional national economical costs for conversion from a double-module to a single-module with a capacity of 10^6 kW per unit amounts to $6\text{-}13 \cdot 10^6$ rubles/yr. It is important to emphasize that these costs are related to the steady-state operating regime of the unit (for the assumed starting data, commencing with the second year after startup of the unit).

TABLE 1. Nuclear Power Station Plant Reliability Data

Plant	Rate of failure per h	Rate of repair per h	Complex reliability index
Reactor facility	10^{-3}	0,040	$\rho = 40,00$
Turbogenerator set, double-module (K-500-65/3000)	$5,7 \cdot 10^{-3}$	0,033	$r = 5,65$
Turbogenerator set, single-module (K-1000-65/3000,	$6,5 \cdot 10^{-3}$	0,0250	$R = 3,85$
K-1000-65/1500)	$6,2 \cdot 10^{-2}$	0,0285	$R = 4,61$

TABLE 2. Power Utilization Factors of Foreign Nuclear Power Stations with PWR and BWR Reactors, %

Year	Nuclear power station capacity, MW		
	400–600	600–900	900–1300
1978	70,4	64,1	62,4
1979	70,5	53,6	57,0
1980	64,1	61,6	59,8
Integrated	64,2	55,7	55,8

As there is still no experience in the production of the K-1000-65/1500 or K-1000-65/3000 turbines, an increase, not a reduction, can be expected in the production cost as compared with the cost of two turbines with a capacity of 500 MW, because of the complex manufacturing technology. In these conditions, the capital costs on the single- and double-modules may be found to be identical, and the advantages of double-modules may increase even more.

We shall also find a natural expression for the additional fuel requirement. Taking account of the specific fuel consumptions in thermal power stations and of the above estimates of the underproduction of power by single-modules, the additional fuel requirement per 10^6 kW of capacity amounts to $20\text{-}100 \cdot 10^3$ ton arb. ton/yr.

We shall dwell briefly on foreign experience. It is well known that in nuclear power stations with pressurized water reactors (PWR) and boiling water reactors (BWR), single-modules are being used. As a result, the capacities are very different [4]. Double-modules are not used. An analysis of the reasons for this is a big independent problem.

It will be interesting to study the power utilization factor (PUF) of foreign nuclear power stations. The statistical data from 113 stations with PWR and BWR in the USA, Great Britain, Sweden, Japan, France, Taiwan, the German Federal Republic, Finland, Switzerland, Belgium, and the Netherlands has been divided into three groups: stations with a capacity of 400-600, 600-900, and 900-1300 MW. These ranges have been chosen because the electrical capacities of commercial thermal reactors operating in the Soviet Union (440 and 1000 MW) lie exactly in the first and third ranges.

The statistical processing of the large quantity of data [5-11] showed that the annual PUF and the integrated factor, taking account of the generation of electric power by the single-modules of nuclear power stations over the whole period of existence of the stations, decreases with an increase of the unit capacity of the single-module of the nuclear power station (Table 2). The average annual PUF of domestic nuclear power stations with a capacity of 1000 MW, with double-modules, amounts to 65.7% [12].

Abroad, during the whole period of development of the concept of pressurized water-cooled/water-moderated reactors, the tendency towards increasing their unit capacity with single-module operation has been preserved. However, at this stage, the further increase of the unit capacity of pressurized reactors in single-module operation above the achieved 1000-1300 MW is considered to be economically unjustified. In addition to the economic factors, the requirements for nuclear safety and the reduction of the power utilization factors of large-scale reactors also influence the tendency to limit the capacity of pressurized reactors (see Table 2).

Thus, as applicable to domestic practice, the following considerations can be expressed in favor of double-modules:

the greater reliability of the power units and, consequently, the greater reliability of the power supplies, resulting from the lower probability of simultaneously putting out of service both turbogenerator sets;

the possibility of operating the unit at a reduced power level, in the case of failure of one turbogenerator set, with the simultaneous recovery of the failed plant, i.e., greater operating flexibility;

reduction of the calculated costs and, what is particularly important, a significant economy of natural organic fuel.

LITERATURE CITED

1. V. S. Emel'yanov and A. I. Klemin, Problems of Nuclear Science and Technology. Physics and Technology of Nuclear Reactors [in Russian], No. 1(10), p. 51 (1980).
2. V. I. Tikhonov and M. A. Mironov, Markoff Processes [in Russian], Sovet-skoe Radio, Moscow (1977).
3. A. A. Makarov and A. G. Vigdorchik, Fuel–Power Generation Complex [in Russian], Nauka, Moscow (1979).
4. B. M. Troyanovskii, Turbines for Nuclear Power Stations [in Russian], Energiya, Moscow (1978).
5. "Generation of electric power by foreign nuclear power stations in 1975-1978," At. Tekh. Rubezhom, No. 12, 22 (1979).
6. Nucl. Eng. Int., 25, No. 307, 40 (1980).
7. Nucl. Eng. Int., 24, No. 282, 66 (1979).
8. Nucl. Eng. Int., 24, No. 286, 60 (1979).
9. Nucl. Eng. Int., 24, No. 286, 54 (1979).
10. Nucl. Eng. Int., 25, No. 304, 54 (1980).
11. Nucl. Eng. Int., 25, No. 296, 48 (1980).
12. Principal Technicoeconomic Operating Indexes of Nuclear Power Stations [in Russian], Minenergo, Moscow (1980).

OPERATING EFFICIENCY OF STEAM SEPARATORS IN POWER PLANTS WITH RBMK REACTORS

V. B. Karasev, Yu. M. Nikitin, O. Yu. Novosel'skii, and E. V. Sakovich

UDC 621.039.577

A special feature of the development of nuclear power generation in the Soviet Union is the construction of nuclear power stations with two types of thermal reactors – RBMK and VVÉR [1]. At the present time, ten power plants with RBMK reactors with a capacity of 1000 MW(elec.) are in industrial operation. Construction of the first line of the Ignalin nuclear power station, with RBMK reactors with a capacity of 1500 MW(elec.), is under way. The enlargement of power plants and, associated with this, the increase of the unit capacity of the plants, the development of standby plants, and the increase in the reliability of the operating plants, impose even higher demands on the organization of thermal hydraulic processes in the components of the multiple forced-circulation circuit (MFC).

Some of the most important components of the MFC are: the drum-separators (DS) with the corresponding framework of steam pipes; steam and water connectors; the make-up water feed system; separation of the steam–water communications; and the monitoring–measurement system (Fig. 1).

The design of the intracontainer equipment (ICE) and the functioning of the steam space and the water volume of the DS are of great importance for ensuring a moisture content of the separated steam of not more than 0.1%. For single-circuit reactor facilities, a reduction of moisture content of the separated steam is favorably expressed on both the operation of the turbine and the radiation environment in the machine hall of nuclear power stations. Moreover, the DS must ensure the necessary operating margin of the water consumed in filling the steam–water channel of the MFC circuit in the case of a sudden reduction of reactor power, as well as the small steam-pickup in the circulating water to avoid cut-out of the main circulatory pumps because of the appearance of steam in the intake branch pipes.

Figure 2 shows schematically a transverse section of a drum-separator of the RBMK-1000 reactor.

These drum-separators are installed in the Leningrad nuclear power station and in the first units of the Kursk and Chernobyl' nuclear power stations. The steam–water mixture reaches the basket 2 through the branch pipes 1, where the kinetic energy of the stream is partially damped. The stream of steam–water mixture is directed under the submerged perforated plate (SPP) 3, which causes a reduction of the steam content in the water volume of the DS. The SPP is

Translated from Atomnaya Énergiya, Vol. 53, No. 2, pp. 70-74, August, 1982. Original article submitted July 24, 1981.

0038-531X/82/5302- 0519$07.50

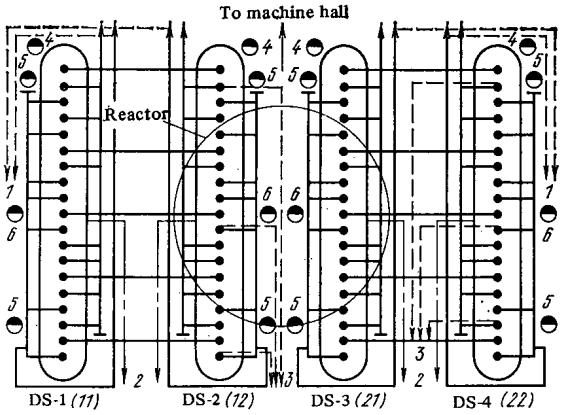

Fig. 1. Diagram of the arrangement of the drum-separators, steam pipes, level meter containers, and steam and water samplers of the first units of the Kursk and Chernobyl' nuclear power stations: 1) steam sampler from the steam collectors; 2) circuit water sampler; 3) steam sampler from the steam outlet branch pipes; 4) end level-meters with base line of the equalizer container of 1600 mm; 5, 6) level-meters with base line of containers of 630 and 400 mm, measuring the water level at the submerged perforated plate (SPP). The numbering of the drum-separators corresponds to that assumed in the Kursk, Leningrad, and (in parentheses) the Chernobyl' nuclear power stations.

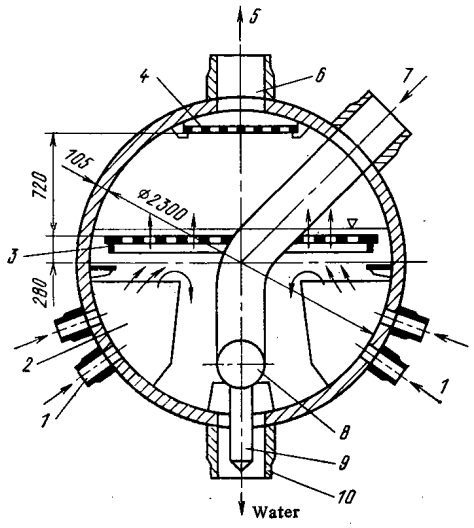

Fig. 2. Transverse section of a drum-separator of the RBMK-1000 reactor.

designed for equalizing the steam loading of the "evaporation meniscus." The overhead perforated plate 4 reduces the perturbing effect on the velocity field of the steam in the steam space of the DS – of the centered steam off-takes 5 in the branch pipes 6. The collector 8 of the feed water 7 is located in the water space of the drum, from which the feed water reaches the water discharge branch pipes 10 through the mixing tank 9. The DS are installed in pairs from the two sides of the reactor, each pair of DS being joined to five steam and two water connectors.

When operating the power plants at nominal power, it was established that the parameters of the principal systems of the unit correspond to the design values. An exception is the excess of the normalized value of the steam moisture content at the outlet from the DS. Thus, e.g., the moisture content of the steam at the outlet from DS-4 of the first unit of the Kursk nuclear power station in October 1977 was equal to 4-5.8%, and at the outlet from DS-12 and DS-21 of the first unit of the Chernobyl' nuclear power station it was 2-2.5%. The permissible capacity of the unit, for the condition

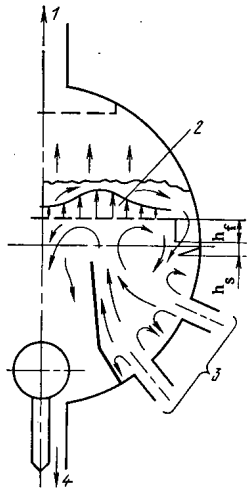

Fig. 3. Flow hydrodynamics in the model of an RBMK-1000 drum-separator (air–water mixture): 1) air; 2) diagram of water discharge; 3) air–water mixture; 4) water.

of ensuring a normalized moisture content of the steam, amounted to 90% of the nominal value. A similar situation was also noted in the first and second units of the Leningrad nuclear power station before redesigning of the ICE.

The appearance and elimination of the causes of exceeding the permissible moisture content of the steam at the outlet from the DS was an urgent problem, on the solution of which depends the high-quality functioning of the power plants at nominal power. In resolving the problem, a wide circle of possible causes was analyzed, in particular the accuracy of assembly of the DS, the effect of differences in the supply of feed water to each pair of the DS, errors in the installation of the throttling disks in the steam takeoff nozzles, nonuniformity of the steam and water loading along the drum and through the drums of each pair. These problems are elucidated in detail in [2], where, in the experience of operating the DS of the first unit of the Kursk nuclear power station, it has been established that the unsatisfactory characteristics of the DS are due to the outburst of steam through the hydroseal channel and, as a consequence of this, the discharge of water into the steam volume of the DS and into the steam collectors.

The hydrodynamic causes of the breaching of the hydroseal in the DS of the RBMK-1000, and the measures to eliminate it, are considered below.

In the drums of the RBMK-1000, two different hydraulically related water levels are measured: at the SPP and the total. The level at the SPP is the principal technological parameter, the maintenance of which within specified limits should ensure the permissible final moisture content of the steam. It is measured by means of level-meters from the base of the equalizer containers of 630 and 400 mm. The total level is measured at the end of the DS and is used as the parameter for regulating and adjusting the emergency shields, and also for determining the volume of water in the drum. The base line of the equalizer containers of the end level-meters amounts to 1600 mm.

A comparison of the readings of these level-meters during operation of the power plants at different power revealed considerable differences in the increase of level with respect to the level-meters with the base line of 630 and 1600 mm. Thus, e.g., for the DS of the left-hand side of the first unit of the Chernobyl' nuclear power station, the rise of the level by 100 mm with respect to the level-meter from the base of the container of 1600 mm increased the readings of the level-meter with the base line of 630 mm, in all, by 40 mm. This fact indicated a breakdown of the hydraulic ratio between the stated levels, and a deviation in the operation of the hydraulic channels of the ICE. These deviations could affect the final moisture content of the steam. Therefore, it was advantageous to investigate the flow hydrodynamics in the DS on a model.

Figure 3 shows schematically the flow of a mixture of air–water in the DS model, on which the investigations were conducted in the Scientific Research Sector of the Hydroproject [2]. With nominal operating conditions of the DS, the two-phase mixture from the steam–water communications (SWC), flows into the basket through the nozzles in jets, with a velocity of $\sim$10 m/sec. The distances from the nozzle outlets to the wall of the basket are approximately equal to the length of the initial sections of the jet. Their relative length amounts to 6-7 nozzle diameters [3]. Therefore, the jets run into the inclined wall of the basket with a high velocity. With the return of the steam–water flow under the action of centrifugal force, redistribution of the actual bulk steam content takes place over the cross-section of the basket. As a result, the stream flows with a sharply increased moisture content in a narrow band from the wall of the basket to the SPP. As a result of the collision of this stream with the SPP, two large vortices are formed. The left-hand vortex, interacting with the symmetrical vortex from the other side of the axis, creates a considerable velocity nonuniformity of dropping motion in the

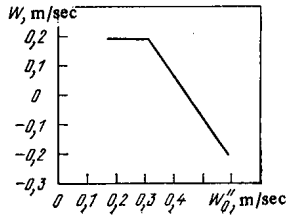

Fig. 4. Dependence of the flow velocity in the overflow channel on the scaled steam velocity at the "evaporation meniscus," for a pressure of 6.85 MPa and a bulk level at the SPP of 100 mm; the "active" cross section of the SPP, related to the surface area of the plate, is equal to 17.7%.

section between the baskets. This nonuniformity is due to the penetration of steam below the rim of the baskets, i.e., to an increase of the steam content in the inter-basket space. The right-hand vortex is replenished with water discharging from the SPP through the slit of the hydroseal; part of it is again drawn into the ascending flow.

Because of the effect of the redistribution of the steam content at the wall of the basket, as mentioned above, and because of the recovery of the kinetic energy of the jet flowing into the SPP, the flow in the vicinity of the frontal points carries out a greater quantity of water at the SPP than the flows of the right- and left-hand vortices along the SPP.

According to the data of the investigations [2], with a height of the overflow slit of the hydroseal of 70-75 mm or more, the two-phase mixture flows out through the hydroseal channel, and its density is insufficient to create a hydrostatic backwater in the hydroseal, which would prevent air (steam) from breaking through below into the steam volume of the DS. The breakthrough of steam under defined conditions is confirmed by the results of investigations on the ICE model of the RBMK drum-separators with the operating parameters. Turbine flow meters, installed in the overflow channel between the wall of the drum and the flange of the SPP, measured the flow and its direction, and also served as indicators of the phases (steam–water) in the overflow channel. Figure 4 shows the characteristic curve of the flow velocity in the overflow channel W versus the scaled steam velocity W_0'' at the evaporation meniscus of the ICE model of the RBMK drum-separators. For the positive direction of the velocity W, the flow motion is assumed to be downward. When $W_0'' < 0.3$ m/sec, i.e., $W \approx 0.2$ m/sec, it exceeds the buoyancy velocity of the steam bubbles for a given pressure and, consequently, the steam–water mixture must exist in the overflow channel.

In the case when $W_0'' = 0.45$ m/sec, the direction of flow of the steam–water mixture reverses.

The breakthrough of steam can be explained by analyzing the equation of motion describing the circulation around the flange of the SPP, which has the form

$$\Delta P_{SPP} + \Delta P_{hs} + \frac{2\sigma}{R} = g(\bar{\rho}_{hs} - \bar{\rho}_f) h_f, \quad (1)$$

where ΔP_{SPP} and ΔP_{hs} are, respectively, the hydraulic drag of the SPP and of the hydroseal channel; $2\sigma/R$ is the excess pressure inside a steam bubble; σ, coefficient of surface tension of water; and R, bursting radius of the bubble.

The values of ΔP_{SPP} and ΔP_{hs} are determined by the formulas

$$\Delta P_{SPP} = \zeta_p \frac{\rho_m W_m^2}{2}; \quad (2)$$

$$\Delta P_{hs} = \zeta_{hs} \frac{\bar{\rho}_{hs} W_{hs}^2}{2}, \quad (3)$$

where ζ_p and ζ_{hs} are hydraulic drag coefficients of the SPP and the hydroseal, respectively; W_m and ρ_m are the velocity and density of the steam–water mixture in the openings of the SPP; W_{hs} and $\bar{\rho}_{hs}$ are the velocity and density of the medium in the hydroseal; $\bar{\rho}_f$ is the average flow velocity below the SPP within the limits of the height of the flange h_f.

The right-hand side of Eq. (1) represents the driving pressure head of the circulation circuit. The quantity $2\sigma/R$ can be neglected because of its smallness.

The average steam velocity at the evaporation meniscus of the DS, with an internal diameter of 2.3 m and for nominal steam loading, is equal to 0.2 m/sec. The coefficient of nonuniformity of the steam flow rate above the SPP

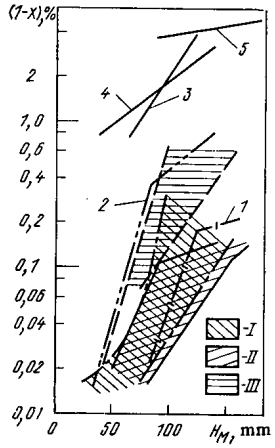

Fig. 5

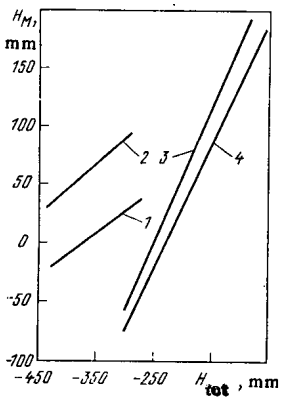

Fig. 6

Fig. 5. Curve of the moisture content of the steam at the outlet from the DS versus the bulk level H_M of water at the SPP (according to the level-meter with a base line of the container of 630 mm), when operating the units with RBMK-1000 reactors at nominal power.

Fig. 6. Comparison of the level-meter readings measuring the bulk level of water at the SPP (compensating containers with a base line of 630 mm, near the machine hall) and the total level (compensating containers with base line of 1600 mm), for the first unit of Chernobyl' nuclear power station: 1, 2) DS-11 and DS-12, respectively, before redesigning of the hydroseal (thermal capacity of the unit 3180 MW); 3) DS-11 and DS-12, capacity of the unit 3140 MW; 4) DS-11 and DS-12, capacity of the unit 3040 MW (3, 4 – after reconstruction of the hydroseal).

reaches 1.5, i.e., the local steam velocity at the evaporation meniscus amounts to $W_0'' = 0.3$ m/sec.

According to our data, the multiplicity of the circulation through the SPP, $K_c = 2$ for a steam velocity at the evaporation meniscus of $W_0'' = 0.3$ m/sec. With hydraulic drag coefficients of $\zeta_p = 1.7$ and $\zeta_{hs} = 2.5$ for operating conditions of the SPP with a loading of the evaporation meniscus of 0.3 m/sec, and taking account of the value given above for K_c, the calculated value of $\Delta P_{SPP} + \Delta P_{hs}$ for a pressure of 7 MPa, amounts to 1200-1300 N/m^2. With this same pressure, the maximum calculated value of $g(\rho_{hs} - \rho_f)h_f$ is 800-900 N/m^2 if there is no steam phase in the overflow channel of the hydroseal, i.e., $\rho_{hs} = \rho'$, and the actual bulk steam content below the SPP within the limits of the height of the flange is $\eta = 0.9\text{-}1$, i.e., $\bar{\rho}_f = 35\text{-}100$ kg/m^3. Before the redesigning of the ICE drum-separators with a diameter of 2.3 m, $h_f = 0.13$ m.

Thus, in the case of factual local values of the steam velocity at the evaporation meniscus attaining 0.3 m/sec, $\Delta P_{SPP} + \Delta P_{hs} > g(\bar{\rho}_{hs} - \bar{\rho}_f)$, i.e., the driving pressure head is less than the hydraulic drag, which causes an "overturn" of the circulation in the overflow channel of the hydroseal. In this case, the steam breaks through the hydroseal channel. The latter becomes like an additional section for the passage of steam into the steam volume of the DS. We note that in reality this phenomenon begins earlier, as $\bar{\rho}_{hs} < \rho'$ always.

It follows from Eq. (1) that for an ICE of given design, an effective means of expanding the zone of burst-free operation of the hydroseal is to increase the density $\bar{\rho}_{hs}$ and the height h_f. In the design of the ICE drum-separators of the RBMK-1000, by increasing the height of the flange, the density $\bar{\rho}_{hs}$ also is simultaneously increased. A reduction of the height of the overflow slit of the hydroseal (because of the increase of h_f) to 50-60 mm, leads to a reduction of the water flow rate through the SPP and, consequently, to a reduction of the steam content in the overflow channel. A further reduction of the height of the slit (to 30 mm or less) has an adverse effect on the water reserve in the DS [2].

As a result, recommendations were put forward, set on the basis of redesigning the ICE drum-separators with a diameter of 2.3 m. In accordance with these recommendations, the main one of which was the reduction of the slit height of the hydroseal because of the increase of the height of the flange, the drum-separators were redesigned at the Kursk, Chernobyl', and Leningrad nuclear power stations. The effect of the redesigning is illustrated in Fig. 5, in which the separation characteristics of the DS are shown (moisture content of the separated steam after the DS versus the bulk level at the SPP) for the first units of the Leningrad (DS-1-4, I), Kursk (DS-4, II), and the Chernobyl' (DS-21, III) nuclear power stations,

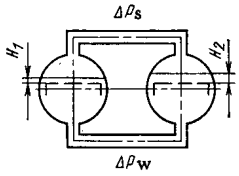

Fig. 7. Hydrodynamic diagram of two adjacent drum-separators in the RBMK-1000 reactor (right-hand DS with breakdown of the hydroseal).

when operating at a nominal electrical capacity of 1000 MW. For comparison, this same figure shows the characteristics of DS-4 of the first unit of the Kursk nuclear power station (curve 5), and of DS-21 and DS-12 of the first unit of the Chernobyl' nuclear power station (curves 3 and 4, respectively) before redesigning. It should be noted that during the separation tests, there was a "misalignment" in the readings of the level-meters (with base line 630 mm), located at different ends of the DS, and in the measured levels of water at the SPP. Therefore, in Fig. 5, the moisture content curves versus the level are shown for the readings of both level-meters. For DS-11 and DS-12 of the first unit of the Chernobyl' nuclear power station (curves 1, 2), this misalignment in the levels was insignificant. It can be seen from the figure that the moisture content of the steam at the redesigned DS had been reduced significantly, and did not exceed 0.1% in the operational range of variation of the bulk water level above the SPP.

After redesigning the hydroseal, the hydraulic relation was established between the water level above the SPP and the total level measured by the end level-meters. It is characteristic in this case that with a rise of the level at the SPP by 50 mm, the total level increases also by 50 mm. In Fig. 6, the readings are compared for the level-meters measuring the level at the SPP and the total level, by the example of DS-11 and DS-12 of the first unit of the Chernobyl' nuclear power station. It can be seen that the end level-meters with a base line of the equalizing containers of 1600 mm, after redesigning of the ICE, react unambiguously to an increase of the bulk level at the SPP.

The determination of the water reserve in the drum-separators results from the readings of the end level-meters. Before redesigning of the ICE, with operating conditions at the SPP according to the level-meter with base line of 630 mm, the end level-meters for a nominal power of the unit read from −320 to −520 mm. The redesigning of the DS increased these values to −250 mm. Thus, not only are the separation characteristics improved but also the operative reserve of water in the DS is increased. We recall that a layer of water with a height of 50 mm near the axis of the DS has a volume of about 3.5 m^3.

The necessity of the simultaneous redesigning of two adjacent DS (located on one side of the reactor) should also be discussed. In the first unit of the Chernobyl' nuclear power station, with nominal power, the water level at the SPP in the central DS, in which the ICE was reconstructed, was 100 mm less than in the peripheral DS. After redesigning of the outermost DS (DS-11), the difference in the readings of the level-meters of the two adjacent drums, for nominal power, did not exceed the measurement errors.

A decisive factor in forming a difference in the bulk levels of water at the SPP is the difference in the hydraulic drag of the SPP of adjacent DS, originating because of bursting of the hydroseal. This factor is illustrated analytically by the corresponding hydrodynamics equation, describing the difference in levels in a separation scheme consisting of two drums (Fig. 7). Taking account of the hydraulic drag of all the components of the scheme, and assuming that the values of the actual bulk steam content of the water volume in both DS being considered are identical, the equation can be written as:

$$H_2 - H_1 = \frac{(\Delta P_{SPP_1} - \Delta P_{SPP_2}) - (\Delta P_W - \Delta P_S)}{\rho' - \rho''}, \quad (4)$$

where ΔP_{SPP_1} and ΔP_{SPP_2} are the hydraulic drag of the SPP of each DS, and ΔP_S and ΔP_W are the hydraulic drag of the steam and water bypass pipes, respectively, between the DS.

An analysis of the data concerning the steam and water flow rate in the operating drum-separators at these nuclear power stations indicates that in adjacent DS the misalignment in the flow rates of the steam−water mixture is small. Consequently, the overflow of steam and water through the steam−water bypass pipes between the two DS being considered is insignificant, and the quantities ΔP_W and ΔP_S in Eq. (4) can be neglected. Thus, the difference in the water levels in the DS is determined entirely by the quantity $\Delta P_{SPP_1} - \Delta P_{SPP_2}$. With identical steam loadings, a difference in the hydraulic drag of the SPP of adjacent DS is possible in the case when bursting of the hydroseal occurs in one of the DS due to the passage of part of the steam through the overflow channel into the steam space.

Thus, a study of the hydrodynamics of the intracontainer equipment of the RBMK-1000 drum-separators on experimental installations, and an analysis of the data of operation and separation tests of the drum-separators, have allowed the cause of the increased moisture content of the separated steam to be established in the first units of the Kursk, Chernobyl', and Leningrad nuclear power stations. It consisted in the breakthrough of steam from the water space of the DS into the steam space, through the overflow channel of the hydroseal. The redesigning of the hydroseal of the DS, carried out at these nuclear power stations (reduction of the height of the overflow slit by increasing the height of the SPP flange), as industrial trials have shown, has allowed a moisture content of the steam of less than 0.1% to be obtained and the operative reserve of water in the DS to be increased, for a nominal capacity of the power generating units.

LITERATURE CITED

1. N. A. Dollezhal' and I. Ya. Emel'yanov, The Channel Nuclear Power Reactor [in Russian], Atomizdat, Moscow (1980).
2. O. Yu. Novosel'skii et al., in: Nuclear Power Stations [in Russian], Énergiya, Moscow, No. 3 (1980).
3. S. S. Kutateladze and M. A. Styrikovich, Hydrodynamics of Gas–Liquid Systems [in Russian], Énergiya, Moscow (1976).

MODELING HEAT AND MASS TRANSFER IN THE CORE OF A HEAT-EMITTING FUEL ELEMENT

V. A. Kornilov and V. D. Yuditskii

UDC 621.039.517.5

By the method of computer modeling, the heat and mass transfer of oxide fuel in a cylindrical heat-emitting fuel element is investigated, with exhaust of the gaseous fission products (GFP) through a gas flue (GF) in the form of a central tube [1]. The mathematical formulation of the nonsteady three-dimensional problem of heat and mass transfer in a fuel element as a problem for a multicomponent system of bodies with moving phase boundaries is given. Three regions are isolated in the fuel element: region v_G with a mobile boundary, occupied by fuel; region v_C with a mobile boundary, occupied by a gas cavity (fuel–vapor phase); and region v_T occupied by the GF tube (with a motionless boundary). For internal phase points, equations of heat and mass transfer in the following form are valid: for regions v_G and v_T

$$c\rho\,(\partial T/\partial\tau) = \operatorname{div}(\lambda \operatorname{grad} T) + q_v(\tau); \tag{1}$$

where q_v is the density of heat liberation; for region v_C

$$\partial\rho/\partial\tau = \operatorname{div}(D \operatorname{grad}\rho). \tag{2}$$

For the GF tube, the heat-transfer condition at the boundary of region v_T is written

$$\lambda(p-0)\frac{\partial T(p-0)}{\partial n} - \theta_1(p)\,\lambda(p+0)\frac{\partial T(p+0)}{\partial n} = \theta_2(p)\,(\mathbf{q}_F(\tau, p)\,\mathbf{n}_0), \tag{3}$$

where p is a point at the phase interface; on the common boundary of the regions v_T and v_C

$$\theta_1(p) = 0,\ \theta_2(p) = 1;$$

on the common boundary of the regions v_T and v_G

$$\theta_1(p) = 1,\ \theta_2(p) = 0.$$

For the moving boundary of the condensed phase v_G, the heat-transfer condition may be written in the form

$$-\lambda(p-0)\,\partial T(p-0)/\partial n = (\mathbf{n}_0\mathbf{q}_F(\tau, p)) + \rho q\left(\frac{dr(p)}{d\tau}\mathbf{n}_0\right), \tag{4}$$

where q is the heat of phase transition.

For motionless external boundaries (the internal surface of the emitter shell of the electricity-generating element, EGE)

Translated from Atomnaya Énergiya, Vol. 53, No. 2, pp. 74-76, August, 1982. Original article submitted August 3, 1981; revision submitted February 22, 1982.

0038-531X/82/5302-0525$07.50

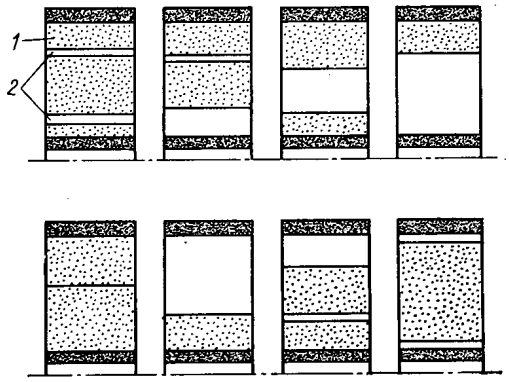

Fig. 1. Calculated cells. Variants of the fuel (1) and gas–cavity (2) positions.

$$T(p) = T_{bo}(\tau, p). \tag{5}$$

For region v_C, the boundary condition is written in the form

$$-D\frac{\partial \rho(p+0)}{\partial n} \equiv \varkappa \frac{P(\tau, p) - P(\tau, p+0)}{\sqrt{2\pi RT(\tau)/M}} = \rho\left(\frac{dr(p)}{d\tau}\mathbf{n}_0\right), \tag{6}$$

where $P(\tau, p)$ is the saturated vapor pressure at the temperature of the gas–cavity boundary at time τ; $P(\tau, p + 0)$, vapor pressure close to the gas–cavity boundary at time τ; $dr(p)/d\tau$, rate of displacement of the boundary point p; $\varkappa$, a factor taking the influence of macroscopic vapor motion into account (the expression for $\varkappa$ may be found in [2, 3]); and R, universal gas constant. The characteristic time of the given transient process is determined by the derivatives $dq_v/d\tau$ and $dr(p)/d\tau$ (the rate of heat-element yield at the working power and the rate of recondensation) and is several orders of magnitude larger than the lag created by heat transfer in the fuel element. This allows the propagation of heat waves in the condensed phase and density waves in the vapor phase to be disregarded and attention to be confined to quasistationary solutions; accordingly, the left-hand sides of Eqs. (1) and (2) are equated to zero, and the nonstationarity of the process is modeled by Eq. (6). The discontinuity of the condensed phase of the fuel and the mobility of the phase interface mean that it is very difficult to obtain a numerical solution in a fixed grid. Therefore, the model is somewhat simplified, and a numerical–analytical approach is used. As shown in [4], the heat flux from the fuel is directed mainly to the cylindrical EGE shell and the GF tube. This allows the longitudinal heat transfer along the fuel to be neglected in calculating the temperature fields. As a result, the projection of the temperature gradient onto the Z axis in the condensed phase reflects the specified temperature at the boundary of the given region. Further simplification is achieved as follows: a calculational region of the fuel element including the GF is isolated; heat transfer between the surfaces of the condensed phase occurs by radiation; the isolated calculational region v_c is divided into cylindrical calculational cells by means of planes perpendicular to the fuel-element axis.

Possible positions of the fuel in the calculational cell are shown in Fig. 1. In the above approximation, the problem of calculating the temperature field in the cell reduces to a combined solution of the equations of heat conduction inside the condensed phase and the equations of radiant heat transfer between the phase boundaries.

Using the well-known Hertz–Knudsen formula [2], the mass flux of fuel recondensing between the walls in the annular gap in the radial direction may be obtained:

$$I = \frac{P_{01}/T_1 - P_{02}/T_2}{1/(T_1k_1) + 1/(T_2k_2) + 1/k_3}, \tag{7}$$

where $k_1 = 2\pi r_1 \varkappa / \sqrt{2\pi RT_1/M}$; $k_2 = 2\pi r_2 \varkappa / \sqrt{2\pi RT_2/M}$; $k_3 = -2\pi DM \Big/ \left(R \ln \frac{r_1}{r_2}\right)$; P_{01} and P_{02} are the saturated vapor pressures at the wall temperatures.

Axial Mass Transfer

The tapering surface forming the boundary of the gaseous pore in the approximation of radial mass transfer is replaced by a system of cones overlapping at the boundaries of the calculational cells. The calculational cell is then divided into elementary layers by means of a system of enclosed truncated cones. Within the limits of each elementary layer, the concentration is determined analytically in the approximation of radial mass transfer, i.e., neglecting the small correction associated with axial mass transfer.

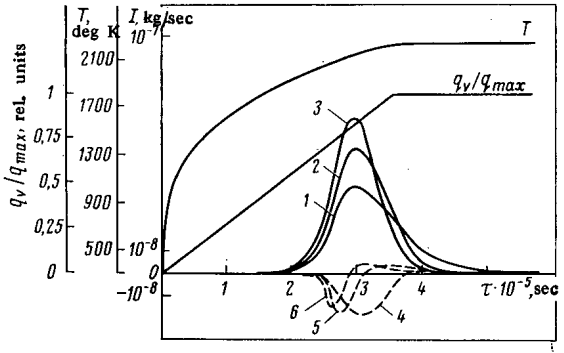

Fig. 2. Change in mass flux of fuel as a function of time (mass fluxes at L/10 are given, λ_G = 2 W/m·deg, λ_T = 125 W/m·deg, v_G/v_c = 0.8).

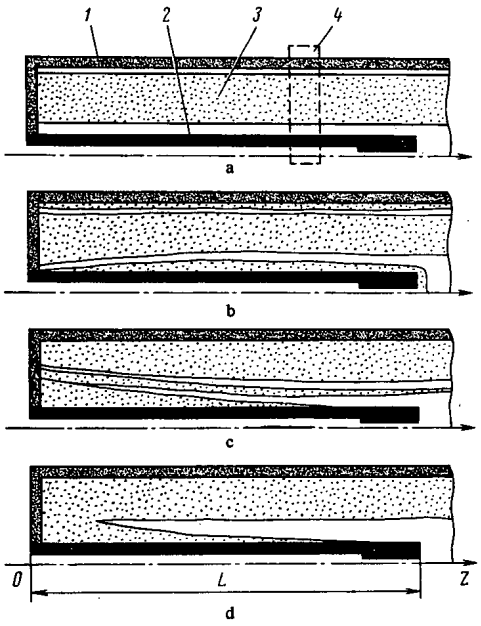

Fig. 3. Change in phase-transition boundary as a function of time; the state of the fuel is shown for τ = 0 (a), $2.9 \cdot 10^5$ (b), $3.6 \cdot 10^5$ (c), and $4.6 \cdot 10^6$ sec (d): 1) fuel-element shell; 2) GF tube; 3) fuel; 4) calculational cell.

The flux of fuel molecules in an arbitrary k-th layer is

$$I_k = D\,(dC/dl)_j\,\pi\,(r_{j,k}^2 - r_{j,k-1}^2), \tag{8}$$

where $(dC/dl)_j$ is the derivative of the fuel concentration in the direction along the generatrix of the annular k-th layer in the arbitrary j-th cross section. The total axial heat flux in the gas pore within the limits of the calculational cell is $I = \sum_k I_k$.

This algorithm is a modification of the method of elementary balances, and is constructed as a perturbation method with respect to analytical calculation of the radial mass transfer. The algorithm for solution of the problem provides for the possibility of realizing various combinations of positions of the two adjacent calculational cells (Fig. 1).

The given method and computer program was used to calculate the heat and mass transfer in the fuel core of an EGE in conditions of the transient process (Figs. 2 and 3). In the given example, a linear law of variation of the mean (over the EGE volume) heat liberation (q_v) was chosen. Assuming that the heat is transferred from the EGE shell by

radiation (this situation may correspond to vacuum conditions of EGE operation), the change in shell temperature T was obtained. Figure 2 shows the mass flux I of fuel at the internal surface of the cylindrical EGE shell (1-3) and at the GF tube (4-6), at various times, for three cross sections z equal to 0, 0.5L, and L.

With increase in heat liberation, the flux of fuel at the GF tube and at the EGE shell increases; subsequently, the flux falls at a rate that is especially high at the hot end of the GF tube, and evaporation of the fuel from the tube begins at $\tau = 2.9 \cdot 10^5$ sec. The change over time in the phase-transition boundary is shown in Fig. 3. As follows from Figs. 2 and 3, the most intense recondensation for the given case is observed in the time interval from $\sim 2 \cdot 10^5$ to $\sim 5 \cdot 10^5$ sec.

LITERATURE CITED

1. V. A. Kornilov, Yu. I. Sukhov, and V. D. Yuditskii, At. Énerg., 49, No. 6, 393 (1980).
2. D. A. Labuntsov, Teplofiz. Vys. Temp., 5, No. 4, 647 (1967).
3. R. Ya. Kucherov and L. É. Rikenglaz, Dokl. Akad. Nauk SSSR, 133, No. 5, 1130 (1960).
4. V. A. Kornilov et al., in: Abstracts of Papers at a Conference on the Thermal-Emission Method of Converting Thermal Energy into Electrical Energy [in Russian], Obninsk (1979), p. 27.

OXIDATION OF URANIUM AND PLUTONIUM MONONITRIDE AND MONOCARBIDE BRIQUETTES

G. P. Novoselov, V. V. Kushnikov, V. A. Baronov, V. P. Serebryakov, and N. M. Stepennova

UDC 621.039.54

The prospects for using oxygen-free compounds of uranium and plutonium in composite fuels [1] have stimulated research on schemes for reprocessing such rods. The scheme for reprocessing mixed nitride and carbide uranium–plutonium fuel should provide for isolating the main portion of the gaseous and volatile fission products. Here an oxidation process can be used, in which the structure of the initial fuel material is altered, with increase in volume and release of these fission products. The purpose of examining the oxidation of unirradiated mixed nitride–carbide uranium–plutonium fuel was to determine the effects of oxidation conditions on the completeness of the oxidative recrystallization in steady and dynamic states, and also on the phase transitions and the grain-size composition of the products.

RESULTS AND DISCUSSION

We used unirradiated briquettes of uranium mononitride and monocarbide, and also mixed nitride–carbide uranium–plutonium fuel, for which the basic characteristics are given in Table 1.

The uranium nitride was made from metallic uranium by the hydronitride method, while the uranium carbide was made by gas carbidization of metallic uranium with propane, and the mixed nitride fuel was made from a uranium–plutonium alloy prepared by three-fold melting of the metals of commercial purity under vacuum at 1300°C. The uranium–plutonium carbide fuel was prepared by mechanical mixing of the initial uranium and plutonium carbides [2, 3]. The plutonium carbide was prepared from metallic plutonium by hydrogenation and carbidization with spectrally pure acetylene black.

The oxidation kinetics of the mononitride and monocarbide briquettes were examined with a derivative-recording system designed by F. and E. Paulik and L. Erdei. The heating rate was 2.5 deg/min.

The kinetic characteristics of the oxidation for the mixed nitride and carbide uranium–plutonium fuel were evaluated from the mass change [4]. The oxidation was performed in the temperature range 325-450°C with continuous supply of 10-15 liter/h of oxygen or air to the reaction space. Oxidative processing under dynamic conditions was examined using vibration at a frequency of 20 Hz with an amplitude up to 1 mm [5]. The phase compositions of the powders obtained by oxidizing the briquettes were examined by x-ray methods (RKU-86 camera with Co radiation). The grain-size composition of the oxidation products was determined by sieve analysis, while the mean particle size was determined with an MBI-11 microscope (× 1000).

Translated from Atomnaya Énergiya, Vol. 53, No. 2, pp. 77-80, August, 1982. Original article submitted October 19, 1981.

0038-531X/82/5302-0528$07.50

TABLE 1. Characteristics of the Specimens of Nitride and Carbide Fuel

Fuel	Contents of main elements, mass %	Oxygen content, mass, %	Lattice constant $a \pm 0{,}001$ Å (1 Å = 10^{-10} m)	Density, % of theoretical
UN	94,45U 5,53N	⩽0,02	4,892	85—90
(U, Pu)N	76,47U 18,11Pu 5,38N	⩽0,04	4,896	85—90
UC	95,27U 4,71C	⩽0,02	4,957	85—90
(U, Pu)C	80,88U 14,37Pu 4,71C	⩽0,04	4,968	85—90

The nitrogen contents of the initial briquettes and the oxidized powder from uranium mononitride and the mixed (U, Pu)N fuel were determined by Kjeldahl's method with an accuracy of ±5% relative, while the carbon contents of the initial briquettes and the oxidized powder from uranium monocarbide were determined with the WR-12 gas analyzer (accuracy ±0.2% relative). The carbon content of the oxidized mixed (U, Pu)C was analyzed with a VK-1C coulometric apparatus made by Kokusai Electric. The errors of analysis at carbon contents of 0.001, 0.01, and 0.1% were ±20, ±5 and ±2%, respectively.

URANIUM MONONITRIDE AND MIXED (U, Pu)N FUEL

Figure 1 shows the results of oxidative processing of UN briquettes with programmed heating. The derivative curves show that the oxidation of UN briquettes in oxygen (Fig. 1a) is accompanied by a considerable exothermic effect in the range 320-350°C; as a result, maximum temperature of 489°C is attained in the reaction zone with a rate of increase in mass of about 50 mg/min. The oxidation of UN briquettes in air is also accompanied by an exothermic effect at 348-474°C. The temperature in the reaction zone rises by 40-50°C. The rate of increase in mass is 10.4 mg/min. Therefore, the mean rate of oxidation of UN briquettes in oxygen is about five times that in air. There is a marked rise in the temperature in the reaction zone (Δt° = 130-170°C). X-ray analysis of the oxidation products showed that they were made of U_3O_8 powder.

As PuN is oxidized more rapidly than UN [6], the oxidation of the (U, Pu)N briquettes was performed in the range 325-400°C. Figure 2 shows the time dependence of the oxidation of the (U, Pu)N briquettes at various temperatures. Figure 2 indicates that the oxidation rate increases with the temperature and attains 160 mg/min at 400°C. A difference from the oxidation of (U, Pu)O_2 briquettes [4] is that in the oxidation of (U, Pu)N briquettes there is virtually no induction period and only the temperature influences the rate of increase in mass.

Table 2 gives data on the grain-size compositions of the oxidation products from (U, Pu)N briquettes in air at various temperatures. Here for comparison we give data on the composition of the powder after oxidation of (U, Pu)N briquettes with vibration (frequency 20 Hz, amplitude 1 mm, time 1.5 h). Table 2 shows that there is a tendency for the proportion of fractions with particle size less than 100 μm to decrease as the temperature is raised (from about 80% at 325°C to about 53% at 400°C). The oxidative processing in the presence of vibration produces a considerable increase in the yield of small fractions. At 350°C, about 93% consists of the fraction of particle size less than 50 μm.

Microscopic examination of this fraction showed that the particle sizes ranged from 3.3 to 49.8 μm (Fig. 3), with a mean size of 12.4 μm. Chemical analysis showed that the nitrogen contents of fractions with particle sizes less than 100 μm was not more than 0.1 mass %.

X-ray examination showed that all the fractions after the oxidation of (U, Pu)N briquettes in the stationary state consisted of a phase with a cubic structure (U, Pu)O_{2+x} (a = 5.422-5.426 Å) and (20-30%) of a (U, Pu)$_3O_8$ phase. The lattice constant of (U, Pu)O_{2+x} corresponded to the superstoichiometric value, evidently due to the excess oxygen content (a_{stoich} = 5.456 Å).

URANIUM MONOCARBIDE AND MIXED (U, Pu)C FUEL

Figure 4 shows derivative recordings of the oxidative processing of UC briquettes. The curves show that the oxidation in oxygen begins at 235°C, with a subsequent rapid rise in temperature to 328°C. The mean oxidation rate was 2.75 mg/min. This corresponds to an exothermic reaction in the temperature range 328-390°C with t^0_{max} = 495°C. Starting at a temperature of 540°C, there was a loss in mass due to burning of the carbon, while above 870°C the mass did not change.

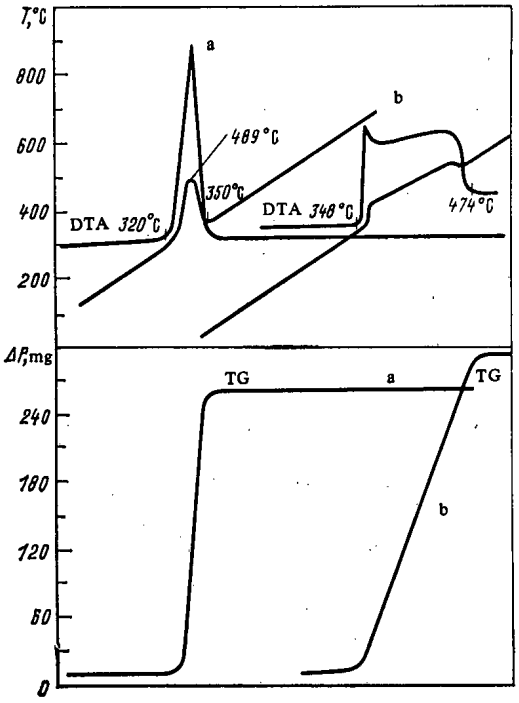

Fig. 1. Derivative recordings for the oxidation of briquettes of uranium mononitride: a) in oxygen (specimen mass 2.388 g); b) in air (specimen mass 2.343 g).

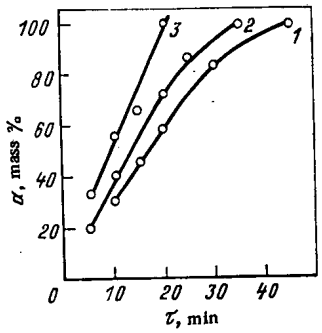

Fig. 2. Time dependence of the completeness of oxidation for (U, Pu)N briquettes at various temperatures in air, °C: 1) 325; 2) 350; 3) 400.

TABLE 2. Grain-Size Composition of Oxidation Products from Mixed (U, Pu)N Fuel

Temp., °C	Fraction, mass %							
	+200 μm		−200+100 μm		−100+50 μm		−50 μm	
	w/o vib.	with vib.	w/o vib.	with vib.	w/o vib.	with vib.	w/o vib.	with vib.
325	3,9	—	15,0	—	40,8	—	40,3	—
350	4,3	3,8	16,8	0,4	42,5	2,8	36,4	93,0
400	22,2	—	24,4	—	30,4	—	22,9	—

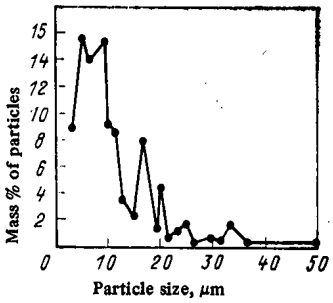

Fig. 3. Size distribution of the particles of powder of oxidized, mixed (U, Pu)N fuel in the fraction less than 50 μm.

TABLE 3. Grain-Size Composition of Oxidation Products from Briquettes of (U, Pu)C Fuel

Temp., °C	Fraction, mass %							
	+200 μm		−200+100μm		−100+50 μm		−50 μm	
	w/o vib.	with vib.	w/o vib.	with vib.	w/o vib.	with vib.	w/o vib.	with vib.
350	22,7	—	10,0	—	36,7	—	30,6	—
400	4,4	2,4	2,4	1,8	44,8	4,3	48,4	91,5
450	11,9	—	21,4	—	43,6	—	23,2	—

The oxidation in air began at 280°C, and the mean rate of oxidation in the range 340-484°C was about 0.88 mg/min. When the temperature was raised above 550°C, the mass of the specimen decreased, and at temperatures above 920°C it did not change. Therefore, the rate of oxidation of UC briquettes in oxygen is 3.5 times that in air, while the temperature rise due to the reaction heat is larger by a factor of three. The reaction is highly exothermic, which indicates that the yield of fine fractions in the oxidation of carbide fuel briquettes should be greater at lower oxygen concentrations and at a temperature close to the start of the oxidation. It is therefore desirable to oxidize (U, Pu)C briquettes in air at 350-450°C. Figure 5 shows the temperature dependence of the reaction completeness in the oxidation of (U, Pu)C briquettes. At 450°C the reaction rate is 71.4 mg/min. Table 3 gives data on the grain-size composition of oxidized (U, Pu)C fuel at various temperatures. For comparison, we give the grain-size composition of the oxidation products from the initial briquettes oxidized in the presence of vibration (frequency 20 Hz, amplitude 1 mm, time 1.5 h).

The largest yield of fractions of grain size less than 100 μm was obtained from oxidation at 400°C, and vibration substantially increased the yield of fractions with particle sizes less than 50 μm. The residual carbon content in the powders of particle size less than 100 μm was not more than 0.09 mass %.

Microscopic examination of the fractions of particle size less than 50 μm gave the size distribution (Fig. 6), with the mean size as 10.8 μm.

X-ray examination showed that the oxidation products of (U, Pu)C briquettes contained approximately equal amounts of two phases: (U, Pu)O_{2+x} with a = 5.425 Å and (U, Pu)$_3O_8$. The lattice constant of (U, Pu)O_{2+x} corresponded to the superstoichiometric value, as in the oxidation of (U, Pu)N briquettes [7].

To elucidate the oxidation mechanism for uranium monocarbide and mononitride in oxygen we performed thermogravimetric studies at the temperature corresponding to the start of reaction (up to 320°C for UN and up to 328°C for UC). The oxidation was halted before the specimens broke up. X-ray examination of a layer to a depth of 10-15 μm revealed the UO_{2+x} phase (base) together with UN and UC. It is assumed [8] that under these conditions it is most likely that solid solutions of UN–UO and UC–UO types are formed. Therefore, the mechanism in the initial and subsequent stages of the oxidation of uranium carbides and nitrides is probably as follows: initially the oxygen enters the lattice of the carbide (nitride) and forms an oxycarbide (oxynitride) of variable composition. Then the UO_2 phase is produced at the surfaces of the grains and at the boundaries. From a certain instant when the protective UO_{2+x} film begins to be disrupted, the reaction rate increases considerably. The oxidation terminates with the formation of U_3O_8. In the case of the monocarbide, there is also a parallel oxidation of free carbon.

The oxidation of mixed carbide (nitride) uranium–plutonium fuel also appears to occur in several stages with the formation of intermediate compounds. The main feature appears to be that the oxidation of the plutonium compounds

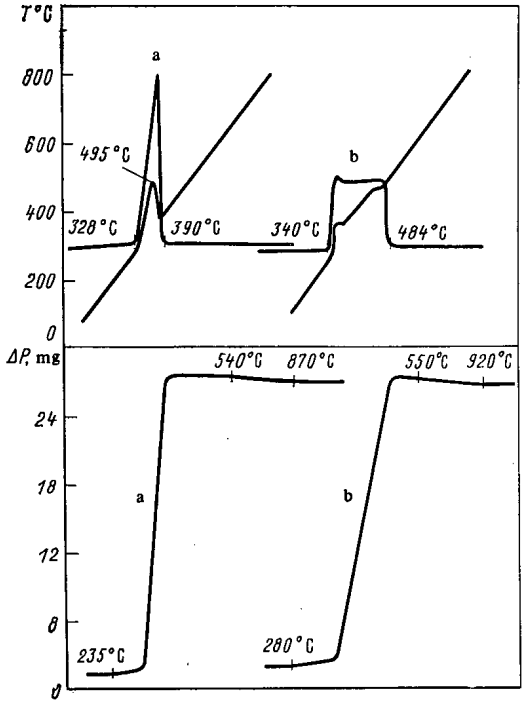

Fig. 4. Derivative recordings for the oxidation of briquettes of uranium monocarbide: a) in oxygen (specimen mass 1.185 g); b) in air (specimen mass 0.197 g).

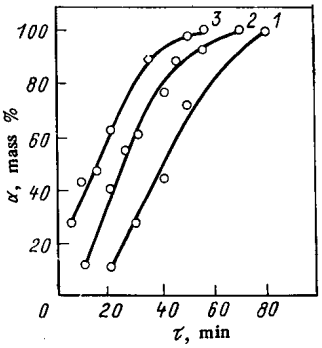

Fig. 5

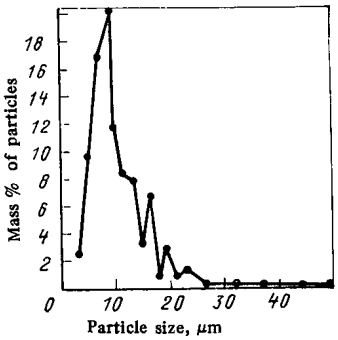

Fig. 6

Fig. 5. Time dependence of the completeness of oxidation for (U, Pu)C briquettes at temperatures, °C: 1) 350; 2) 400; 3) 450.

Fig. 6. Size distribution of powder of oxidized mixed (U, Pu)C fuel in the fraction less than 50 μm.

as components of the solid solution occurs in a single stage. For this reason, as a rule not all the uranium present in the specimen is oxidized to U_3O_8. For example, in the oxidation products for the (U, Pu)C solid solution about half is accounted for by $(U, Pu)O_{2+x}$.

LITERATURE CITED

1. F. G. Reshetnikov, At. Énerg., 50, No. 2, 118 (1981).
2. A. Bauer, React. Technol., 15, No. 2, 87 (1972).
3. V. V. Gagarin, At. Tekh. Rubezhom, No. 4, 6 (1976).
4. G. P. Novoselov et al., At. Énerg., 46, No. 4, 254 (1979).
5. G. P. Novoselov et al., At. Énerg., 37, No. 6, 460 (1974).
6. A. N. Vol'skii and Ya. M. Sterlin, Plutonium Metallurgy [in Russian], Nauka, Moscow (1967), p. 58.
7. V. G. Vlasov et al., Oxygen Compounds of Uranium [in Russian], Atomizdat, Moscow (1964).
8. N. M. Voronov, High-Temperature Chemistry of Uranium Oxide Compounds [in Russian], Atomizdat, Moscow (1971).

INFLUENCE OF PRELIMINARY NEUTRON IRRADIATION UPON HELIUM BLISTERING IN OKh16N15M3B STEEL

I. I. Chernov, B. A. Kalin, D. M. Skorov,
G. N. Shishkin, and M. V. Ivanov

UDC 621.039.531

Experimental research on radiation-induced erosion of materials under ion bombardment has shown that the form of the surface destruction depends significantly upon the mobility of the induced gas atoms and vacancies and on the growth mechanism of gas bubbles [1]. The first wall in a thermonuclear reactor is subjected to irradiation by neutrons, helium ions, and hydrogen isotopes. Previous investigations have shown that surface erosion in the first stage of reactor operation results mainly from helium blistering. Some researchers believe that in prolonged reactor operation, blister formation will be suppressed either by sputtering of the surface layer of the material before the critical dose of blister formation has been reached [2, 3] or by nonmonochromatic compositions of the ion beams [4, 5]. Yet, so far, the simultaneous influence of the various ions and the neutrons upon radiation-induced erosion has not been clarified. Experiments with successive [6, 7] and simultaneous [7, 8] irradiation by helium ions and hydrogen isotopes indicate that the simultaneous implantation of D^+ and He^+ ions reduces the critical dose [8] and enhances surface erosion [7] vis-à-vis irradiation by ions of a single type (D^+ or He^+).

The development of point defects obviously must modify the kinetics of blister formation. For example, Kornelsen [9] has shown that preliminary implantation of 5 keV Kr^+ ions in tungsten (dose of $8\cdot10^{15}$ ions/m^2) produces vacancies and vacancy clusters which in the subsequent bombardment by 250 keV He^+ ions form helium–vacancy complexes of the type He_nV_m. Similar results were obtained by Wilson [10], Caspers [11, 12], and others.

In order to simulate the conditions of a thermonuclear reactor, research on the formation of blisters and scaling in materials irradiated with neutrons is necessary and it is of interest for both applied and pure science. We therefore studied the influence of preliminary neutron irradiation upon helium blistering of stainless OKh16N15M3B steel.

Experimental Technique. Steel samples were irradiated by neutrons in nonstationary operation in the IGR reactor [13] at a thermal neutron flux density of about $1.5\cdot10^{19}$ neutrons/m$^2\cdot$sec and a thermal and fast ($E > 0.1$ MeV) neutron flux of $2.21\cdot10^{22}$ and $6\cdot10^{20}$ neutrons/m^2, respectively. The sample temperature did not exceed 573°K. Subsequent bombardment by 20 keV helium ions and doses of $(1\text{-}10)\cdot10^{21}$ ions/m^2 took place in a mass monochromator with double focusing [14] and target temperatures not exceeding 373°K. In order to increase the accuracy of the relative tests, the neutron-irradiation samples and control samples were cut from the same steel sheet, and the ion irradiation was made in the "pair" technique (the neutron-irradiated sample and the control sample were set up in a row and irradiated by the same helium ion beam at each of the doses indicated). Some of the samples irradiated with neutrons were additionally annealed for 15 min at 1173°K before the ion bombardment took place. The surface topography of the irradiated samples was studied on an REM-200 raster electron microscope; the steel structure was studied with the thin foil technique on an EVM-100L electron microscope.

Experimental Results. Typical electron-microscope pictures of the surface topography of steel samples are shown in Fig. 1; the results of the evaluation of the pictures are listed in Table 1 and Fig. 2. It follows from Table 1 that the blister formation on the surface of steel previously irradiated by neutrons is shifted toward higher doses. At a dose of $3\cdot10^{21}$ ions/m^2, blisters are observed on both types of samples: the surface of the control sample has only a small destroyed portion, whereas the surface of the sample irradiated by neutrons shows blisters which are already stable. When the dose is increased, the erosion coefficient S* increases owing to the scaling of the blister domes, but (see Fig. 2) scaling on the previously irradiated samples begins at higher doses and is less intense in the range from $4\cdot10^{21}$ to $7\cdot10^{21}$ ions/m^2 than on control samples. But at doses of $(8\text{-}10)\cdot10^{21}$ ions/m^2, the erosion coefficient of the control samples reaches its maximum and, as is known from [15], decreases thereafter. A sharp increase in scaling of the neutron-irradiated steel is observed at the same doses, but a maximum does not appear.

The typical feature characterizing the influence of preliminary neutron irradiation is that the damage to the blister domes changes: on the control samples a number of blisters appear which are broken over the dome periphery (see Fig. 1b),

Translated from Atomnaya Énergiya, Vol. 53, No. 2, pp. 80-83, August, 1982. Original article submitted July 28, 1981.

0038-531X/82/5302-0533$07.50

TABLE 1. Blistering of OKh16N15M3B Steel

State of the steel	Dose of the induced helium (10^{21} ions/m^2)				
	1	2	3	4	5–10
Initial	—	Blisters	Beginning of scaling	Scaling	
After neutron irradiation	—	—	Blisters	Beginning of scaling	Scaling

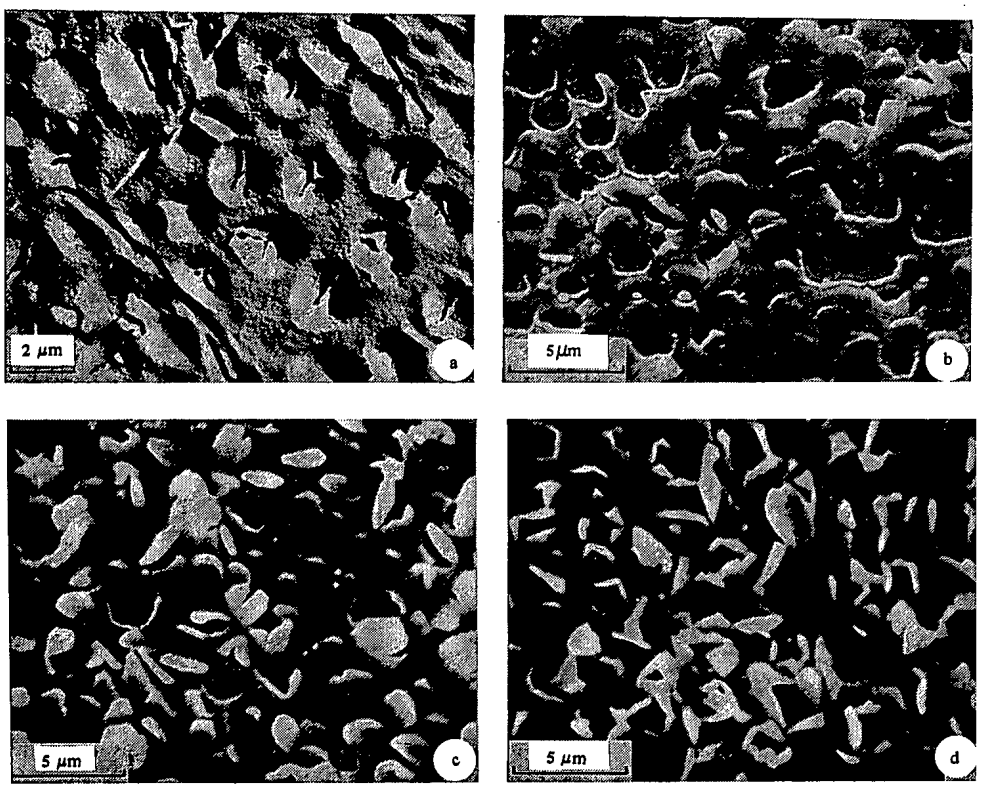

Fig. 1. Topography of the OKh16N15M3B steel surface irradiated with He^+ ions at E = 20 keV and T < 373°K; a) neutron irradiation + He^+ irradiation up to a dose of $5 \cdot 10^{21}$ ions/m^2; b) He^+ irradiation to a dose of $6.5 \cdot 10^{21}$ ions/m^2; c) neutron irradiation +He^+ irradiation to a dose of $6.5 \cdot 10^{21}$ ions/m^2; d) neutron irradiation + 15 min annealing at 1173°K + He irradiation to a dose of $6.5 \cdot 10^{21}$ ions/m^2.

whereas the majority of blisters are destroyed on the top of the dome in samples exposed to neutron irradiation (see Figs. 1a, c); the average size of the blisters is smaller but their density is higher.

Neutron irradiation has practically no influence upon the suppression of radiation-induced erosion, provided that the sample has been annealed for 15 min in vacuum at 1173°K before the ion bombardment. It follows from Fig. 2 that in this case S* = 0.45 atoms/ion, i.e., the coefficient of erosion is practically equal to that obtained for the control sample (S* = 0.47 atoms/ion). In the annealed samples, the form of the surface destruction is the same as in the irradiated samples, i.e., the destruction of the tops of the domes dominates. In this case, scaling causes bursting of the domes in the section close to the top (see Fig. 1d).

Discussion of the Results. The results which we obtained indicate that blistering depends significantly upon the neutron irradiation. High-intensity neutron irradiation at a relatively low (as far as the mobility of vacancies is concerned) temperature implies the development of a noticeable number of point defects and of defect clusters in the steel. When thin steel foils are inspected in a transilluminating electron microscope, it is observed that preliminary neutron irradiation under the conditions specified above favors the development of a dislocation net in addition to the point defects (Fig. 3). The consequence is a substantial increase in the number of sites where clusters develop. When the dose of the bombarding ions does not change, the merging of blisters must be delayed because the growth of each individual bubble is slowed down.

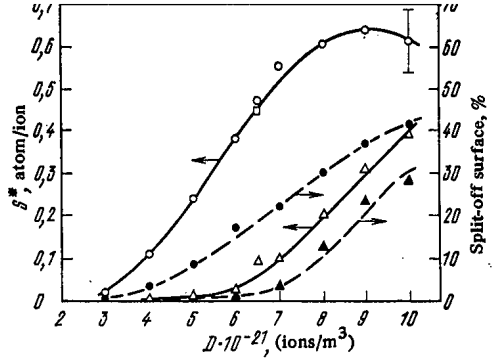

Fig. 2. Dose dependence of the erosion coefficient of 0Kh16N15M3B steel irradiated with He^+ ions at E = 20 keV and T < 373°K: Δ and ▲) preliminary irradiation with neutrons; ○ and ●) control sample; □) neutron irradiation + 15 min annealing at 1173°K.

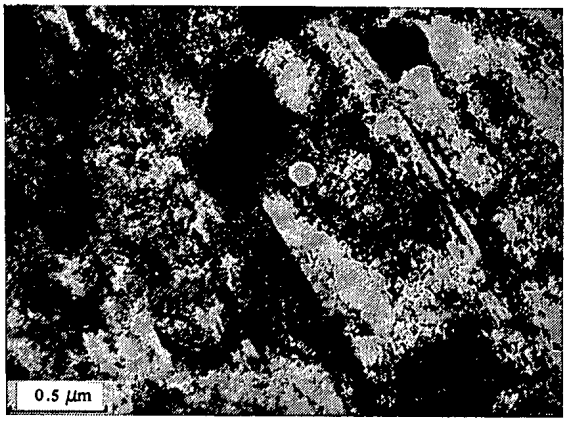

Fig. 3. Dislocation structure of 0Kh16N15M3B steel irradiated in nonstationary operation with a thermal neutron flux density of $\sim 1.5 \cdot 10^{19}$ neutrons/m^2·sec to a total flux of thermal and fast (E > 0.1 MeV) neutrons of $2.21 \cdot 10^{22}$ and $6 \cdot 10^{22}$ neutrons/m^2, respectively.

After an incubation period, the erosion coefficient of neutron-irradiated steel increases sharply. This can be explained with the assumption that the doses of seed formation, growth, and scaling of blisters are controlled by two factors: the influence of subdispersed microinhomogeneities in the material upon the kinetics of helium bubble formation and the influence of the mechanical properties of the material upon the erosion stability. The first factor dominates in the stage in which gas-filled pores are formed and, probably, merged into a void (the blister). The second factor determines the stability of the blister roofs against destruction under the influence of lateral stresses and internal gas pressure. At relatively low doses of the bombarding ions, the helium ions introduced are delayed by the neutron defects created. This obviously determines the observed incubation period. However, we can assume that at a spatial ion dose of up to $7 \cdot 10^{21}$ ions/m^2, saturation of the defects by helium atoms rapidly begins, and the subsequent blister formation proceeds in the usual fashion. In addition to the elastic properties of the surface layer of the material, the radiation-induced erosion can be affected by certain interactions and complexes which were formed during the incubation period. According to the results of M. I. Guseva et al. [16], the formation of pores in the irradiation can substantially enhance the radiation-induced erosion in blistering. The simultaneous irradiation of a material by neutrons, ions, and other particles can multiply this effect because the vacancies formed in the bombardment by fast particles, and the clusters of these vacancies, will be stabilized by the gas atoms which are present in excess.

The importance of preliminarily generated radiation defects during blister formation is also experimentally corroborated in the thermal annealing of samples before ion bombardment. When the samples are kept for 15 min at 1173°K, the defects are obviously annealed and, accordingly, the radiation-induced erosion is enhanced to that observed in the control samples.

Summarizing, preliminary neutron irradiation shifts the beginning of the blister formation and the intensive scaling of the surface toward higher ion doses. But when a certain critical dose of the helium ions ($7 \cdot 10^{21}$ ions/m^2) is reached, the scaling of the surface increases sharply and possibly reaches the steel erosion level in the initial stage at higher helium ion doses (>$1 \cdot 10^{22}$ ions/m^2).

LITERATURE CITED

1. D. Caletta, in: Ion Implantation in Semiconductors and Other Material, Plenum Press, New York (1973).
2. J. Martel et al., J. Nucl. Mater., 53, 142 (1974).
3. B. A. Kalin et al., At. Énerg., 47, No. 1, 53 (1979).
4. M. I. Guseva et al., J. Nucl. Mater., 63, 245 (1976).
5. J. Roth, et al., J. Nucl. Mater., 57, 365 (1975).
6. D. M. Skorov et al., Problems of Atomic Science and Technology. Physics of Radiation-Induced Damage and Radiation Materiology, No. 1(6), 46 (1978).
7. B. G. Vladimirov et al., At. Energ., 50, No. 1, 25 (1981).
8. M. Kaminsky et al., in: Int. Conf. on Low Energy Ion Beams, Salford, Sept. 5-8 (1977).
9. E. Kornelsen, Rad. Effects, 13, 227 (1972).
10. W. Wilson and R. Johnson, in: Interatom. Potent. and Simul. Lattice Defects, Plenum Press, New York (1972), p. 375.
11. A. Van Veen and L. Caspers, in: Proc. 7th Int. Vacuum Congress and 3rd Int. Conf. on Solid Surfaces, Vienna (1977), p. 2637.
12. L. Caspers et al., Phys. Status Solidi A, 46, 541 (1978).
13. I. V. Kurchatov et al., At. Energ., 17, No. 6, 463 (1964).
14. L. B. Begrambekov et al., in: Reports of the 4th All-Union Conf. on the Interaction of Atomic Particles with Solids [in Russian], Khar'kov, Press of the Khar'kov Physicotechnical Institute, 1, 100 (1976).
15. B. A. Kalin et al., Problems of Atomic Science and Technology. Physics of Radiation-Induced Damage and Radiation Materiology, No. 2(13), 72 (1980).
16. I. N. Afrikanov et al., At. Énerg., 50, No. 3, 183 (1981).

AVERAGE NUMBER $\bar{\nu}_p$ OF PROMPT NEUTRONS IN THE FISSION OF ^{236}U NUCLEI BY NEUTRONS IN THE ENERGY RANGE 0.8-6 MeV

V. V. Malinovskii, V. G. Vorob'eva, B. D. Kuz'minov, V. M. Piksaikin, and N. N. Semenova

UDC 539.185

The average number $\bar{\nu}_p$ of prompt fission neutrons is one of the important characteristic parameters of nuclei undergoing fission. The present work deals with research on the energy dependence of $\bar{\nu}_p$ in the fission of ^{236}U by neutrons. The authors of [1] have presented results obtained in measurements of $\bar{\nu}_p$ in the fission of nuclei of this isotope. But the measurements were not sufficiently detailed to evaluate the possible deviations of the energy dependence of $\bar{\nu}_p$ from a linear law. Furthermore, measurements made with an independent technique give reason for deriving recommended values of the quantity under inspection and for determining the errors. Preliminary and incomplete results of $\bar{\nu}_p$ measurements in the fission of ^{236}U nuclei by neutrons were earlier presented in [2].

The technique of the $\bar{\nu}_p$ measurements and the scheme of the experimental setup have been described in detail in [3]. Neutrons of various energies were obtained with the Li(p, n), T(p, n), and D(d, n) reactions. The neutron energy resolution in work on solid targets amounted to 30 keV for lithium and tritium targets and 80 keV for a deuterium target. In order to include the background neutrons resulting from the D(d, n) reaction under consideration, special measurements with a hollow target identical with the experimental target, but not filled with deuterium, were made. The detector of the fission neutrons was assembled from 16 ^{3}He-filled counters mounted in a cylindrical polyethylene block. Ionization chambers were the detectors of the fission fragments. The ^{236}U enrichment exceeded 99%. The operational assembly consisted of six uranium chambers and one californium chamber, the latter being located in the center of the setup. Owing to the high α-activity of the ^{237}Np nuclei in [3] the pulses taken from the fission chamber were amplified with fast current amplifiers. In the α-measurements on ^{236}U, spectrometric amplifiers with a time constant of 0.5 μsec of the pulse-shaping circuits were

Translated from Atomnaya Énergiya, Vol. 53, No. 2, pp. 83-86, August, 1982. Original article submitted October 6, 1981.

0038-531X/82/5302-0536$07.50

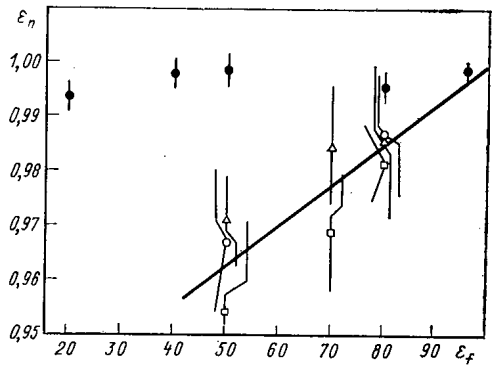

Fig. 1. Dependence of the number of recorded neutrons (rel. units) upon the fission-fragment recording efficiency: ●) ^{252}Cf; ○, Δ, □) ^{236}U at the energies 2, 2.5, and 3 MeV, respectively.

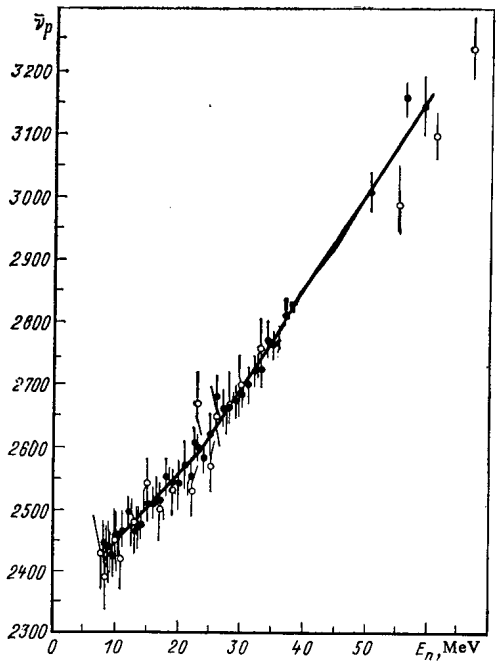

Fig. 2. Energy dependence of $\bar{\nu}_p$ in the fission of ^{236}U nuclei by neutrons: ○) [1]; ●) present work; ——) recommended dependence.

employed. In this manner, the entire circuitry obtained additional stability against interference. In the operational threshold of discrimination, the recording efficiency of fission fragments of ^{236}U and ^{252}Cf nuclei was 80 and 96%, respectively.

In the fission of ^{236}U nuclei by neutrons, $\bar{\nu}_p$ was determined from the formula $\bar{\nu}_p = \bar{\nu}_p^0 \beta K$, where $\bar{\nu}_p^0 = 3.733$ denotes the average number of prompt neutrons in the spontaneous fission of ^{252}Cf nuclei; β denotes the experimental value of the ratio of the average number of prompt neutrons in the fission of ^{236}U by neutrons to that in the spontaneous fission of ^{252}Cf; $K = (1 + \delta_1)(1 + \delta_2) \ldots (1 + \delta_i)$, where δ_i denotes corrections accounting for the various energy spectra of the fission neutrons of the ^{236}U and ^{252}Cf nuclei (δ_1), dependence of the efficiency of fission-neutron recording upon the position of the ^{236}U layers on the axis of the neutron detector (δ_2), various diameters of the ^{236}U and ^{252}Cf layers (δ_3), counting losses (δ_4, δ_5), dependence of the number of recorded neutrons upon the recording efficiency of fission fragments (δ_6), difference of the probability of full slowing down in the layer of the material undergoing fission for fragments with different kinetic energies (δ_7), difference of the angular distributions of the fragments in the fission of ^{236}U and ^{252}Cf nuclei (δ_8), and the presence of background neutrons in the D(d, n) reaction (δ_9). The determination of the corrections δ_i has been described in detail in [3]. The corrections δ_6 and δ_7 were experimentally determined (Fig. 1). In contrast to [4, 5], layers

TABLE 1. Results of the $\bar{\nu}_p$ Measurements for the Fission of ^{236}U Nuclei by Neutrons

Neutron energy (MeV)	Corrections and their errors			$\bar{\nu}_p$	Statistical error*	Total error
	δ_1	δ_4	δ_5			
0,80	−0,019±0,005	0,002±0,001	−0,019±0,002	2,451	0,029	0,034
0,85	−0,019±0,005	0,003±0,001	−0,019±0,002	2,446	0,027	0,033
0,90	−0,019±0,005	0,003±0,001	−0,019±0,002	2,434	0,022	0,034
0,95	−0,019±0,005	0,004±0,001	−0,019±0,002	2,430	0,023	0,035
1,00	−0,019±0,005	0,004±0,001	−0,019±0,002	2,465	0,033	0,038
1,10	−0,019±0,005	0,002±0,001	−0,019±0,002	2,472	0,022	0,029
1,20	−0,018±0,005	0,005±0,001	−0,017±0,002	2,501	0,017	0,025
1,30	−0,018±0,005	0,002±0,001	−0,017±0,002	2,469	0,030	0,035
1,35	−0,018±0,005	0,001±0,001	−0,017±0,002	2,476	0,031	0,036
1,40	−0,018±0,005	0,002±0,001	−0,017±0,002	2,480	0,015	0,024
1,50	−0,018±0,005	0,002±0,001	−0,017±0,002	2,514	0,020	0,030
1,60	−0,018±0,005	0,002±0,001	−0,017±0,002	2,515	0,017	0,025
1,70	−0,018±0,005	0,003±0,001	−0,017±0,002	2,518	0,023	0,030
1,80	−0,018±0,005	0,001±0,001	−0,017±0,002	2,556	0,026	0,032
1,90	−0,017±0,004	0,003±0,001	−0,017±0,002	2,549	0,012	0,021
2,00	−0,017±0,004	0,003±0,001	−0,017±0,002	2,545	0,035	0,039
2,10	−0,016±0,004	0,001±0,001	−0,017±0,002	2,575	0,033	0,037
2,20	−0,016±0,004	0,002±0,001	−0,017±0,002	2,558	0,024	0,030
2,25	−0,015±0,004	0,004±0,004	−0,017±0,002	2,611	0,016	0,024
2,30	−0,015±0,004	0,002±0,001	−0,017±0,002	2,604	0,015	0,023
2,40	−0,015±0,004	0,005±0,001	−0,017±0,002	2,588	0,015	0,023
2,50	−0,015±0,004	0,005±0,001	−0,017±0,002	2,626	0,029	0,034
2,60	−0,014±0,004	0,001±0,001	−0,016±0,002	2,684	0,028	0,034
2,70	−0,014±0,004	0,009±0,001	−0,016±0,002	2,667	0,023	0,029
2,80	−0,014±0,004	0,003±0,001	−0,016±0,002	2,669	0,032	0,037
2,90	−0,014±0,004	0,004±0,001	−0,016±0,002	2,678	0,024	0,030
3,00	−0,014±0,004	0,003±0,001	−0,016±0,002	2,690	0,013	0,023
3,10	−0,014±0,004	0,002±0,001	−0,016±0,002	2,704	0,023	0,030
3,20	−0,014±0,004	0,004±0,001	−0,016±0,002	2,727	0,016	0,025
3,30	−0,014±0,004	0,002±0,001	−0,016±0,002	2,732	0,021	0,029
3,40	−0,012±0,003	0,004±0,001	−0,015±0,002	2,780	0,022	0,029
3,50	−0,012±0,003	0,003±0,001	−0,015±0,002	2,772	0,015	0,023
3,60	−0,012±0,003	0,005±0,001	−0,015±0,002	2,775	0,022	0,029
3,70	−0,012±0,003	0,005±0,001	−0,015±0,002	2,819	0,019	0,026
5,05 †	−0,009±0,003	0,005±0,001	−0,013±0,002	3,007	0,016	0,030
5,60	−0,007±0,002	0,002±0,001	−0,010±0,002	3,167	0,026	0,034
5,90	−0,007±0,002	0,002±0,001	−0,010±0,002	3,154	0,042	0,046

*The error calculated from the spread of the results of measurements in the individual series is stated whenever the error exceeded the statistical error.

†At the energies 5.05, 5.60, and 5.90 MeV, the following values are obtained for δ_9: -0.002 ± 0.003; 0.008 ± 0.003; and 0.011 ± 0.003, respectively.

of natural uranium of various thicknesses with ^{252}Cf uniformly distributed in the layers (intensity of the spontaneous fission events about 20 fissures/sec) were employed in our experiments. Table 1 lists the results of the ν_p measurements. We indicate below the corrections which do not depend upon the neutron energy, and the errors of these corrections:

δ_2 ... 0.048 ± 0.002 $\quad$ δ_7 ... 0.003 ± 0.001
δ_3 ... -0.003 ± 0.002 $\quad$ δ_8 ... 0.000 ± 0.001
δ_6 ... 0.015 ± 0.003

Figure 2 shows the results of the present work in comparison with the results of [1]. The overall discrepancies of the results are not beyond the error limits of the measurements; the neutron energy interval of 4-6 MeV is an exception. All the experimental results of both investigations were described with the least-square method which led to the straight line $\bar{\nu}_p = (2.297 \pm 0.009) + (0.1363 \pm 0.034)E_n$ in the neutron energy range below the threshold of the (n, n'f) reaction.

The statistical weight of the points was taken in accordance with the total errors stated in the work. But it is generally accepted that the average kinetic energy of the fission fragments of the nuclei begins to decrease above a certain neutron energy [6]. Assuming that this decrease is unrelated to the change in the total fission energy of the nuclei, we may expect a corresponding increase in the growth rate of ν_p above this neutron energy.

An inflection of the energy dependence of $\bar{\nu}_p$ has been observed in several other nuclei [7, 8]. The experimental data were therefore described by two straight lines obtained with the least-square method. The boundary separating all the experimental $\bar{\nu}_p$ values into two portions for describing each part with a respective straight line was varied in the neutron energy range between 2 and 3 MeV; the optimal description of the energy dependence of $\bar{\nu}_p$ by two straight lines was selected with the χ^2 minimum condition. This condition could be used to confirm that the representation of the energy dependence of ν_p by two straight lines is much better than the description of the experimental data by a single straight line.

The following energy dependence of $\bar{\nu}_p$ in the fission of ^{236}U nuclei by neutrons is recommended for practical applications: $\bar{\nu}_p = (2.346 \pm 0.012) + (0.1072 \pm 0.0071)E_n$ for $E_n \leqslant 2.35$ MeV; and $\bar{\nu}_p = (2.236 \pm 0.024) + (0.1539 \pm 0.0068)E_n$ for 2.35 MeV $\leqslant E_n \leqslant 5.9$ MeV.

The errors indicated do not include the error of the average number $\bar{\nu}_p$ of prompt neutrons from the ^{252}Cf standard employed. The value $\bar{\nu}_p^0 = 3.733$ was assumed for the estimate.

LITERATURE CITED

1. H. Condé and M. Holmberg, Nucl. Energy, 25, 331 (1971).
2. V. G. Vorob'eva et al., in: Neutron Physics [in Russian] (Reports of the 5th All-Union Conference), Moscow, Press of the Central Sci.-Research Inst. of Atomic Inf., Vol. 3, 95 (1980).
3. V. G. Vorob'eva et al., Problems of Atomic Science and Technology. Nuclear Constants [in Russian], No. 3(38), 44 (1980).
4. J. Boldeman and J. Frehaut, Nucl. Sci. Eng., 76, No. 1, 49 (1980).
5. H. Condé and M. Holmberg, Ark. Fys., 29, No. 4, 33 (1965).
6. N. P. D'yachenko et al., Problems of Atomic Science and Technology. Nuclear Constants [in Russian], No. 1(40), 53 (1981).
7. V. G. Vorob'eva et al., Problems of Atomic Science and Technology. Nuclear Constants [in Russian], No. 1(40), 62 (1981).
8. V. G. Vorob'eva et al., Problems of Atomic Science and Technology. Nuclear Constants [in Russian], No. 1(40), 60 (1981).

NUCLEAR REACTIVITY OF EXTRACTORS WITH A VARIATION IN THE CONCENTRATION OF FISSIONABLE MATERIALS IN A NONSTEADY REGIME

T. Żółtowski

UDC 66.061.5:621.039.59

The criticality of extraction units has important significance. The extraction process performed in a multistage device (in the counterflow) is highly nonlinear; therefore, it is accurate to describe the phenomena occurring in the unit as very complicated. The distribution and variation of the concentration in the individual stages of the device depend on the initial parameters; the plutonium concentration in the aqueous phase can be subjected to the greatest perturbation.

A device for the extraction of a large amount of fissionable materials cannot always have absolutely safe geometry. In this connection, control of the criticality of the device is directly related to control of the concentration distribution in the stages of the device. The appearance of nonuniformity in the distribution of fissionable materials in an extraction can result in too large an increase in the nuclear reactivity of the system.

A. M. Rozen et al. [1-4] have calculated the profiles of the plutonium concentration and determined the conditions under which a peak in the plutonium concentration is created in a steady-state or transitional process. They assume that this can lead to a critical state.

The goal of this paper is to check the postulate of A. M. Rozen et al. and to determine the variations of the reactivity when a critical concentration profile is attained.

Method of the Investigation. The variation of the concentration profiles in the extraction device has been calculated with the help of the SEPHIS computer program [2]. This program permits calculating the time dependence of the process of counterflow extraction by the Purex-process scheme. An analytic representation of the extraction isotherms is used in it. The concentration profiles are determined by means of iterations using mass balance.

The calculation of the nuclear reactivity is performed with the help of the KENO II Monte Carlo method [6]. The Hansen–Rock 16-group capture cross sections supplemented by the Aerojet Company (USA) capture cross sections were used. The programs were run on a Cyber-73 computer.

Initial Data for Calculation of the Concentration Profiles of Uranium and Plutonium in a Counterflow Extractor of the Mixing–Settling-Tank Type. The variations in time of the concentration profiles in an extractor of the mixing–settling-tank type containing 16 stages were calculated. Data on the supply of the extractor are given in Table 1. The ratio of the flows of the phases (the flow of the organic phase is taken as unity) for the aqueous phase is 0.1065 for stages 1-5 (washing) and 0.3435 for stages 6-16 (extraction).

The calculations were performed for 1484 time intervals. An approach to 95% of the steady state (according to the mass balance) was obtained after 918 intervals, and an approach to 99.9% was obtained after 1484 intervals.

Results of the Calculation of the Variation of the Concentration Profiles. The distribution of the plutonium concentration obtained as a result of the calculation by the SEPHIS program for 500, 700, 920, and 1484 time intervals is presented in Fig. 1. The profiles for an individual interval were taken to correspond to a steady state.

It follows from the results that after 920 intervals a peak in the plutonium concentration appears, which reaches 20 g Pu/liter in the organic phase and 50 g Pu/liter in the aqueous phase. With the fact that the extractor is supplied with a plutonium solution having a concentration of 2 g/liter taken into account, this is an appreciable increase in the concentration. After 920 intervals the plutonium concentration decreases, reaching ∿3.5 g/liter in the organic phase and 10 g/liter in the aqueous phase. It follows from this that the steady state is appreciably removed from the nonsteady state with respect to the ratio of the observed increase in the plutonium concentration. One should add that the plutonium peak appears in all of the more removed stages of the extractor and reaches its maximum value in the 14th stage for the aqueous phase and in the 15th stage for the organic phase.*

*Such regimes, which are characterized by an appreciable discharge of valuable components to a refinery, are called out-of-bounds. The internal accumulation of plutonium during such processes is a maximum in the nonsteady (transitional) regime; in the steady state, the peak of the concentrations is small due to the discharge of plutonium to a refinery [1] – Editor's Note.

Institute of Nuclear Research, Warsaw, Poland. Translated from Atomnaya Énergiya, Vol. 53, No. 2, pp. 86-88, August, 1982. Original article submitted August 28, 1981.

 0038-531X/82/5302-0540$07.50

TABLE 1. Data on Supply of the Extractor

Phase	Stage	Uranium, g/liter	Plutonium, g/liter	HNO_3, moles/liter
Aqueous	1	0,0	0,0	3,0
Aqueous	6	300,0	2,0	3,0
25% Tributyl phosphate	16	0,0	0,0	0,0

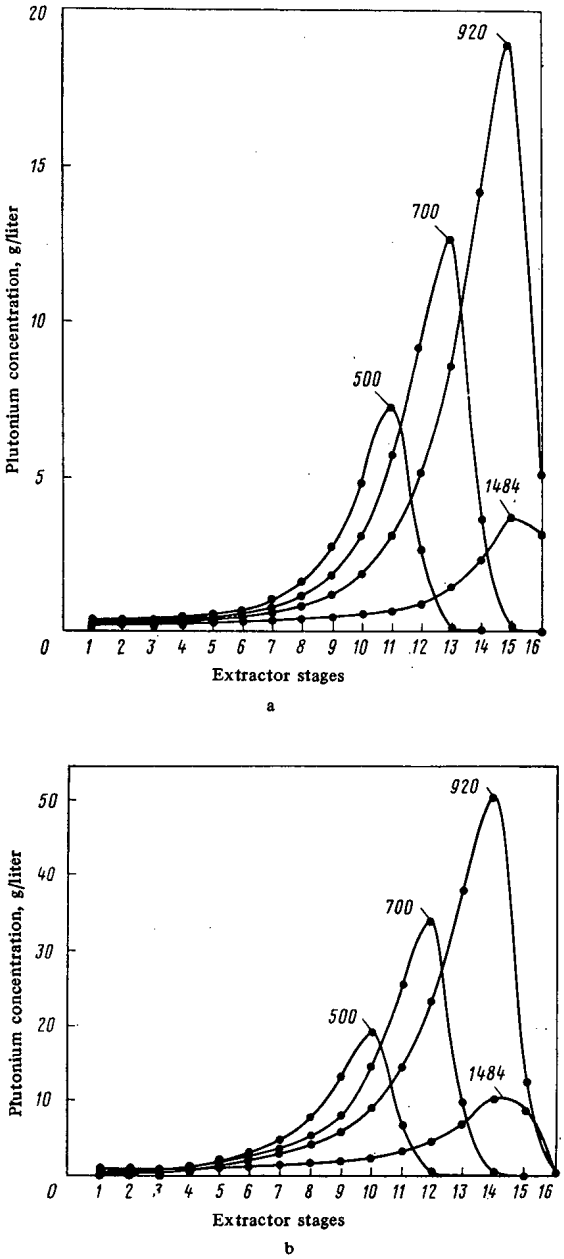

Fig. 1. Variations in time of the profile of the plutonium concentration in the (a) organic and (b) aqueous phases.

Calculation of the Criticality by the Monte Carlo Method. Three geometric configurations of a horizontal extractor with settling tanks in the shape of a rectangular parallelepiped made out of acid-resistant steel are adopted for the calculations.

The layout of one stage of the extractor is presented in Fig. 2. The volumes of solution in the stage were (a) 2, (b) 5, and (c) 12 liters, respectively. An 80%-enrichment of ^{235}U and a 100%-enrichment of ^{239}Pu is specified.

The results based on the Hansen–Rock capture cross-sections are supplemented with the capture cross-sections worked out by the Aerojet Company.

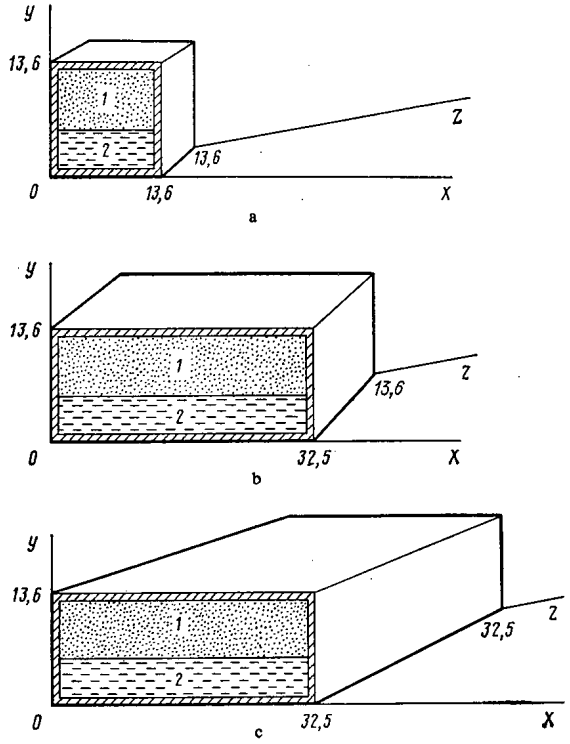

Fig. 2. Geometry of an individual stage of the exterior (the dimensions are indicated in centimeters): 1, 2) organic and aqueous phases in the stage, respectively.

TABLE 2. K_{eff} of the Extractors

Regime	Stage vol., liters	K_{eff}	Standard deviation
1	2	0,4626	0,0077
2	5	0,7102	0,0070
3	12	1,1449	0,0101
4*	12	1,1391	0,0086

*Calculated for the profile corresponding to time interval 700.

For extractors with a stage volume of 2 and 5 liters, 50 generations were calculated for 300 initial neutrons (15,000 events). The average value of the effective neutron multiplication factor K_{eff} was calculated using the results obtained for the last 40 neutron generations; the first 10 generations were discarded. A total of 39 neutron generations from 300 initial neutrons were calculated for an extractor with a stage volume of 12 liters; the results for the last 29 generations were used to calculate K_{eff}.

The necessary correction to the capture cross sections of the fission nuclides has been applied with potential scattering (the fissionable nuclide dilution effect) taken into account. A cosinusoidal distribution of the initial neutrons was assumed in all the calculations. Reflectors were not taken into account in the calculation. Modeling of each regime required calculations lasting 10 min (CPU time) on a Cyber-73 computer.*

Results of the Calculations of the Nuclear Reactivity of an Extractor by the Monte Carlo Method. As a result of the calculations with the indicated geometrical configurations for the case in which the plutonium concentration becomes a maximum, values of the criticality K_{eff} are obtained. The values of K_{eff} and the standard deviations are presented in Table 2.

*In view of the simple geometry of the extractors, calculation of the criticality of a single stage is possible with the help of simple engineering formulas without using the Monte Carlo method; it is advisable to use the latter when calculating the criticality of a bank of extractors as a whole – Editor's Note.

As is evident from Table 2, extractors with a stage volume of 2 and 5 liters are appreciably distant from the critical state, notwithstanding an increase in the plutonium concentration, and only the extractor with a volume of 12 liters is supercritical. One should note that a state of supercriticality is also attained for the profile which precedes the profile having the maximum plutonium concentration.

Discussion of the results. The determination of the criticality parameters of extractors during perturbation of the concentration profile of the fissionable materials confirms the conclusions of A. M. Rozen et al. [1-4], although a different mathematical model of the process was used [5]. One can achieve a critical state of the system and the onset of a self-maintaining valuable reaction in some cases in which extractors with large-volume settling tank stages are used in the engineering process. Limiting the number of sections may be sufficient to control the criticality. One should note that the mixing chambers of the extractor were not taken into account in the calculations presented. They should be taken into account for an accurate calculation of the nuclear reactivity of an extractor. In addition, it is necessary to provide for the calculation of a bank of extractors as a whole.

The results of this paper show that in the case of large process banks of extractors, one should use continuous control of the variations of the nuclear reactivity as suggested by T. Zoltowski et al. [7].

LITERATURE CITED

1. A. M. Rozen et al., in: Transactions of the COMECON Symposium "Investigations in the Area of Reprocessing of Irradiated Fuel," Marianske Lazne, 1971, Prague (1972), p. 118.
2. A. M. Rozen et al., At. Energ., 37, No. 3, 187 (1974).
3. A. M. Rozen et al., At. Energ., 46, No. 5, 333 (1979).
4. A. M. Rozen et al., Radiokhimiya, 18, No. 4, 572 (1976).
5. W. Gronier, ORNL-4746 (1972).
6. G. Whitesides and N. Gross, ORNL CTC-5 (1969).
7. Z. Zoltowski et al., Trans. Am. Nucl. Soc., 39, 519 (1981).

STATUS AND PROSPECTS OF THE PRODUCTION OF RADIOISOTOPE-TAGGED COMPOUNDS IN THE USSR*

E. I. Mikerin

UDC 547.02

Compounds tagged with radioisotopes are used today as a precise instrument for investigations in various fields of the natural sciences and also as a means for diagnosing many diseases. In our country their production was begun in 1948. The gradual development of this field of chemistry resulted in the production of about 200 different preparations by the end of the first decade. These were mainly key compounds, relatively simple organic and inorganic substances, and preparations for medicinal purposes. By the end of the 1960s, the total range was close to 600 compounds, and by the mid-1970s it was large enough to meet most of the current needs of the domestic market and the COMECON member-nations for specialized products.

As a result of the development of the biological sciences, increasing importance came to be attached to biologically active substances tagged with radioactive biogenic elements such as ^{3}H, ^{14}C, and ^{32}P. Today the range of tagged organic compounds includes over 600 products. During the tenth five-year plan, 150 new compounds were brought into production and the quality of other previously developed preparations was substantially improved, making possible a significant improvement in the supply of these products to scientific research organizations. The production of tagged compounds is today an independent branch of precision chemical technology combining the development of efficient methods for introducing appropriate isotopes and the organization of the mass production of tagged compounds. The available range of tagged compounds includes practically all of the most important classes of biologically active substances. Among them are the compounds nucleic acids, amino acids, lipids, steroid hormones, and carbohydrates. The most important organizations producing and supplying tagged organic compounds are the State Institute of Applied Chemistry, the V. G. Khlopin Radium Institute, the Molecular Genetics Institute of the USSR Academy of Sciences, and the "Radiopreparat" Enterprise of the Nuclear Physics Institute of the Academy of Sciences of the Uzbek SSR.

The expansion of the available range of biologically active substances tagged with tritium is due not only to the availability and low price of the initial isotope raw material and the fact that it is easier to conduct synthesis operations on the basis of tritium than on the basis of ^{14}C but also to the valuable nuclear-physics properties of the isotope itself. In our country, we produce 226 tritium-tagged organic compounds, the most important of which are the components of nucleic acids, amino acids, and steroid hormones. In addition to monomer compounds, there is considerable interest in tritium-tagged biopolymers, particularly polyribo- and polydeoxynucleotides, which are the synthetic analogs of RNA and DNA. Today there is a wide variety of tritium-tagged D- and L-amino acids with high-quality indicators which are as good as foreign specimens. The method of their production is based on the use of an improved procedure for the hydration of the appropriate precursors, with subsequent ligand-exchange chromatography to separate the mixture of optically active isomers. The variety and output of anabolic steroid hormones, which are a necessary component of diagnostic kits for radioimmunological analysis, have been expanded. The need to supply biological experiments with nucleic acid components possessing high and superhigh molar activity stimulated the development of methods for obtaining multiply tagged purine and pyrimidine bases. The subsequent use of enzymes from purine and pyrimidine metabolism revealed a simple and reliable method of obtaining a large variety of multiply tritium-tagged components of nucleic acids.

The assortment of compounds tagged with ^{14}C includes 293 substances. This assortment has been expanded much more slowly than that of tritium-tagged compounds. A total of about 50 new preparations has been produced. Compounds tagged with ^{14}C constituted 50% of the total volume of isotope production in our country in 1981, whereas the percentage in 1969 was about 68%. A similar trend is observed in the development of the assortments supplied by leading firms in the capitalist countries. The transition to more-complex biological installations has considerably complicated the setups for chemical synthesis, which in some cases makes it very difficult to work with compounds tagged with ^{14}C. In accordance with the Agreement on Multilateral International Specialization and Cooperation in the Production of Isotope Products, the USSR has concerned itself mainly with the development of methods for obtaining steroids tagged with ^{14}C.

The assortment of compounds tagged with ^{32}P has been considerably expanded, since radioactive preparations containing this isotope are widely used in biological research, experimental medicine, and agriculture. In particular, the most significant advances made during recent years in deciphering the structure of nucleic acids and in experiments in genetic engineering were

*This is the journal version of a report presented at the second symposium of the COMECON member-nations entitled "Organic Compounds Tagged with Radioactive Isotopes" (Leningrad, December 8-11, 1981).

Translated from Atomnaya Énergiya, Vol. 53, No. 2, pp. 89-91, August, 1982. Original article submitted March 12, 1982.

0038-531X/82/5302- 0544$07.50

achieved by using ^{32}P-tagged fragments of nucleic acids. The most important initial substance for the synthesis of ^{32}P-tagged nucleotides is [^{32}P]orthophosphoric acid without a carrier. The USSR developed an industrial technology for its production based on the irradiation of pure sulfur in a nuclear reactor and on a distillation method for producing ^{32}P which ensures a stable output of preparations with high molar activity practically equal to the theoretical value. Through the use of [^{32}P] orthophosphoric acid it has been possible to set up an industrial technology for obtaining nucleotide triphosphates with high molar activity (up to 1000 kCi/mole, 37 PBq/mole), as well as tagged fertilizers and pesticides for agriculture. Today the range of ^{32}P-tagged organic compounds includes about 30 substances. In biological research, preparations containing ^{33}P are sometimes used. The production of compounds containing this isotope was organized in 1977, and in some cases their properties give them advantages over analogous preparations containing ^{32}P.

The importance and timeliness of using radioisotopes for the development of fundamental molecular-biology research and for the discovery of scientific principles of medicine may be illustrated by specific examples. As a part of international cooperation among the COMECON member-nations on the "Revertase" project, work was done on the synthesis of globin, a blood protein, outside of the organism by means of enzymes. This work was made possible by the use of isotope techniques. Using isotope methods the researchers discovered a new class of subcellular units known as informosomes. This work forms the basis of a new branch of molecular biology, the study of the transmission of genetic information. The use of specially synthesized valine with high molar activity (60 kCi/mole) made it possible to measure the rest mass of the anti-neutrino. The production of tritium-tagged anabolic steroid hormones enabled the Sports Committee of the USSR to develop a method to check the doping of athletes at the Moscow Olympic Games. The synthesis of chemotherapeutic preparations intended for combating diseases in humans and animals (eleutheroside B, chemococcids, antitumor preparations, etc.) containing ^{3}H and ^{14}C as the radioactive indicators made it possible to study their pharmacokinetic behavior in detail.

There has been a significant increase in the molar activity of newly developed compounds and an improvement in those produced earlier. For nucleic-acid components singly tagged with tritium, the value averages 15-20 kCi/mole (555-740 TBq/mole), and for multiply tagged compounds it is no less than 40-50 kCi/mole (1.48-1.85 PBq/mole). Tritium-tagged L- and D, L-amino acids are available with a molar activity of 15-60 kCi/mole (0.6-2.2 PBq/mole). There has been an increase in the molar activity of tritium-tagged steroid hormones (in some cases up to 100 kCi/mole (3.7 PBq/mole) or higher).

An equally important class of indicators consists of the characteristics which show the presence of radioactive and chemical impurities in tagged compounds since in many cases the presence of such substances even in minute quantities may seriously distort the results of the biological experiment. The wide use of modern methods for producing and purifying compounds based on the use of different forms of preparatory and analytic chromatography, as well as of modern physico-chemical and biological methods of analysis, makes it possible to obtain tagged compounds with high indicators of radio-chemical and chemical purity.

Interest in compounds containing ^{125}I has increased as a result of its nuclear-physics properties. Tests of radioimmuno-logical kits for diagnosing various diseases have been developed and are being continued. The assortment of kits for radio-immunological analysis is expected to be expanded in the near future.

An analysis of the development of tagged-compound production during the past decade enables us to detect some trends which will probably continue to prevail in the near future:

1. We observe the further "biologization" of the assortment of compounds developed in the laboratory and mass-produced, accompanied by an increase in complexity.

2. A greater complication of the structure of tagged, biologically active compounds leads to a constant increase in the role of enzyme methods of synthesis, as well as of isotope-exchange methods, based on the introduction of radioisotopes directly into the final product.

3. The molar-activity requirements for tagged compounds are becoming steadily higher. With regard to ^{125}I and ^{32}P this means a need to produce compounds with a molar activity close to the theoretical value, while with regard to ^{3}H and ^{14}C it means the increasingly widespread development of methods for synthesizing multiply tagged compounds.

4. The purity requirements for tagged compounds are growing more rigorous, leading to the use of the most modern methods for their production and analysis (high-efficiency liquid and ligand-exchange chromatography, etc.) and to the inclusion of biological-activity tests in the technical requirements for tagged compounds.

The development of the production of tagged compounds in the USSR is a good example of the fraternal cooperation established among the COMECON member-nations. An important role in this has been played by the 1974 Agreement on Multilateral International Specialization and Cooperation in the Production of Isotope Products. Today our country's specialization includes about 200 organic compounds tagged with radioisotopes (85 tagged with ^{3}H, 106 with ^{14}C, and 14 with ^{33}P). At the same time, a considerable number of tagged compounds are being imported from other COMECON member-nations for which they are being reserved. A further advance in the cooperation between the COMECON member-nations was the exchange of information on plans for the development of new isotope products and the harmonization of these plans among different countries.

EXPERIENCE FROM APPLICATION OF RADIOLYOLUMINESCENCE AND ELECTRON PARAMAGNETIC RESONANCE TO DOSIMETRY OF ACCIDENTAL IRRADIATION

I. A. Alekhin, S. P. Babenko, S. N. Kraitor, K. K. Kushnereva, A. V. Barabanova, S. R. Ginzburg, R. D. Drutman, and V. N. Petushkov

UDC 539.12.08

It was proposed [1] that the dose from accidental irradiation be measured by using radiolyoluminescence (RLL), i.e., the luminescence which occurs during the dissolution of samples of human biological tissue (hair, nails), clothing, documents, and other objects which accompany a person under the conditions of an accident. Radiolyoluminescence is caused by free radicals which are formed when organic substances are irradiated, which can be detected by the method of electron paramagnetic resonance (EPR). The possibility of employing EPR to measure the dose of accidental irradiation was considered in [2, 3].

In the work reported here, we made a comparative study of the EPR and RLL of human hair, cotton fabric used to make protective clothing for the personnel of sections with an accident hazard, as well as synthetic and woolen fabrics used in everyday clothing. We investigated the characteristics of RLL and EPR which are of interest for dosimetry of accidental irradiation. For the first time, RLL and EPR have been used to measure the dose of accidental irradiation of accelerator personnel.

Radiolyoluminescence. To observe the RLL, we used a detector with an FÉU-29 photomultiplier whose current pulse was recorded by an NTA-512 multichannel analyzer. The samples were dissolved in a glass cell placed above the photocathode of the photomultiplier. Sodium sulfide was the solvent used for hair and sulfuric acid was used for fabrics. The samples were irradiated in an apparatus with a ^{60}Co source.

Before being placed in the cell, the hair was ground in a porcelain mortar for several minutes. After such preparation, the sample, weighing up to several milligrams, dissolves quickly in an aqueous solution of sodium sulfide. The RLL pulses from the hair are fairly short, and, 30-40 sec after the onset of dissolution, the intensity of the luminescence decreases tens of times [1]. When the samples weigh no more than 15 mg, the intensity of the RLL of hair is proportional to their mass.

The dependence of the intensity of RLL from hair on the γ-ray dose (Fig. 1) is linear right up to 25 krd (1 rd = 0.01 Gy). The background luminescence during dissolution of unirradiated hair is determined to a considerable degree by the hair pigment (melanin); light is emitted when melanin reacts with the solvent. In particular, black hair, which contains more pigment, has a higher background luminescence.

The intensity of the RLL and the background luminescence depend on the technology used to prepare the hair samples and on the dissolution conditions (Fig. 2). Although the intensity of the luminescence increases in both cases, in the case of background luminescence a tendency toward saturation at a grinding time of 10-15 min is observed. This may be due to the fact that the main contribution to the background luminescence is made by the outer part of the hair, which contains the pigment, while in the case of RLL the inner part makes the main contribution. With prolonged grinding the solvent gets improved access to the inner part of the hair, and this increases the ratio of the RLL to the background luminescence by a factor of 2.5. The intensity of the RLL from hair also increases when the concentration of the solvent is increased and its temperature is raised (the intensity at 50°C is double that at room temperature). The maximum RLL yield is observed for a saturated solution of sodium sulfide, which was used to determine the characteristics of the RLL of hair.

In the first several hours, and even minutes after irradiation, the intensity of RLL of hair decreases severalfold (Fig. 3). The decrease slows down in 10-20 h, and then in 1-4 days the RLL intensity falls by half. It was found that the RLL has long-lived components which result in RLL from hair being observed even 1.5-2 yr after irradiation.

The most intensive RLL from cotton fabric is observed when the fabric is dissolved in sulfuric acid (Fig. 4). The shape of the RLL pulse displays a fast component due to short-lived free radicals or radicals with a high mobility in the solvent, or due to the background chemiluminescence, and also displays a slow component due to comparatively long-lived

Translated from Atomnaya Énergiya, Vol. 53, No. 2, pp. 91-95, August, 1982. Original article submitted June 17, 1981; revision submitted December 21, 1981.

0038-531X/82/5302- 0546$07.50

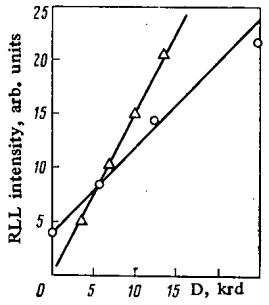

Fig. 1. Intensity of the RLL of hair (○) and cotton fabric (Δ) as a function of the radiation dose.

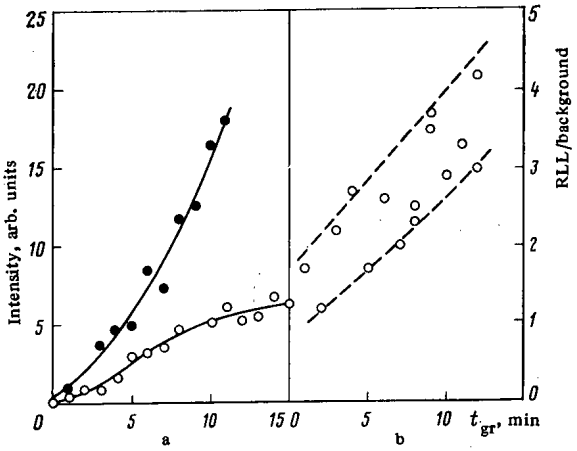

Fig. 2. Intensity of luminescence (a) of irradiated (●) and unirradiated (○) hair and ratio of RLL to background luminescence (b) as a function of the grinding time of sample.

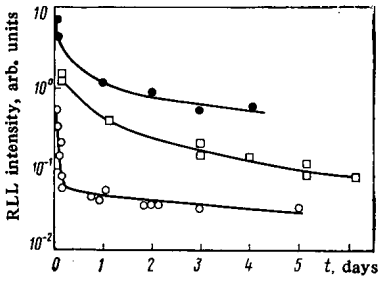

Fig. 3

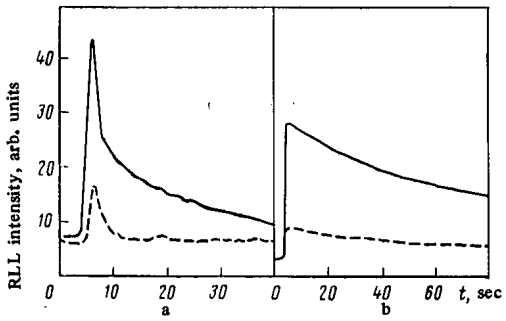

Fig. 4

Fig. 3. Decrease in the intensity of RLL of hair (●), cotton fabric (○), and synthetic fabric (□) as a function of the time after irradiation.

Fig. 4. Shape of RLL pulse at irradiation dose of 10 krd from cotton fabric (a) and synthetic fabric (b) (solid lines) and background luminescence of unirradiated fabric (dashed lines).

or low-mobility radicals. In the signal from unirradiated fabric, because of the absence of slow chemical reactions, the slow component is rather indistinct against the background of the photomultiplier dark current. In this way cotton fabric differs from hair, in which background luminescence of a nonradiative character is stronger.

The dependence of the intensity of RLL from cotton fabric on the mass of the sample and the radiation dose is linear for masses of 5-50 mg and doses of up to 15 krd (see Fig. 1). Increasing the mass (>50 mg) makes the sample poorly transparent to the luminescence emitted. If the sample is prepared in the form of finely chopped threads, the intensity of the luminescence increases by a factor of 1.7-2 in comparison with the unchopped sample since the conditions for dissolution improve and absorption of light in the sample diminishes.

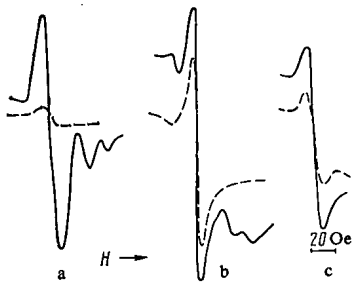

Fig. 5. Shape of EPR signals from cotton (a), woolen (b), and synthetic (crimplene) (c), fabrics irradiated with a dose of 12.5 krd (solid line) and unirradiated (dashed line).

In the first 3-4 h, the intensity of RLL from cotton fabric falls off 10-20-fold (see Fig. 3). Further change with time is slight (by roughly 1.5 times in 2 weeks). At the same time, the existence of a long-lived component enables the dose to be measured even after a long time has elapsed.

The RLL intensity depends in great measure on the conditions under which the cotton fabric is dissolved in sulfuric acid, in particular, on the temperature of the solution and the concentration of the acid. The optimal values are a 60-65% concentration of sulfuric acid and a solution temperature of 65-75°C. Under these conditions we studied the RLL of synthetic fabrics based on elastique, caprone, and Dederon, which are used in everyday clothing. The dependence of RLL on the mass of the sample and the radiation dose is linear, just as for cotton fabric. Synthetic fabric dissolves more slowly in acid and, consequently, the fast component in the RLL pulse of this fabric is indistinct (see Fig. 4). As in the case of cotton fabric, the intensity of RLL from synthetic fabric decreases substantially in the first several hours after irradiation (see Fig. 3) and in 1-6 days it falls off roughly five-fold.

Electron Paramagnetic Resonance. An RE-1306 radiospectrometer was used to detect free radicals in fabrics. The samples were irradiated in an apparatus with a ^{60}Co source. The samples to be measured were prepared in the form of finely chopped threads which were introduced into a molybdenum glass tube with an inner diameter of about 3 mm. The tube containing the sample was placed in the sensitive volume of the radiospectrometer used to measure the EPR spectra (Fig. 5). The spectra were measured 1 day after irradiation at a magnetic field strength of 3200 Oe and a scanning length of 200 Oe (1 Oe = 79.5775 A/m). The signal due to free radicals of a radiative origin is probably caused by radicals of various types and its width is several tens of oersteds. Unirradiated cotton fabric does not give such a signal, but there is slight resonance absorption in near fields, and it must be taken into account when measuring the dose.

After irradiation, woolen fabric – like cotton fabric – gives a signal with a different shape, which indicates the formation of a different type of radical. Unlike cotton, wool gives an intense EPR background signal, which is similar in shape to the signal from the unirradiated fabric as well as to the previously observed EPR signal from hair samples [3]. The existence of this background signal limits the possibility of measuring a comparatively low dose of radiation from samples of woolen clothing. Accordingly, the dose sensitivity of woolen fabric is several times poorer than that of cotton.

Synthetic fabric is not always characterized by a narrow resonance and at times there is only a wide region of paramagnetic absorption. If such a resonance is observed after irradiation, a substantial background signal occurs in the same range of magnetic field strength, even though it is a smaller signal than in woolen fabrics.

In the hours immediately after irradiation, the most short-lived radicals disappear and this causes a change in the shape of the EPR spectrum [3]. Radicals with roughly identical lifetimes remain, and only the signal amplitude decreases while the shape of the spectrum does not change. In the case of cotton fabrics the intensity decreases by roughly one order of magnitude in the first 4-5 h and 1.8 times in the next 10 days (Fig. 6). The intensity of the EPR signal from woolen fabric decreases 1.5-2 times more rapidly than from cotton in the first 10 days after irradiation. In the case of synthetic fabric, the intensity decreases even more rapidly (14 times in 6 days).

Comparing the time characteristics of EPR and RLL (see Figs. 3 and 6), we find that they are very similar for the same type of fabric. This confirms the assumption in [1] that RLL and EPR are caused by free radicals which were formed under irradiation and whose lifetime determines the drop in intensity with time elapsed after irradiation.

The dose dependence of EPR is linear in the range of interest in accident situations (Fig. 7). The signal amplitude also depends on the type of radiospectrometer, the power of its klystron and the level of intrinsic noise, the mass of the sample, and the technique used to prepare the sample prior to the measurements. In particular, the prior pressing of fabrics into pellets, other conditions remaining the same, increases the EPR signal amplitude 15-20 times (see Fig. 7).

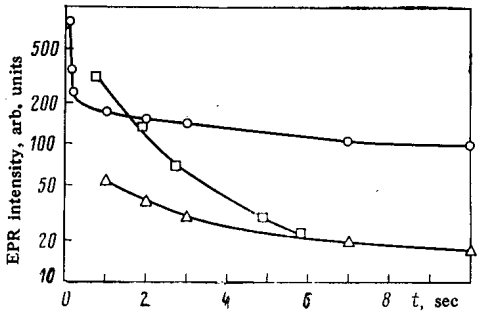

Fig. 6. Intensity of EPR of cotton (○), woolen (Δ), and synthetic (□), fabrics as a function of time after irradiation.

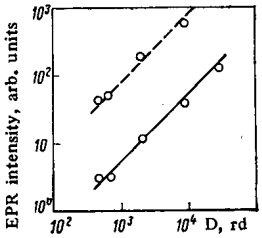

Fig. 7. Intensity of EPR of cotton fabric as function of irradiation for dense packing of sample (solid line) and after pressing into a pellet (dashed line).

Free radicals, at least those which are comparatively long-lived, are fairly stable under external influences (increased humidity and temperature). In particular, only a slight decrease in signal amplitude is noticeable after the fabrics are washed in hot water. This is equally true of the RLL of the fabrics. As in the case of RLL, the possibility of isolating the EPR signal of a radiative nature against the background of the signal from unirradiated fabric depends on its color. As a rule, the color of the fabric results in an increase in the background signal and a reduction of the ratio of the intensity of the EPR of free radicals to the background. For example, this ratio is reduced 2-3 times when cotton fabric is colored blue.

Dosimetry of Accidental Irradiation in Accelerators. The methods described above were used to measure the dose of accidental irradiation of personnel in high-energy particle accelerators. In the first such case, worker C. of an enterprise, contravening the technical safety regulations, entered the experimental room of a U-250 proton accelerator through an open door with the interlocking system switched off. In his left hand C. held a daylight lamp, which he was preparing to place between the poles of the deflecting magnet so as to determine the exit point of the proton beam from the light of the lamp. While he was setting up the lamp he saw that it lit up, and he realized that the accelerator was turned on. As a result, he had been exposed to a 40-MeV proton beam. It turned out that his left forearm and hand, as well as his right hand, with which he had held the other end of the lamp, had been exposed. Unfortunately, the victim did not have any personal dosimeters. There was no reliable information about the beam current, the duration of the irradiation, and the exact position of the irradiated parts of the body relative to the proton beam. From the distinct nature of the primary reaction of the skin, the estimated level of irradiation was several kilorads while the depth of tissue damage could reach the range of 40-MeV protons, which is roughly 1.5 cm.

To determine the proton dose on the surface of the forearm, we used the EPR of samples from the smock which the victim had worn. On the left sleeve of the smock we found the spot which had covered the part of the skin with the highest degree of radiation burn. Then we took samples of the fabric from the perimeter of this spot and measured the intensity of the EPR signal from each sample; the maximum signal was attributed to the maximum proton dose.

To determine the absolute dose, samples of fabric taken from parts of the smock which had certainly been outside the proton beam were bombarded with protons in a known dose in the same accelerator. On the basis of these data we determined the proton dose sensitivity of the smock fabric and a correction for the time decrease of the readings. Estimation from the intensity of the EPR gave a value of 1.0 ± 0.2 krd for the dose on the surface of the left forearm. Analysis of the irradiation conditions showed that such a surface dose corresponds to a proton dose of 3-4 krd at the Bragg maximum. Since the beam passed at a tangent to the forearm, this maximum was a depth of only 1-1.5 mm and resulted in intense radiation burn of the skin, with greater damage to the subcutaneous connective tissue. For this reason, the clinical picture of the burn corresponded to a dose of several kilorad, although the surface dose did not exceed 1 krd. The

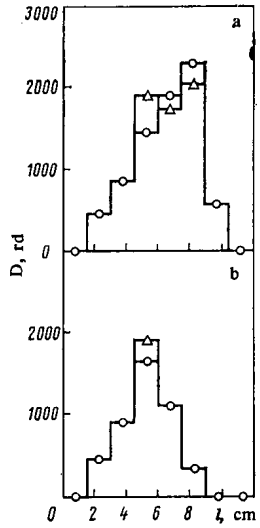

Fig. 8. Distribution of the electron dose over the radiation burn in the horizontal (a) and vertical (b) directions through the center of the burn: ○) EPR; Δ) RLL.

dosimetric data obtained proved to be useful in treating the victim.

Another case of accidental irradiation occurred in an LUE-15 electron linac in which work was done with a 12.7-MeV electron beam. When the irradiation was completed, a timer cut off the voltage to the controlling electrode of the electron gun of the linac. A worker P. entered the experimental room of the accelerator and stood with her back to the exit window of the accelerator. She then turned 180° so that she had her chest in front of the accelerator window. Since the high voltage to the accelerating tube was still turned on, a dark current of accelerated electrons was passing through the accelerator. For this reason, P. turned out to have been irradiated twice: first on the back slightly to the left of the spinal column and then on the chest. According to estimates made at the site of the accidental irradiation and on the basis of the primary reaction of the skin, the electron dose on the back was 4-6 krd, and that on the chest was about 2 krd with a low degree of reliability.

To determine the electron dose, we measured the RLL and EPR of samples of the synthetic fabric of the jacket the victim had been wearing. Samples of the fabric were taken from the areas of the jacket opposite the places on the chest and back where the skin had reddened. Samples of fabric from parts of the jacket which had certainly been outside the electron beam were irradiated with a known dose of electrons in order to obtain the dependence of the RLL and EPR intensity on the irradiation dose. To eliminate the need to introduce corrections for the time decrease of the readings, in calibrating we determined the intensity with the same lapse of time as in measuring irradiation suffered by the victim. In this way we obtained the absolute values of the dose.

Figure 8 gives the distribution of the dose over the radiation burn in different directions. It is seen that in the horizontal direction the dose distribution is asymmetric, which indicates that the victim had moved during the irradiation. The maximum value of the dose in this case is about 2 krd. The maximum dose on the chest is 0.8 krd. The measured values of the dose turned out to be substantially smaller than those obtained on the basis of the pattern of the accidental irradiation; the clinical character of the development of the radiation burn confirmed that they were correct.

On studying the whole of the dosimetric characteristics of RLL and EPR of samples of human tissue, clothing, etc., and the application of these methods to the accidental irradiation of accelerator personnel, we must emphasize that because of them it has become possible for the first time to measure the dose and its distribution over the body in the absence of safety dosimeters or in the case of inadequate dosimetric monitoring. Radiolyluminescence and electron paramagnetic resonance provided reliable dosimetric information which played a major role in selecting the tactics for treating the victims. Further development of these methods will permit successful solution of a wide range of problems in dosimetry of accidental irradiation.

LITERATURE CITED

1. I. A. Alekhin et al., At. Energ., 45, No. 2, 347 (1978).
2. T. Nakajima and S. Watanabe, Nucl. Sci. Technol., 11, 575 (1974).
3. S. N. Kraitor, Dosimetry in Radiation Accidents [in Russian], Atomizdat, Moscow (1979).

METHOD FOR AUTOMATIC MONITORING OF IODINE RADIOACTIVITY IN THE WATER COOLANT OF AN ATOMIC POWER PLANT

L. N. Moskvin, V. W. Miroshnikov, V. A. Mel'nikov,
I. S. Orlenkov, and V. V. Chetverikov

UDC 543.53

The use of a rapid chromatographic method for separating the reference radionuclides from water media on block selective sorbents greatly simplifies radiochemical monitoring of the coolant in an atomic power plant [1]. The maximum use of the capabilities of instrumental analysis on which the method is based, as well as the simplification and great decrease in the number of chemical operations, permits creating comparatively easily automated radiochemical monitoring systems, which is the purpose of the present work. We specifically studied the possibility of automating the monitoring of iodine radionuclides in the water coolant, which are reference nuclides for evaluating the hermetic seal of fuel-element jackets from radiochemical data [2].

The scheme for the automated setup (Fig. 1) is based on combining the selective separation of the radioelement being monitored from a complex mixture on a porous sorbent block with the recording of the level of γ radiation from the sorbent. Structurally, this is achieved by combining the sorbent element and the detector in a single unit, namely, the sample analysis block. The other functional elements of the setup are: specimen selecting line; block, based on a peristaltic pump which is coupled with a time delay of for measuring the radiation dose from the specimen; and a line for transmitting spectrometric information. The cycle of operations includes selecting the sample specimen, dosing it, selective separation of radioiodide, and detection of γ radiation. Two variants for operation of the setup are possible: discrete and continuous. In the first case, the increment to the radioactivity of the sorbent after passage of a fixed volume of coolant is recorded. In continuous monitoring, the coolant passes through the setup at a constant flow rate, and an equilibrium level of radioactivity of the nuclide is attained on the sorbent according to the content of the radionuclide in the coolant, the half-life, and the flow rate of the coolant through the sorbent:

$$A_e = \frac{GA_{sp}}{\lambda}(1-e^{-\lambda t}), \quad (1)$$

where A_e is the equilibrium activity of the radionuclide on the sorbent, Bq; A_{sp}, specific radioactivity of the coolant according to the given nuclide, Bq/liter; G, flow rate of the coolant through the sorbent, liters/sec; t, time from the beginning of operation of the setup, sec; λ, half-life of the radio nuclide, sec^{-1}.

Under equilibrium conditions ($e^{-\lambda t} \ll 1$)

$$A_e = GA_{sp}/\lambda. \quad (2)$$

The deviation of the level of radioactivity being monitored corresponds to any processes occurring in the first loop that change the fission-product content of the coolant.

The advantage of this scheme for automated monitoring lies in the use of accessible and simple-to-use standard scintillation detectors for γ radiation, but due to their low (compared to semiconducting detectors) resolution, the sorbents in the system must have a very high selectivity for the radionuclides being monitored. Another important condition for the applicability of the sorbents is their chemical stability (stability of their properties during prolonged use of the setups in the sample collecting lines). In this case, traditional materials such as ion-exchange resins or extracting agents fixed on porous carriers are not suitable. Starting from the assumption that metals whose iodides have low solubility are selective to iodide sorbents, we chose to study the absorption properties of bismuth, copper, and silver.

It was established with experiments under static conditions, using finely dispersed powders of these metals obtained by reducing them from solutions of the corresponding salts, that the equilibrium coefficients of distribution of ^{131}I with pH = 6-8 attained high values ($\geqslant 5 \cdot 10^3$). For the process of sorption on metals under dynamic conditions, we deposited metal layers on an extended surface of porous polytetrafluoroethylene by impregnating it with salt solutions in a vacuum, followed by working with a reducing agent (hydrazine hydrate). The dimensions of block sorbents conformed with the dimensions of sorbents used in rapid chromatographic analysis (d = 25 mm, h = 20 mm) [1]. The total porosity of the sorbents was 50-60% and the average pore radius was 50 μm.

Translated from Atomnaya Énergiya, Vol. 53, No. 2, pp. 101-102, August, 1982. Original article submitted January 16, 1981; revision submitted December 7, 1981.

0038-531X/82/5302-0551$07.50

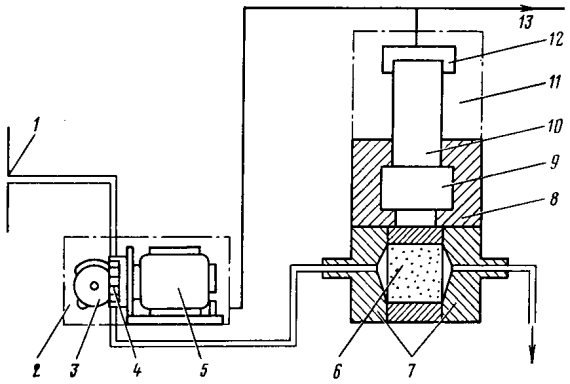

Fig. 1. Setup for radiochemical monitoring of the radioactivity of iodine in a water coolant: 1) sample collecting line; 2) block for dosing the specimen; 3) doser cylinders; 4) pushers; 5) SD-54 electrical motor; 6) block sorbent in mandrel; 7) pressing inserts; 8) lead screen; 9) NaI(Tl) crystal; 10) FEU; 11) radiochemical analysis block; 12) emitter repeater; 13) line for transmitting γ spectrometric information.

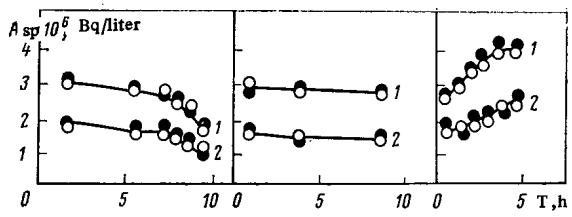

Fig. 2. Change in the specific radioactivity of ^{135}I (1) and ^{133}I (2) in the coolant (interval between each cycle is 5 days): ●, ○) are data obtained with the help of the setup (copper was used as the sorbent) and a semiconducting spectrometer, respectively.

We checked the characteristics of the sorbents under laboratory conditions on model solutions of ^{131}I, simulating the uncorrected water regime. In order to estimate the stability of the sorption setups under conditions of prolonged operation, we passed desalinated water with known content of ^{131}I through columns containing the block sorbents and monitored the radioactivity of the filtrate. We passed 250 liters of solution ($2.5 \cdot 10^4$ sorbent volumes) with a flow rate of 0.3 liters/min, created by constant excess pressure of 1.5 MPa, through each sorbent. During the entire experiment, the completeness of extraction of radioiodide on silver remained constant ($\geqslant$99%), on copper at the end of the experiment it decreased to 92%, and on bismuth to 79% due to partial oxidation of the metal surface. In subsequent work, we used sorbents based on copper and silver.

We checked the efficiency of the setup on model solutions of ^{131}I, simulating an uncorrected water regime. We estimated the reproducibility of the results obtained with the operation of the setup using data on measurements of radioactivity of the sorbent after passing specimens with a volume of 0.1 liters and a flow rate of 0.02 liters/min through the radiochemical analysis block. The coefficients of variation, found from five parallel experiments, for the specific radioactivities of $4 \cdot 10^1$, $4 \cdot 10^4$, $4 \cdot 10^6$ Bq/liter were 23, 4, and 2%, respectively.

We tested the setup under real conditions using the sample collecting lines of the main technological loop of the atomic power plant with a boiling coolant. In order to avoid contamination of the sorption element by suspended radioactive impurities originating with corrosion, we placed a mechanical filter tablet made of porous polytetrafluoroethylene with pore sizes of $\sim$1 μm in front of the doser. The radioactivity of the iodine nuclides and fission products of the coolant and impurities (^{18}F, ^{24}Na, ^{56}Mn, ^{99}Mo and others) amounted to 10^6 Bq/liter. We performed the tests in the discrete mode with fixed periodicity. We recorded the γ emission from the sorbent before and after filtration of 0.1 liters of the coolant specimen with a flow rate of 0.02 liters/min. In order to obtain spectrometric information, we used an AI-256-6 pulse-height analyzer. We determined the area of the photopeaks of the separated iodine radionuclides by subtracting out the area of the photopeaks before and after alternate separation. We monitored the reliability of the results obtained by direct γ-spectrometric measurement of simultaneously collected specimens of coolant using a Ge(Li) detector (Fig. 2). The satisfactory agreement between the results of the measurements indicates the absence of noticeable accumulation of impurity radionuclides on the sorbent, which affect the accuracy of the determination of radioiodine.

LITERATURE CITED

1. L. N. Moskvin, V. S. Miroshnikov, and V. A. Mel'nikov, Radiokhimiya, 21, No. 2, 311 (1979).
2. A. A. Chubakov et al., Preprint IAE-1034, Moscow (1966).

γ-RADIATION ALBEDO OF HYDROGEN-CONTAINING PLANE LAYERS

V. I. Kulikov and K. K. Popkov

UDC 621.039.51.17

The differential characteristics of the γ-radiation albedo of flat plates of various thicknesses made out of polyethylene, paraffin, Plexiglass, and layers of water are calculated with the help of the Monte Carlo method implemented in a previously published program [1]. The statistical error of the calculations was 5-10% for the angular characteristics of the albedo and 5-30% for the spectroangular characteristics. Analysis of the results obtained shows that the spectral, number, energy, and dosage albedos a can be calculated with the help of the empirical formula

$$a(d) = a_1(d) + a_2(d), \tag{1}$$

where d is the thickness of the scattering plate; and a_1 and a_2, contributions of single and multiple scattering, respectively. Expressions which permit calculating a_1(d) have been given previously [1], and the component a_2(d) can be determined from the formula

$$a_2(d) = [a(\infty) - a_1(\infty)]\left[1 - \exp\left(b\frac{\mu d^c}{\cos\theta_0 \cos\theta}\right)\right], \tag{2}$$

where θ_0 and θ are the angles of incidence and reflection; μ, linear attenuation coefficient of the γ radiation; and b, c empirical constants whose values are presented in Table 1.

TABLE 1. Empirical Constants b and c

Calculated albedo	b	c
Spectral	-0,0712	1,82
Number	-0,0712	1,82
Energy	-0,115	1,75
Dosage	-0,117	1,73

TABLE 2. Relative Deviations of the Differential Spectral (Numerator) and Differential Energy (Denominator) Albedos of Water Layers Calculated from Formulas (1)-(2) and by the Monte Carlo Method, % (E_0 in MeV)

θ_0	θ	$\mu d = 0.25$			$\mu d = 1.0$			$\mu d = 3.0$		
		$E_0 = 0.5$	$E_0 = 2.0$	$E_0 = 8.0$	$E_0 = 0.5$	$E_0 = 2.0$	$E_0 = 8.0$	$E_0 = 0.5$	$E_0 = 2.0$	$E_0 = 8.0$
0	0	84/12	62/17	56/35	35/4	34/9	12/8	2/-1	0*/0	0/0
	30	103/14	51/19	46/34	32/2	30/7	9/6	2/-1	0/0	0/0
	80	95/13	75/2	8/-2	28/-9	7/-2	3/-2	1/-1	1/0	0/0

Translated from Atomnaya Énergiya, Vol. 53, No. 2, pp. 102-103, August, 1982. Original article submitted April 8, 1981.

0038-531X/82/5302-0553$07.50

TABLE 2 (continued)

t_0	θ	$\mu d = 0,25$			$\mu d = 1,0$			$\mu d = 3,0$		
		$E_0 = 0,5$	$E_0 = 2,0$	$E_0 = 8,0$	$E_0 = 0,5$	$E_0 = 2,0$	$E_0 = 8,0$	$E_0 = 0,5$	$E_0 = 2,0$	$E_0 = 8,0$
80	0	78 / −3	35 / −3	8 / −3	16 / −9	5 / −3	1 / 0	1 / 0	0 / 0	0 / 0
	30	70 / 1	49 / 2	35 / −3	14 / −5	4 / −2	2 / 0	0 / 0	0 / 0	0 / 0
	80	31 / −3	14 / −1	10 / −2	6 / 0	2 / 0	0 / 0	0 / 0	0 / 0	0 / 0
	−30	71 / −6	42 / −9	5 / −5	18 / −9	4 / −4	3 / 0	0 / 0	0 / 0	0 / 0
	−80	72 / −15	19 / −11	11 / −8	23 / −2	6 / −1	1 / 0	0 / 0	0 / 0	0 / 0

*Deviation of the calculated results is less than 1%.

The error of the calculations according to formulas (1) and (2) basically decreases as the energy of the γ radiation increases and as d increases. The relative deviations of the results of the calculations based on formulas (1) and (2) from the results obtained by the Monte Carlo method are given in Table 2.

The order of magnitude and the variation trend of the errors for polyethylene, paraffin, and Plexiglass do not differ greatly from the order of magnitude and the variation trend of the errors for water.

Formulas (1) and (2) can be used for calculations of the albedo of materials with $Z < 10$.

LITERATURE CITED

1. V. I. Kulikov et al., At. Energ., 44, No. 1, 85 (1978).

QUASILINEAR APPROXIMATION IN THE STATISTICAL ANALYSIS OF THE SIMPLEST NONLINEAR DYNAMIC MODEL OF A POWER REACTOR

Yu. V. Volkov, A. G. Kostromin, and V. K. Nazarov

UDC 621.039

In the statistical analysis of dynamic properties, and also in estimating the thermotechnical reliability of power reactors (PR), it is necessary to know the probabilistic characteristics of their power. The basic such characteristics are the one- and two-dimensional laws of power and reactivity distribution, and also the first two moments of these distributions. The distribution laws play the dominant role, since they provide the basis for the construction of probability functions and the estimation of the probability of exceeding the specified PR power. The complexity of the algorithms for the statistical derivation and estimation of the thermotechnical reliability demands that the probabilistic characteristics of the PR power assumed be sufficiently simple (preferably, standard) and that the real physical process be correctly described.

It is known [1, 2] that the basic random perturbing factor influencing the PR power is the fluctuation in reactivity. This influence is analyzed within the framework of dynamic models of PR. In [1], an accurate and complete statistical analysis of the simplest nonlinear dynamic model (NDM) of a reactor operating in steady conditions was performed. Account was taken of the lagging-neutron effect in the effective lifetime and also of the power effect, and it was assumed that the reactivity is a "white noise" with a finite spectral density. However, for the fluctuations of the reactivity, white noise is not always a correct idealization, and the conditions of its applicability must be investigated. Usually, the estimates of the self-correlation functions (SCF) of the reactivity with respect to experimental data decrease monotonically with time, and the approximation of these estimates by an exponential function

$$R_\rho(t)=\sigma_\rho^2\exp(-\varkappa|t|), \tag{1}$$

where $\varkappa = 1/t_C$, t_C is the correlation interval of the reactivity, and σ_ρ is the norm of the reactivity fluctuations, is in sufficiently good agreement with experimental data. In [2], in a quasilinear approximation (logarithmic linearization), and in the Barrett approximation (small-parameter method), expressions were obtained for the moments of the power distribution in a point model of a PR, taking a single group of lagging neutrons into account, with an arbitrary form of the spectral density of reactivity. However, the power effect was not included in the model, and knowledge of only the moments of the PR power distribution is insufficient for the solution of the above-noted problems.

In the present work, a complete statistical analysis of the simplest NDM, analogous to that in [1], is conducted in the quasilinear approximation of [2] for exponentially correlated fluctuations of the reactivity.

Suppose that the PR dynamics in steady conditions are described, as in [1], by the simplest nonlinear model

$$l\frac{dn}{dt}=[k_0+\rho(t)-\gamma n]\,n, \tag{2}$$

where n is the reactor power; l, effective neutron lifetime, taking the lagging neutrons into account; $\gamma > 0$, reactivity power coefficient; $\rho(t)$, random perturbation of the reactivity; and $k_0 = \gamma\bar{n}$, total power effect with a steady reactor power $\bar{n}$. Suppose that the random process $\rho(t)$ has an SCF of the form in Eq. (1) and hence obeys the stochastic differential equation

$$\frac{d\rho}{dt}+\varkappa\rho=\sqrt{2\varkappa}\sigma_\rho\xi(t), \tag{3}$$

where $\xi(t)$ is Gaussian white noise, for which $\langle\xi(t)\rangle = 0$, $R_\xi(t) = \langle\xi(t_0)\xi(t_0+t)\rangle = \delta(t)$ (the angle brackets correspond to an averaging operator over all possible realizations of the corresponding random process). The system of Eqs. (2) and (3) describes the two-dimensional Markov process $\{n(t), \rho(t)\}$ [3], where $\langle n(t)\rangle = \bar{n}$. It is required to find $w_n(n, \rho, t\,|\,n_0, \rho_0)$, the transient density of the process $\{n(t), \rho(t)\}$, i.e., the probability density that the system will be in state ρ at time t under the condition that it is in the state n_0, ρ_0 initially. The transient density $w_n(n, \rho, t\,|\,n_0, \rho_0)$ completely describes the probabilistic properties of the process $\{n(t), \rho(t)\}$.

Translated from Atomnaya Énergiya, Vol. 53, No. 2, pp. 103-105, August, 1982. Original article submitted June 2, 1981; revision submitted March 10, 1982.

0038-531X/82/5302-0555$07.50

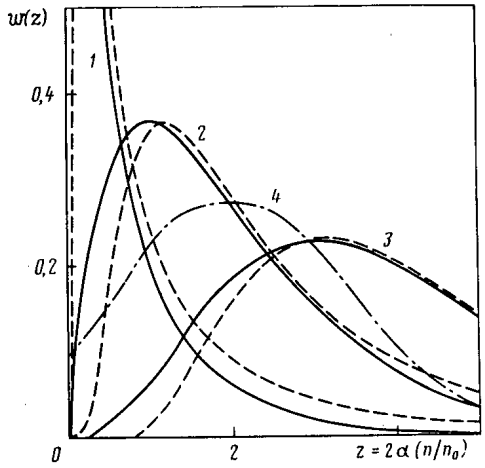

Fig. 1. Probability density of the reactor power distribution: continuous curves correspond to the accurate solution [1], dashed curves to the quasilinear approximation, and dash-dot curves to the linear approximation: 1) $\alpha = 0.25$; 2) $\alpha = 1$; 3) $\alpha = 2$; 4) Gaussian law ($\alpha = 1$) [1].

An accurate and sufficiently simple analytic solution of the Kolmogorov equation [3] written for the system in Eqs. (2) and (3) for the transient density $w_n(n, \rho, t \mid n_0, \rho_0)$ cannot be obtained. In these conditions, the quasilinear approximation of Eq. (2) may be used to estimate $w_n(n, \rho, t \mid n_0, \rho_0)$. The variable change

$$x(t) = \ln(n(t)/\bar{n}). \tag{4}$$

is introduced. Then, when $|x| \ll 1$, i.e., when the fluctuations of n(t) about $\bar{n}$ are sufficiently small, it follows from Eq. (2) that

$$\frac{dx}{dt} = -\frac{k_0}{l}x + \frac{1}{l}\rho(t), \tag{5}$$

where $\langle x(t) \rangle = 0$. Equation (5) is also a quasilinear approximation (logarithmic linearization) of the simplest NDM. The system in Eqs. (2) and (5) describes the two-dimensional Markov process $\{x(t), \rho(t)\}$. The transient densities $w_n(n, \rho, t \mid n_0, \rho_0)$ and $w_x(x, \rho, t \mid x_0, \rho_0)$ of the processes $\{n(t), \rho(t)\}$ and $\{x(t), \rho(t)\}$ are related as follows:

$$w_n(n, \rho, t \mid n_0, \rho_0) = \frac{1}{n} w_x\left[\ln\left(\frac{n}{\bar{n}}\right), \rho, t \mid \ln\left(\frac{n_0}{\bar{n}}\right), \rho_0\right], \tag{6}$$

and therefore it is not difficult to pass from the probabilistic characteristics of the process $\{x(t), \rho(t)\}$ to the characteristics $\{n(t), \rho(t)\}$.

Since the system in Eqs. (2) and (5) is linear and $\xi(t)$ is Gaussian white noise, it is not necessary [3] to solve the Kolmogorov equation for the transient density $w_x(x, \rho, t \mid x_0, \rho_0)$ in the given case, and the following expression may be written directly:

$$w_x(x, \rho, \tau \mid x_0, \rho_0) = \frac{1}{2\pi\sqrt{\Delta(\tau)}} \exp\left\{-\frac{1}{2\Delta(\tau)}\left(\sigma_\rho^2 r_{\rho\rho}(\tau)[x-\bar{x}(\tau)]^2 - 2\sigma_x\sigma_\rho r_{x\rho}(\tau)[x-\bar{x}(\tau)][\rho-\bar{\rho}(\tau)] + \sigma_x^2 r_{xx}(\tau)[\rho-\bar{\rho}(\tau)]^2\right)\right\}, \tag{7}$$

where σ_x is the norm of fluctuations of the process $x(t)$; $\tau = \varkappa t$; and

$$\bar{x}(\tau) = \langle x(\tau) \mid x_0 \rangle = x_0 e^{-\lambda\tau} + \rho_0 \frac{e^{-\tau} - e^{-\lambda\tau}}{l_1(\lambda - 1)}; \tag{8}$$

$$\bar{\rho}(\tau) = \langle \rho(\tau) \mid \rho_0 \rangle = \rho_0 e^{-\tau} \tag{9}$$

are conditional (with respect to x_0, ρ_0) mean values of the processes x(t) and $\rho(t)$; also

$$r_{xx}(\tau) = \frac{1}{\sigma_x^2}\langle [x(\tau)-\bar{x}(\tau)]^2 \rangle = 1 - \frac{1}{(\lambda-1)^2}[4\lambda e^{-(\lambda+1)\tau} - \lambda(\lambda+1)e^{-2\tau} - (\lambda+1)e^{-2\lambda\tau}]; \tag{10}$$

$$r_{x\rho}(\tau) = \frac{1}{\sigma_x\sigma_\rho}\langle [x(\tau)-\bar{x}(\tau)][\rho(\tau)-\bar{\rho}(\tau)] \rangle = \sqrt{\lambda(\lambda+1)}\left[\frac{1}{\lambda+1} - \frac{1}{\lambda-1}e^{-2\tau} + \frac{2}{\lambda^2-1}e^{-(\lambda+1)\tau}\right]; \tag{11}$$

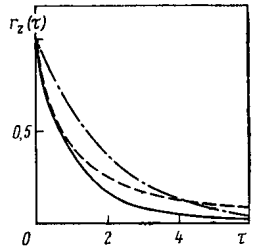

Fig. 2. Comparison of normalized SCF of the reactor power (white noise reactivity): Continuous curve corresponds to the quasi-linear approximation, dashed curve to the accurate solution [1], and dash-dot curve to the linear approximation [1].

$$r_{\rho\rho}(\tau)=\frac{1}{\sigma_\rho^2}\langle[\rho(\tau)-\bar{\rho}(\tau)]^2\rangle=1-e^{-2\tau} \tag{12}$$

are the normalized correlational moments of the processes x(t) and ρ(t); $r_{x\rho}(\tau) = r_{\rho x}(\tau)$; and

$$\Delta(\tau)=\begin{vmatrix}\sigma_x^2 r_{xx}(\tau) & \sigma_x\sigma_\rho r_{x\rho}(\tau)\\ \sigma_x\sigma_\rho r_{x\rho}(\tau) & \sigma_\rho^2 r_{\rho\rho}(\tau)\end{vmatrix}. \tag{13}$$

In Eqs. (8)-(12), $l_1 = \varkappa l$, $\lambda = k_0/l_1$.

When $\tau \to \infty$, Eq. (7) yields, with the appropriate integration, the one-dimensional steady Gaussian distributions of the processes x(t) and ρ(t):

$$w(x)=\frac{1}{\sqrt{2\pi}\sigma_x}\exp\left(-\frac{x^2}{2\sigma_x^2}\right), \tag{14}$$

$$w(\rho)=\frac{1}{\sqrt{2\pi}\sigma_\rho}\exp\left(-\frac{\rho^2}{2\sigma_\rho^2}\right). \tag{15}$$

Thus, in the quasilinear approximation of the NDM, the PR power has a logarithmically normal one-dimensional distribution law.

It may also readily be shown that the normalized SCF of the process takes the form

$$r_x(\tau)=\frac{1}{\lambda-1}(\lambda e^{-|\tau|}-e^{-\lambda|\tau|}) \tag{16}$$

and is related to the normalized SCF of the process z(t) = n(t)/$\bar{n}$ as follows:

$$r_z(\tau)=\left\{\exp\left[\frac{r_x(\tau)}{2\alpha}\right]-1\right\}\Big/\left[\exp\left(\frac{1}{2\alpha}\right)-1\right], \tag{17}$$

where

$$\alpha=\frac{1}{2\sigma_x^2}=\frac{k_0(k_0+l_1)}{2\sigma_\rho^2}. \tag{18}$$

For the ratio of the norm of fluctuations of the power logarithm to the norm of fluctuations of the reactivity, the following formula holds:

$$C=\frac{\sigma_x}{\sigma_\rho}=\frac{1}{\sqrt{k_0(k_0+l_1)}}, \tag{19}$$

by means of which the sensitivity of the fluctuations in PR power may be estimated.

It is of interest to compare the results obtained under the assumption that ρ(t) is white noise ($\varkappa \to \infty$) with the accurate solutions obtained in [1] and also with the solutions derived from the linear model (complete linearization of the problem). The results of calculating the one-dimensional density of the distributions w(z) and $r_z(\tau)$ from the accurate, quasi-linear, and linear models are shown in Figs. 1 and 2. It is evident that the numerical values of w(z) from the accurate and quasilinear models are not too different at all α, and are considerably different from the Gaussian law obtained from the linear model at small α. In addition, in contrast to the linear model, the quasilinear approximation, like the accurate model, gives a physically realizable solution: w(z) = 0 when $z \leqslant 0$. Comparison of the normalized SCF obtained by the three

models shows that at small τ the quasilinear approximation gives solutions that are practically no different from the accurate solutions and, at large τ, solutions no worse than those obtained by the linear model.

From the relations obtained, it is not difficult to determine the conditions of applicability of the white-noise approximation for the reactivity and the linear approximation in the statistical analysis of NDM: when $\varkappa l = l/t_c \gg k_0$ ($\lambda \gg 1$), the white-noise model is applicable for the reactivity; when $\varkappa l = l/t_c \gg 9\sigma_\rho^2/2k_0$, the linear approximation is applicable. In addition, these relations lead to a conclusion with a sufficiently clear physical meaning: First, with increase in $\varkappa$ and/or k_0, the density w(x) tends to a delta function, i.e., the fluctuations in the PR power must be practically absent; second, with decrease in $\varkappa$, the PR power becomes almost completely correlated with the reactivity, and a good approximation for the PR NDM is

$$k_0 + \rho(t) - \gamma n(t) = 0. \tag{20}$$

As a result of the statistical analysis of the simplest NDM of a power reactor with exponentially correlated fluctuations of the reactivity, a sufficiently simple approximate expression is obtained for the transient density of the two-dimensional Markov process, which is represented by fluctuations of the PR power and reactivity. It is shown that a logarithmically normal one-dimensional distribution law of the PR power is a sufficiently good approximation of the real distribution law, and the quasilinear approximation of the NDM is sufficiently accurate. The conditions of applicability of the linear dynamic model and the white-noise approximation for the reactivity are obtained, taking the power effect into account. It should be noted that the given approach is completely applicable to the statistical analysis of the NDM of a power reactor with piecewise-rational spectral density of the reactivity fluctuations of general form.

LITERATURE CITED

1. W. Dutre et al., Nucl. Sci. Eng., 62, No. 3, 355 (1977).
2. E. Quabili and M. Karasulu, Ann. Nucl. Energy., 6, No. 3, 133 (1979).
3. A. A. Sveshnikov, Applied Methods of Random Functions [in Russian], Nauka, Moscow (1968).

SPUTTERING OF THE SURFACE OF GOLD BY FISSION FRAGMENTS

V. V. Obnorskii, I. A. Baranov, N. V. Badadzhanyants, and B. G. Yarullov

UDC 537.226.539.173

Both bulk samples (foil 20 μm thick) and thin, finely granular layers deposited by thermal sputtering in a vacuum on substrates made out of a dielectric (glass) and a metal (platinum) have been used in connection with the determination of the sputtering coefficients K of gold by fission fragments from an external source [1]. The value of K of finely granular layers of gold is $\sim 10^3$ atoms/fragment. Larger values of K have been observed previously [2, 3] in the case of finely granular layers made out of nonconducting materials. Such anomalously large sputtering coefficients can be explained, e.g., within the framework of the isolated-grain model [4-6]. The value of K obtained for bulk gold was 26 atoms/fragment [1], which is significantly less than that found for finely granular layers, but higher than the value calculated from Sigmund's model (3 atoms/fragment) [4]. In order to clarify the sputtering mechanism of bulk gold by heavy, multiply-charged ions of the fission-fragment type, the dependence of K on the variation of the mean fragment energy has been investigated.

The samples were sputtered in a vacuum chamber using a mechanism [3] for the replacement of the collectors and retarding films without disrupting the high vacuum, which was 5×10^{-5} Pa. The sputtered gold was foil 20 μm thick. Prior to the irradiation, the foil surface was degreased and etched by means of successive scrubbing in CCl_4, nitric acid, and ethanol, with alternate rinsing in distilled water. The state of the surface was controlled in a UÉMB-100K electron microscope (Fig. 1). A thin layer of ^{252}Cf with an intensity of 7×10^6 fragments/sec into 4π sr served as the source of fission fragments. Collimators ($\sim 16°$) were used for more accurate definition of both the stream of fission fragments itself and of the fragments' energy spectra. The energy spectrum of the fission fragments of the calibrated source, as well as the spectra of "nonretarded" and "retarded" fragments from a working ^{252}Cf source, are presented in Fig. 2. It is evident that in the nonretarded source (see Fig. 2b) the main part of the fragments had an energy of 37-80 MeV, and in the retarded source (see Fig. 2c), 10-30 MeV. The amount of sputtered gold collected on the thin nickel collectors was determined by the method of thermal neutron activation in the JINR reactor of the USSR Academy of Sciences. The gamma spectra were determined with the help of a spectrometer with a Ge (Li)-detector.

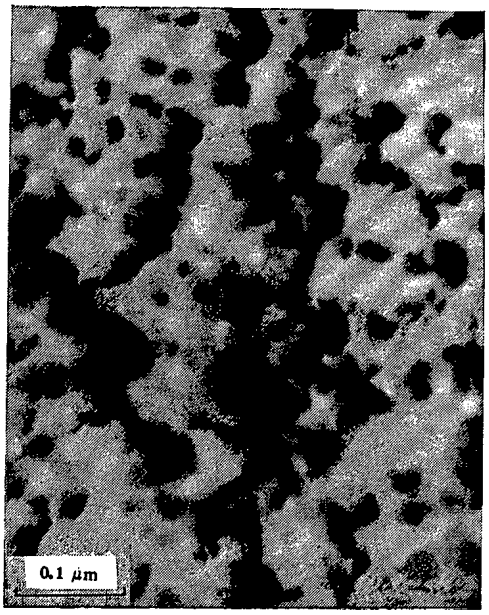

Fig. 1. Electron micrograph of the surface of the bulk sample of gold (carbon replica shadowed by platinum).

Translated from Atomnaya Énergiya, Vol. 53, No. 2, pp. 105-106, August, 1982. Original article submitted June 22, 1981.

0038-531X/82/5302- 0559$07.50

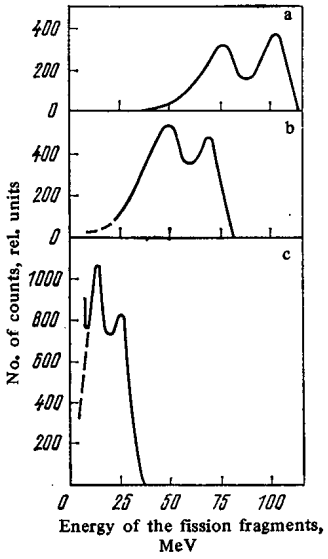

Fig. 2. Energy spectra of the fission fragments of a ^{252}Cf calibrated source (a) and the working sources [the fission fragments passed only through (b) a protective nickel film and (c) through protective and retarding nickel films]. For an energy <10 MeV, the spectrum of the α-particles is superimposed on the energy spectrum of the fission fragments.

The processing of the results (with an error of $\pm 20\%$) carried out by the known procedure [1] showed that in the case of sputtering of bulk gold by fission fragments whose spectrum is presented in Fig. 2b, K = 55 atoms/fragment. When the same sample was sputtered by fission fragments whose spectrum is presented in Fig. 2c, this coefficient is equal to 25 atoms/fragment. The sputtering coefficient of bulk gold by fission fragments whose spectrum is shifted appreciably into the low-energy region ($\lesssim$ 20 Mev) was measured as an estimate; it was $\sim$7 atoms/fragment. Thus, it is evident that in the case of irradiation of a bulk metal by fission fragments, the value of K is reduced in proportion to the decrease in the energy of the fragments. Consequently, nonelastic interactions of fission fragments with atoms of the material play the principal role in the sputtering of the surface of a metal. It is evident from the electron micrograph (see Fig. 1) that there are grains on the surface of bulk gold with a size mainly $\gtrsim$300 Å (1 Å = 10^{-10} m). In this connection, one should note that the result obtained contradicts the conclusions of the isolated-grain model, according to which fission fragments can sputter layers with grains no more than 100 Å in size due to ionization energy losses [4]. Here one can suggest two explanations: in connection with the sputtering of bulk gold either a small fraction of the ionization energy losses of some fragments (in the region of the greatest specific losses [7]) participates in the sputtering of atoms from the surface, or a small difficult-to-control amount of fine gold grains is present on the surface of the samples used. Thus, e.g., in order to obtain a mean sputtering coefficient of $\sim$100 atoms/fragment (we have assumed for simplicity's sake that 99% of the surface is not sputtered), it is sufficient that 1% of the sample be covered by gold grains 70 Å in diameter, for which the sputtering coefficient is equal to $\sim 10^4$ atoms/fragment [8]. Experiments either with preliminary ion etching of bulk gold samples or performed under conditions of a variable dosage of fission fragments can introduce definite clarity.

In conclusion, the authors thank V. P. Eismont for the interest exhibited in the research as well as E. G. Lebedev, G. V. Solov'ev, and A. N. Smirnov for help in conducting the irradiation of the samples by fission fragments and in performing the activation analysis.

LITERATURE CITED

1. B. M. Aleksandrov et al., At. Energ., 41, No. 6, 417 (1976).
2. M. Rogers, J. Nucl. Mater., 16, No. 3, 298 (1965).
3. B. M. Aleksandrov et al., At. Energ., 38, No. 1, 47 (1975).
4. I. A. Baranov and V. V. Obnorskii, Preprint RI-120 (1980).
5. A. Goland and A. Paskin, J. Appl. Phys., 35, No. 7, 2188 (1964).
6. I. S. Bitenskii, At. Energ., 49, No. 4, 232 (1980).
7. N. Demidovich, J. Nakhutin, V. Shatunov, and M. Shapovalov, Nucl. Instrum. Methods, 171, 551 (1980).
8. M. Rogers, J. Nucl. Mater., 15, No. 1, 65 (1965).

BUILDUP OF ^{233}U WITH A SPECIFIED CONTENT OF ^{232}U BY THE IRRADIATION OF THORIUM IN A WATER-COOLED/WATER-MODERATED REACTOR (VVÉR)

A. A. Polyakov, V. P. Rukhlo, Yu. E. Titarenko, and S. F. Komin

UDC 621.039.51

When thorium is irradiated in reactors, it is necessary to reduce the buildup of ^{232}U with respect to ^{233}U [1, 2]. It is shown in [3], that a reduction of $N^{232}U/N^{233}U$ can be achieved by inserting certain inert diluents into the thorium rods. Based on an analysis of the nuclear-physics and technological properties, zirconium dioxide was chosen as such an inert diluent. A detailed investigation of the effect of a different concentration of ZrO_2 in ThO_2 rods on the formation of ^{233}U and the determination of the ratio of the concentrations $N^{232}U/N^{233}U$ was conducted on a subcritical uranium–water test-rig, for which the neutron source was the IRT reactor [4]. For this purpose, a slug of $ThO_2 + ZrO_2$ rods was installed at the center of the UO_2-H_2O lattice modulating the VVÉR core, with 6.5% enrichment with respect to ^{235}U. The buildup of ^{233}U in the thorium was simulated by the introduction into the thorium rods of another fissile isotope of ^{235}U of different concentration. Measurements were conducted by the activation method for rods of thorium and two compositions of $ThO_2 + ZrO_2$: ThO_2 + 20%-by-mass ZrO_2, and ThO_2 + 40%-by-mass ZrO_2, with different concentrations of ^{232}U (0, 1, 5, and 10 kg ^{235}U per ton ^{232}Th).

As the neutron flux in the subcritical assembly is inadequate for direct measurements of the rate of formation of ^{232}U in the irradiated samples, an indirect method was used. The reaction $^{232}Th(n, 2n)$ was simulated by another threshold

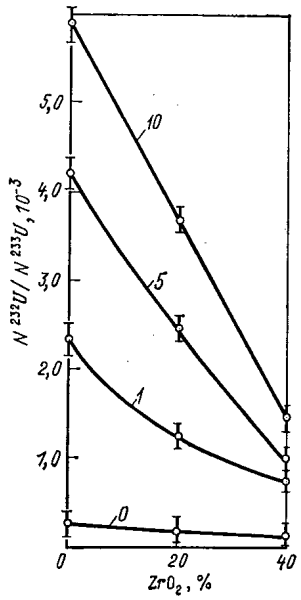

Fig. 1. Dependence of the relative buildup of $N^{232}U/N^{233}U$ on the concentration of ZrO_2 and ^{235}U in thorium, when irradiated in the fourth unit of the Novovoronezh nuclear power station, thermal-fissile assembly, of the $ThO_2 + ZrO_2$ rods during 1 yr (figures on the curves are the concentration of ^{235}U in ^{232}Th, kg ^{235}U/ton ^{232}Th).

Translated from Atomnaya Énergiya, Vol. 53, No. 2, pp. 106-107, August, 1982. Original article submitted July 14, 1981.

0038-531X/82/5302-0561$07.50

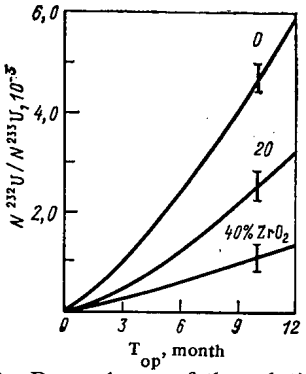

Fig. 2. Dependence of the relative buildup of $N^{232}U/N^{233}U$ on the duration of irradiation in the TFA of $ThO_2 + ZrO_2$ rods, taking account of the continuous buildup of ^{233}U in them.

reaction $^{27}Al(n, \alpha)$, the effective threshold of which is close to the effective threshold of the (n, 2n)-reaction on thorium, and the rate of the $^{231}Pa(n, \gamma)$-reaction was estimated from the measured cadmium-to-dysprosium ratio in R_{Cd}^{Dy}. The rate of formation of ^{233}U was determined by directly recording the γ-radiation of ^{233}Pa in the irradiated ThO_2 samples:

$$\frac{N^{232}U}{N^{233}U} = K \frac{A^{24}Na}{A^{233}Pa}\left(1 + \frac{I_\infty^{231Pa}}{\sigma_{0,n,\gamma}^{231Pa}} \frac{\sigma_{0,n,\gamma}^{Dy}}{I_\infty^{Dy}} \frac{1}{R_{Cd}^{Dy}-1}\right),$$

where K is a coefficient obtained during normalization; $A^{24}Na$, $A^{233}Pa$, activity of the recorded isotopes; $\sigma_{0,n,\gamma}$ and I_∞, thermal neutron radiative capture cross sections and the true resonance integral.

In order to reduce to absolute values, an indirect method was used in the measurements in the reactor of the fourth unit of the Novovoronezh nuclear power station jointly with a direct determination of the buildup of ^{232}Pa and ^{233}Pa in the irradiated thorium samples. The thermal neutron flux density at the site of irradiation of the samples was $\varphi_T = 3.5 \cdot 10^{13}$ neutrons/(cm^2·sec).

The results of the measurements on slugs of different sizes were extrapolated on a thermal-fissile assembly (TFA) of a VVÉR of 126 rods. By simulating the buildup of ^{233}U in the thorium by the introduction of ^{235}U into the thorium rods, the change of rate of formation of ^{232}U was established in different operating periods of the reactor. It can be seen in Fig. 1 that the small buildup of fissile isotopes in the thorium TFA leads to a sharp increase of the rate of formation of ^{232}U. At the same time, the introduction of zirconium oxide into the thorium allows the relative buildup of ^{232}U to be reduced. Using these results, conclusions can be drawn about the realistic conditions of irradiation of thorium in the case of the continuous buildup of ^{233}U. Figure 2 shows the results of calculations of the relative buildup of ^{233}U and ^{232}U in the thorium TFA of the VVÉR, obtained by taking account of the experiment.

LITERATURE CITED

1. Rev. Mod. Phys., 50, No. 1, 2 (1978).
2. S. V. Marin, At. Tekh. Rubezhom, No. 5, 3 (1978).
3. L. N. Yurova et al., At. Energ., 45, No. 1, 21 (1978).
4. L. N. Yurova et al., At. Energ., 44, No. 6, 518 (1978).

ESTIMATION OF STACKING-FAULT ENERGY OF FRANK LOOPS IN 0Kh16N15M3B AUSTENITIC STAINLESS STEEL

Yu. V. Konobeev and S. I. Rudnev

UDC 621.039.531

It was reported earlier [1] that vacancy pores and dislocation loops form in 0Kh16N15M3B austenitic steel under bombardment with iron ions of an energy of 12-18 MeV in the internal beam of the U-300 cyclotron. Electron-microscope examination of the microstructure of steel irradiated with a damaging dose of 80 displacements/atom showed that dislocation loops are observed in the range 400-600°C. At a temperature above 450°C, all of the loops were prismatic, while the dislocation loops were primarily Frank loops. The temperature dependences obtained for the mean diameter $\langle d_l \rangle$ and maximum diameter $d_{l_{max}}$ of the loops are given in Fig. 1.

The observed facts make it possible to estimate the stacking-fault energy of Frank loops. For this purpose we can use the expression for the energy of prismatic loops and Frank loops which Johnson [2] found for fcc metals:

$$E_{pr} = \frac{\mu(T)\, b_{pr}^2}{2[1-\nu(T)]} R_l \left[\left(1 - \frac{\nu(T)}{6}\right) \left(\ln \frac{4R_l}{b_{pr}} + 2\ln 2\right) - \frac{4}{3}\left(1 - \frac{\nu(T)}{4}\right)\right];$$

$$E_F = \frac{\mu(T)\, b_F^2}{2[1-\nu(T)]} R_l \left[\ln \frac{4R_l}{b_F} + 2\ln 2 - 1\right] + \gamma_{s.f.} \pi R_l^2,$$

where $\mu(T)$ is the shear modulus which depends on the temperature T; $\nu(T)$, Poisson ratio (see Table 1); $b_{pr} = a\sqrt{2}$ and $b_F = a\sqrt{3}$, Burgers vectors of prismatic and Frank loops, respectively; a, lattice constant; R_l, loop radius; and $\gamma_{s.f.}$, stacking-fault energy.

It is natural to assume that the disappearance of a stacking fault as a result of restructuring of a Frank loop into a prismatic loop according to the dislocation reaction [3] $\frac{a}{6}[112] + \frac{a}{3}[111] \rightarrow \frac{a}{2}[110]$ occurs when the energy of the latter becomes the smallest. Having determined the "critical diameter" D_c at which $E_{pr} = E_F$ for a number of values of $\gamma_{s.f.}$, and having compared it with the experimentally established maximum loop diameter at various temperatures, we can find the value of $\gamma_{s.f.}$ which corresponds to the observed transformation of loops from the intersection of the curves of D_c and $d_{l_{max}}$ as a function of the temperature at 450°C (the upper temperature limit for the existence of Frank loops). The

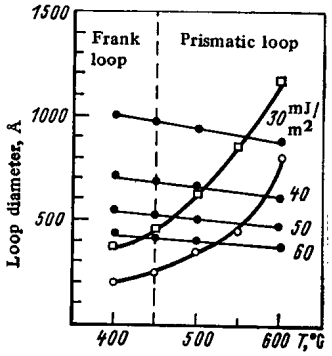

Fig. 1. Temperature dependence of the mean (○), maximum (□), and critical (●) diameter of loops (1 Å = 10^{-10} m) at different values of the stacking-fault energy (numbers next to curves).

Translated from Atomnaya Énergiya, Vol. 53, No. 2, pp. 107-108, August, 1982. Original article submitted July 15, 1981.

0038-531X/82/5302- 0563$07.50

TABLE 1. Temperature Dependences $\mu(T)$ and $\nu(T)$

T, °C	$\mu(T)$, GPa	$\nu(T)$
400	65,0	0,294
450	63,5	0,298
500	61,5	0,302
600	57,5	0,309

results of such analysis are given in Fig. 1, from which it is seen that the best agreement with experiment is attained if the stacking-fault energy of 0Kh16N15M3B steel is $\sim$55 mJ/m^2.

We were unable to find published results of measurements of $\gamma_{s.f.}$ by other methods for 0Kh16N15M3B stainless steel, apart from attempts at a systematic study of the dependence of $\gamma_{s.f.}$ on the composition of Fe–Cr–Ni ternary alloys [4]. In [4], the method of regression analysis of experimental data for different alloys was used to obtain the following empirical formula for determining the stacking-fault energy: $\gamma_{s.f.} = -53 + 6.2\,C_{Ni} + 0.7\,C_{Cr} + 3.2\,C_{Mn} + 9.3\,C_{Mo}$ [mJ/m^2], where C_x is the content of the alloying elements [at.%]. Calculation with this formula for 0Kh16N15M3B steel gives $\gamma_{s.f.} = 70$ mJ/m^2, which is in fair agreement with the value found, $\gamma_{s.f.} \approx 55$ mJ/m^2, if we consider the fairly large scatter of the $\gamma_{s.f.}$ values measured in [4] as well as the error stemming from the difference between the composition of the 0Kh16N15M3B steel studied and the nominal composition.

Thus, in studying the temperature dependence of the characteristics of the microstructure of 0Kh16N15M3B stainless steel bombarded with Fe^{3+} ions, we found that the value of the stacking-fault energy is $\sim$ 55 mJ/m^2.

LITERATURE CITED

1. E. D. Vorob'ev et al., Preprint 18-80-646, Joint Institute for Nuclear Research, Dubna (1980).
2. R. Johnson, Philos. Mag., 16, 553 (1967).
3. Derek Hull, Introduction to Dislocations, Pergamon (1976).
4. R. Schramm et al., Metall. Trans., 6A, No. 7, 1345 (1975).

DENSITY AND VISCOSITY OF FUSED MIXTURES OF URANIUM CHLORIDES AND POTASSIUM CHLORIDE

S. F. Katyshev, Yu. F. Chervinskii,
and V. N. Desyatnik

UDC 531.756:532.13:546.791.131

The possibility of using fused uranium chlorides as an electrolyte in obtaining and refining uranium metal as well as in reprocessing spent nuclear fuel necessitates a profound and comprehensive study of the physicochemical properties of multicomponent systems. In the present paper we give the results of investigations of the density and viscosity of fused three-component $KCl-UCl_3-UCl_4$ mixtures and the viscosity of $KCl-UCl_4$ mixtures over wide ranges of temperature and concentration.

The density was determined by the method of maximum pressure in an argon bubble [1], while the viscosity was found by the method of torsional vibrations of a cylindrical crucible containing the melt [2]. The initial salts were prepared by familiar techniques. The experimental data were processed by the method of least squares. As an indicator of the accuracy of the chosen type of equation, we used the value of the standard deviation S. The values of the density and viscosity of the systems were determined earlier [1, 3, 4].

Tables 1 and 2 give the results of measurements in the form of the temperature dependences of the density ρ and the kinematic (ν) and dynamic (η) viscosities of the fused mixtures. To ascertain the character of the reaction of the salts when mixed, on the basis of the experimental data we calculated the molar volumes V and their relative deviations $\Delta V/V_{ad}$ from additivity (Fig. 1), and the molecular viscosity (Fig. 2). As is seen from the data presented, this reaction is of a complex nature in the $KCl-UCl_3-UCl_4$ system. Positive deviations $\Delta V/V_{ad}$ are observed in the region of primary crystallization of the chemical compounds K_2UCl_5 and K_2UCl_6 [5] and are probably explained by the formation of complex UCl_5^{2-} and UCl_6^{2-} ions.

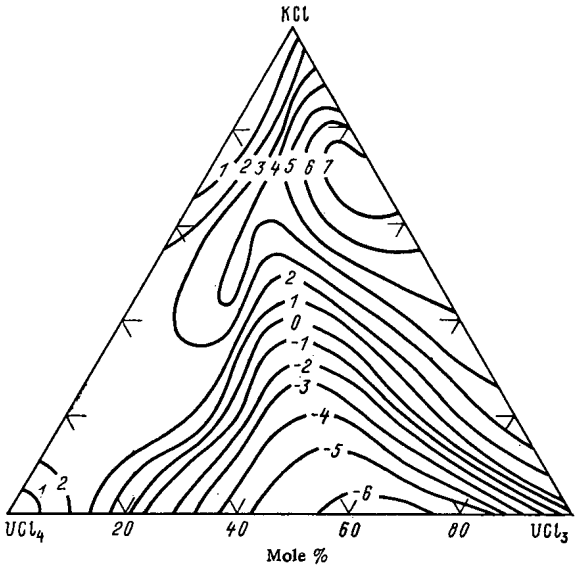

Fig. 1

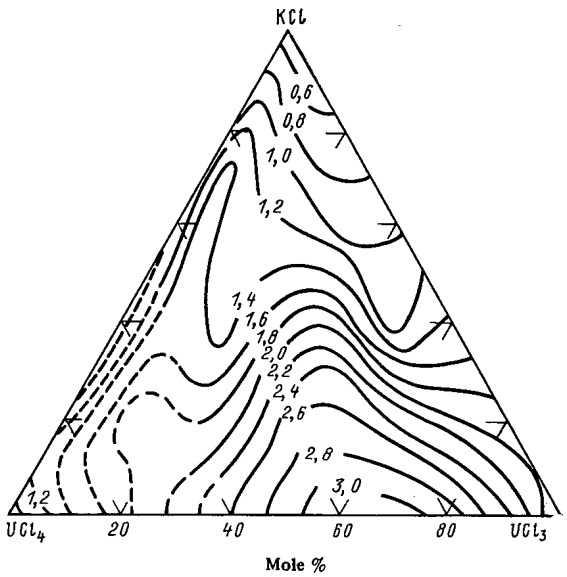

Fig. 2

Fig. 1. Relative deviations of the molar volumes from the additive values for fused $KCl-UCL_3-UCl_4$ mixtures at 1023°K, %.

Fig. 2. Lines of equal molecular viscosity (10^4 J·sec/kmole)of fused $KCl-UCl_3-UCl_4$ mixtures at 1130°K.

Translated from Atomnaya Énergiya, Vol. 53, No. 2, pp. 108-109, August, 1982. Original article submitted July 23, 1981; revision submitted January 6, 1982.

0038-531X/82/5302- 0565$07.50

TABLE 1. Density of Fused $KCl-UCl_3-UCl_4$ Mixtures

KCl content, mole %	$\rho = a - b \cdot T$, g/cm^3			Temperature range, °K
	a	$b \cdot 10^3$	$S \cdot 10^3$	
	(79,9 % UCl_3 + 20,1 % UCl_4) − KCl			
14,0	5,6732	1,4470	4	1068—1196
19,8	5,1600	1,1462	1	1098—1196
39,9	4,5458	1,0602	3	958—1049
54,9	3,9524	0,9276	2	885—1041
70,0	3,3814	0,8236	1	965—1078
75,0	3,0980	0,6910	2	963—1108
84,9	2,7874	0,6638	2	969—1109
	(60,1 % UCl_3 + 39,9 % UCl_4) − KCl			
20,2	5,6536	1,7304	1	1031—1105
29,9	4,8920	1,2367	1	991—1091
50,0	4,0879	0,9847	1	873—990
60,0	3,4649	0,6870	1	398—1054
75,0	3,0951	0,7178	1	928—1056
85,0	2,7680	0,6640	1	976—1083
	(45,0 % UCl_3 + 55,0 % UCl_4) − KCl			
20,2	5,6426	1,9278	3	1002—1086
35,0	4,7098	1,3243	1	957—1057
50,0	4,1978	1,1889	1	912—1047
60,1	3,6750	0,9341	2	873—1007
70,0	3,1889	0,7024	1	950—1046
80,0	2,9480	0,6942	1	978—1086
	(30,0 % UCl_3 + 70,0 % UCl_4) − KCl			
20,0	5,1131	1,7134	2	851—943
40,0	4,5531	1,5201	2	827—942
50,8	4,0378	1,1722	2	887—977
60,0	3,6809	1,0112	2	916—1028
75,0	3,2131	0,8374	1	834—951
85,0	2,7886	0,6873	1	1001—1137
	(14,9 % UCl_3 + 85,1 % UCl_4) − KCl			
20,0	4,9069	1,7116	3	869—948
39,0	4,1017	1,1407	2	770—949
50,0	4,0622	1,2573	2	781—941
60,0	3,5865	0,9534	2	884—985
70,0	3,4068	0,9439	2	904—1024
80,0	3,0616	0,8094	3	928—1039
90,0	2,5970	0,6444	1	1030—1153

TABLE 2. Viscosity of Fused $KCl-UCl_3-UCl_4$ Mixtures

KCl content, mole %	$\log \nu = A_\nu + B_\nu/T$ (ν, m^2·sec^{-1})			$\log \eta = A_\eta + B_\eta/T$ (η, Pa·sec)			Temperature range, °K
	$-A_\nu$	B_ν	$S \cdot 10^3$	$-A_\eta$	B_η	$S \cdot 10^5$	
	$KCl - UCl_4$						
0,0	8,7389	2401	1,1	5,4640	2650	3,6	870—1003
10,0	8,0138	1769	1,0	4,7420	2002	3,4	852—1002
23,0	7,9360	1597	2,3	4,6419	1789	6,9	823—1005
36,5	7,6932	1375	2,1	4,3830	1529	6,7	774—1013
50,0	7,5590	1338	2,6	4,2302	1449	4,4	678—1009
58,0	7,5412	1384	1,0	4,2620	1526	2,8	864—1048
66,7	7,6071	1538	0,7	4,3732	1701	1,7	949—1096
75,0	7,5617	1529	1,4	4,3567	1691	3,2	919—1095
83,0	7,4150	1395	1,4	4,2701	1580	3,2	968—1145
90,0	7,1932	1144	0,9	4,1119	1350	1,5	1042—1173
	(79,9 % UCl_3 + 20,1 % UCl_4) − KCl						
19,8	8,0390	2162	1,3	4,5961	2326	5,2	1073—1179
39,9	7,7343	1583	0,8	4,3480	1740	2,8	990—1173
54,9	7,4668	1322	1,3	4,1239	1458	3,8	874—1166
70,0	7,5119	1354	1,4	4,2618	1512	3,8	968—1150
84,9	7,3660	1202	1,6	4,1993	1363	3,3	1000—1150
	(60,1 % UCl_3 + 39,9 % UCl_4) − KCl						
20,2	7,6891	1852	1,6	4,3300	2089	5,9	1022—1156
29,9	7,4637	1604	2,2	4,0858	1790	7,7	1025—1198
50,0	7,5842	1604	1,8	4,2381	1747	5,0	875—1193
60,0	7,7601	1728	1,8	4,4281	1838	5,6	864—1187
85,0	7,5980	1544	1,6	4,4370	1716	3,3	1018—1138
	(30,0 % UCl_3 + 70,0 % UCl_4) − KCl						
20,2	7,8022	1763	1,8	4,5130	2005	6,5	968—1131
40,0	7,8009	1709	1,1	4,5581	1947	3,5	941—1131
60,0	7,7630	1797	1,8	4,5178	1978	5,0	954—1134
75,0	7,5251	1611	1,3	4,3190	1781	2,8	954—1141
85,0	7,3148	1386	1,6	4,1691	1564	3,4	1030—1174
	(14,9 % UCl_3 − 85,1 % UCl_4) − KCl						
20,0	7,5971	1550	2,2	4,3310	1788	7,5	937—1083
39,0	7,6228	1563	1,4	4,3167	1728	4,0	888—1111
50,0	7,7720	1784	1,7	4,5042	1960	5,2	817—1130
70,0	7,7039	1866	1,4	4,5051	2059	3,3	974—1157
90,0	7,1900	1249	1,4	4,0900	1443	2,6	1085—1191

In the range of compositions which are characterized by negative deviations of the molar volumes from additivity (see Fig. 1) and a molecular viscosity maximum (see Fig. 2), the predominant processes are apparently those of dissociation of unstable U(III) ions with the formation of more unwieldy complex groupings of the UCl_6^{2-} type.

LITERATURE CITED

1. V. N. Desyatnik, S. F. Katyshev, and S. P. Raspopin, At. Energ., 42, No. 2, 99 (1977).
2. A. N. Vokhmyakov et al., in: Proceedings of the Higher Institutions of Learning of the USSR [in Russian], Uralsk. Politekh. Inst., Sverdlovsk, No. 2 (1974), p. 70.
3. V. N. Desyatnik et al., Zh. Fiz. Khim., 50, No. 10, 2522 (1976).
4. V. N. Desyatnik, S. F. Katyshev, and Yu. F. Chervinskii, At. Energ., 49, No. 4, 261 (1980).
5. V. N. Desyatnik et al., At. Energ., 31, No. 6, 631 (1971).

PROBLEMS IN SUMMARIZING EXPERIMENTAL DATA ON THE HEAT-TRANSFER CRISIS IN BOILING

Yu. V. Mironov and S. V. Shpanskii

UDC 536.248.2:621.039.534.44

The heat-transfer crisis is one of the main thermophysical factors that restrict increased specific power in nuclear-power systems. Therefore, there are many experimental studies on the crisis, and extensive experimental evidence has been accumulated. Much attention has recently been given to the physical essence of the process. This has provided a reasonably sound qualitative picture that indicates how the individual parameters influence the process. However, at present it is impossible to predict the crisis reliably on the basis of a detailed description of the hydrodynamics of the flow in a channel with fuel-rod elements. A decisive role in thermophysical calculations is assigned to semiempirical models and to correlations derived from statistical processing of the experimental data.

The reliability of these correlations is dependent on the correctness of the physical arguments and on the volume of the empirical evidence used. The latter is improved by the use of a data bank on the heat-transfer crisis in rod assemblies, namely an automatic system for acquiring and storing information [1].

This bank has now accumulated data on 8561 experimental points derived from 133 experimental sections that have been published in Soviet and foreign sources. These parameters correspond approximately to the forecasts made in [1]. The distribution of the experimental points by design parameters of the working sections [1] has hardly varied during the assembly of the bank, although there has been a tendency for the number of experiments performed on models with various levels of energy production in the fuel rods to increase. The distribution of the experimental points by working parameters (Fig. 1) shows that the range of pressures above 6 MPa and of mass flow rates below 4000 kg/m^2·sec is adequately and uniformly covered by the experimental studies. On the other hand, most of the points have been obtained on assemblies with a positive steam-content balance at the point of crisis.

The expansion of the bank has enabled one to compare theoretical methods of calculating the heat-transfer crisis for practically all the experimental data accumulated in various countries. For this purpose, the calculation recommendations of [2, 3] were adopted, which are the most widely used in the design of nuclear power systems, together with some more recent recommendations [4]. The basic statistical parameters for these formulas are given in Table 1. The volume of the sample is determined by the physical and design constraints that the authors propose to incorporate into the calculations. Note that in calculations from the recommendations of [4] some simplifications were introduced concerning the interaction between the hottest cells. However, the simplifications affect the theoretical results only for a very restricted number of experiments and are not reflected in any appreciable fashion on the statistical results given here. Also, in those

TABLE 1. Results from Statistical Analysis of the Theoretical Recommendations

Parameters	For recommendations of		
	[2]	[3] *	[4]
Volume of working file, % of bank volume	68,9	17,4	82,2
Arithmetic mean deviation	0,029	- 0,029	0,073
Mean-square deviation	0,179	0,155	0,085
Percent of experimental points deviating from theor. ones by more than 38%	5,6	4,3	5,4
Percent of experimental points agreeing with theory within limits of ± 24%	80,5	90,5	87,9

*In the pressure range from 6.5 to 7.5 MPa.

Translated from Atomnaya Énergiya, Vol. 53, No. 2, pp. 110-111, August, 1982. Original article submitted August 7, 1981.

0038-531X/82/5302- 0567$07.50

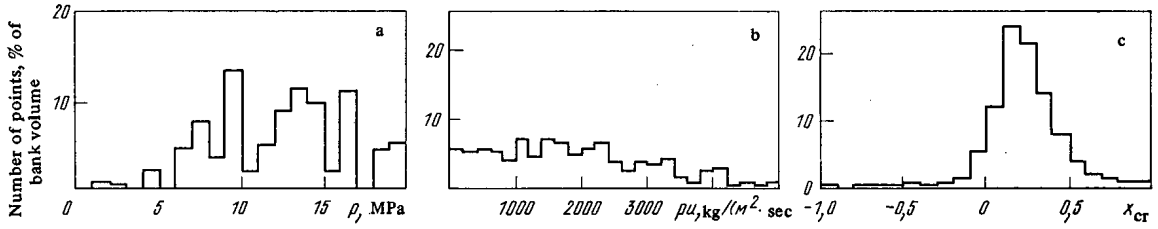

Fig. 1. Distribution of the experimental points by flow parameters: pressure (a), mass flow rate (b), and critical steam content (c).

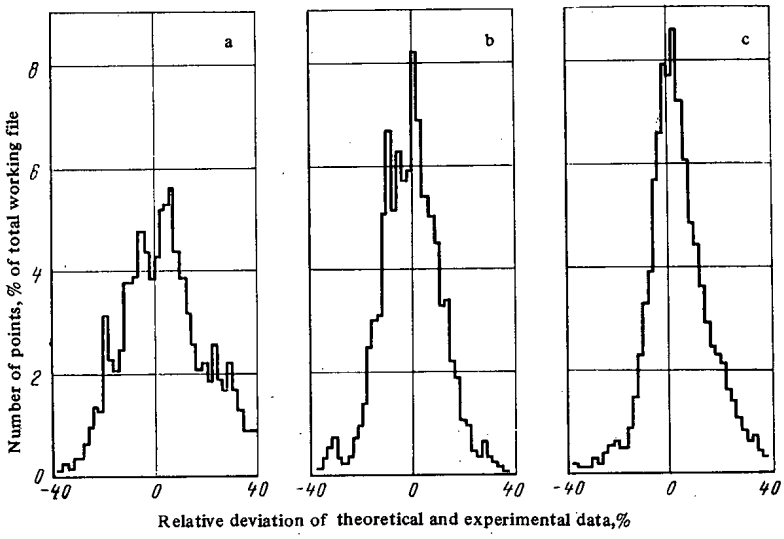

Fig. 2. Histograms for the distribution of relative deviation of the theoretical values for the critical power: a-c) from recommendations of [2-4] correspondingly.

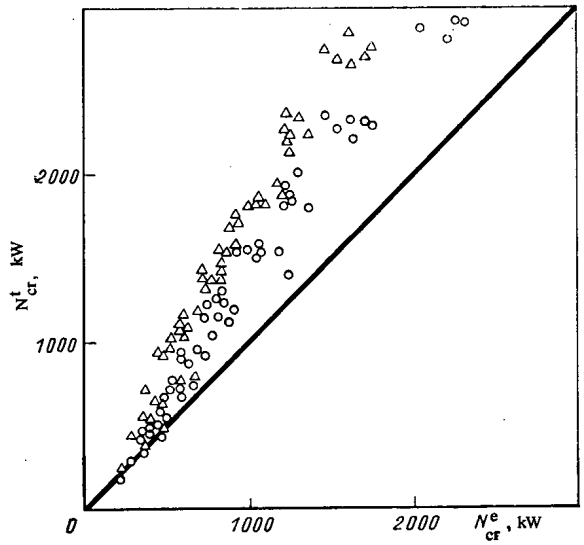

Fig. 3. Comparison of theoretical and experimental values of the critical heat flux from the experimental data of [6]: Δ, ○) calculations from the recommendations of [2, 4] correspondingly.

recommendations there were no constraints on the nonuniformity of the energy production over the cross sections of the models. Figure 2 shows histograms for the deviations of the theoretical values of the critical heat flux for these correlations. The shapes of the curves confirm that calculations on the recommendations of [3] lead in most cases to an underestimate of the critical heat flux, whereas the correlations of [2, 4] give a more symmetrical shape for the histograms, although in these cases there is somewhat of an overestimate in the theoretical values of the critical heat flux. More detailed examination revealed some differences between the working formulas arising from the features of the initial volume of experimental material used in deriving the correlations. For example, the formulas of [3] give a much smaller spread in processing the experimental data obtained on assemblies with square packing. The recommendations of [2] also have considerably better statistical parameters for models that simulate the channels of the RBMK and VVÉR reactors operated in the USSR. In [2], for example, the correlation describes a set of 206 experimental points with a standard deviation of 6.2%.

The experimental data that are poorly described by all these correlations relate to a small number of points obtained on relatively short sections in which the inlet was supplied with a steam–water mixture, or else to data for assemblies with a very large gradient in the energy production (e.g., the data of [5], where the difference in energy production was by a factor of more than nine). However, the data from assemblies with actual nonuniformity in the energy production over the cross section may also agree poorly with the general correlations, particularly when this factor is combined with appreciable thermal or hydraulic lack of equivalence between the cells. Figure 3 compares the theoretical and measured values for the critical heat flux from the experimental data of [6] for a 20-rod assembly with a square lattice with nonuniformity in heat production of a factor of up to 1.5. In this case, the experimental data again deviate appreciably from the theoretical predictions, with the arithmetic mean deviations ranging from 25% (for the correlations of [4]) to 35% (for the correlations of [3]).

This all indicates that at present the scope for constructing general correlations for the critical heat flux in relation to thermohydraulic characteristics averaged over the section is largely exhausted. It would seem that in this respect one should not expect any appreciable improvement in the recommendations of [2, 4]. In the future, it will be necessary to use a more detailed description of the internal structure of the flow in the fuel-rod assembly. In that respect, it is notable that there is a certain advantage in the recommendations of [4], which approximately incorporate the effect of the thermohydraulic nonuniformity of the most heavily loaded cells in the section of the assembly on the critical heat flux.

LITERATURE CITED

1. Yu. V. Mironov et al., Teploenergetika, No. 9, 65 (1978).
2. V. S. Osmachkin and N. N. Lystsova, Preprint IAE-2558, Moscow (1975).
3. R. Macbeth, AEEW-R358, Winfrith (1964).
4. V. N. Smolin and V. K. Polyakov, in: Thermophysical Studies to Provide Reliability and Safety in Nuclear Reactors of Water–Water Type: TF-78 Seminar [in Russian], Vol. 2 (1978), p. 475.
5. V. I. Abramov et al., ibid., p. 791.
6. B. Letourneau et al., Nucl. Sci. Eng., 54, No. 2, 214 (1974).

LIBERATION OF HELIUM IN THE HEATING OF IRRADIATED BORON CARBIDE

V. G. Kovyrshin

UDC 621.039.531.661.65:620.181.4

Radiation damage to boron carbide is produced primarily by the formation and accumulation of helium atoms. The interaction of these atoms with the original and radiation defects at increased temperatures promote an escape of helium to the surface and diffusion into the material, which is accompanied by the formation of gas porosity and swelling. Therefore, special attention is being paid to the investigation of the behavior of helium in boron-containing materials [1-4].

In the course of the experiments, we studied the kinetics and determined the energy characteristics of processes of thermal desorption during the heating of irradiated samples of unenriched boron carbide. The conditions of irradiation of B_4C powders of various particle sizes (up to 10, 10-100, and above 100 μm) in a VVR-M [water-moderated–water-cooled] reactor ensured a temperature of the samples no higher than 100°C. The flux densities of thermal neutrons, $\sim 5 \cdot 10^{13}$ neutrons/(cm^2·sec), and that of fast neutrons, ($E \geqslant 1$ MeV) $\sim 10^{13}$ neutrons/(cm^2·sec), were determined by the method of activation indicators. The thermal neutron fluxes for two exposures of B_4C powder were $1.2 \cdot 10^{19}$ and $9 \cdot 10^{19}$ neutrons/cm^2; those of fast neutrons, five times lower.

The method of mass spectrometric measurement of the helium concentration during its thermodesorption from heated irradiated samples described earlier [3] and improved was used.

Figure 1 presents typical temperature dependences of the relative rate of liberation of helium from B_4C, identical with those obtained in an investigation of irradiated boron carbide particles, sintered in a carbon–graphite base [3]. The reproducibility of the temperature of the maxima T_{max} in the thermodesorption spectra at the same rate of heating proved no poorer than $\pm 2\%$. The activation energy E_i of the steps of liberation of helium were determined by analysis of the curves of heating at the rates of ~ 0.3 and 0.1°C/s according to the experimental values of the characteristic temperature [5].

The temperature of the first peak (see Fig. 1), equal to 100-135°C at a rate of heating 0.3°C/sec, increases by ~ 35°C for larger particles of B_4C at a flux of $1.2 \cdot 10^{19}$ neutrons/cm^2, while at a flux of $9 \cdot 10^{19}$ neutrons/cm^2 it remains constant (~ 140°C). This may be associated with a change in the effective length of migration under the influence of the particle size and neutron flux. The low-temperature step I (activation energy $E_1 = 0.3 \pm 0.1$ eV) is evidently controlled by an interstitial mechanism of migration of helium atoms, uncaptured during irradiation by the vacancy and other traps, from the surface layer of B_4C particles.

With a further increase in the temperature, two stages of liberation of helium are observed: the activation energy of step II, $E_2 = 1.2 \pm 0.2$ eV, and of step III, $E_3 = 2.3 \pm 0.3$ eV. An increase in the flux is accompanied by a decrease of 100-150°C in the values of T_{max} for processes with the same activation energy. The parameters of the high-temperature steps are evidence of a vacancy mechanism of the liberation of helium. Evidently, it is precisely by a change in the nature of the migration of helium in comparison with the low-temperature step that a certain (20-50°C) decrease in the characteristic temperatures T_2 and T_3 in the case of an increase in the particle size of B_4C, irradiated up to a flux of $1.2 \cdot 10^{19}$ neutrons/cm^2, can be explained. The parameters of these steps were calculated according to the experimental data for B_4C particles up to 10 μm in size. The value of E_2 is somewhat less than the activation energy of the migration of helium in boron carbide obtained earlier [4], $E_m = 1.5$ eV, while the value of E_3 is ~ 0.8 eV greater than E_m and may include the bond energy and other energy characteristics of complexes of "radiation defect–helium."

Thus, at different fluxes, helium is liberated from irradiated boron carbide in the course of three main steps. Although the experimental procedure used permits a determination of the activation energy with an error of $\sim 20\%$, the absence of other steps of gas evolution in the temperature interval 700-1000°C permits us to consider the processes of diffusion of helium in the material, which control the liberation of helium at steps II and III at different fluxes, as identical.

Translated from Atomnaya Énergiya, Vol. 53, No. 2, pp. 112-113, August, 1982. Original article submitted September 4, 1981.

0038-531X/82/5302-0570$07.50

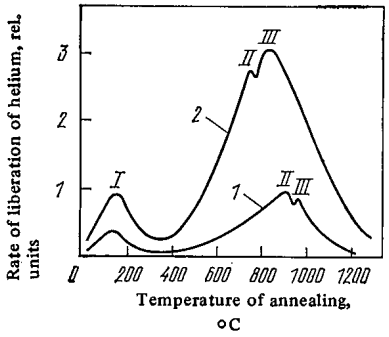

Fig. 1

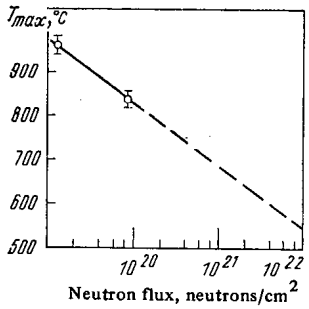

Fig. 2

Fig. 1. Spectra of the thermodesorption of helium from irradiated boron carbide at a flux of $1.2 \cdot 10^{19}$ (1) and $9 \cdot 10^{19}$ (2) neutrons/cm^2; rate of heating, 0.3°C/sec.

Fig. 2. Dependence of the characteristic temperature T_{max} of step III of the liberation of helium from B_4C on the neutron flux (dashed line – extrapolation to a flux of 10^{22} neutrons/cm^2).

The linear dependence of the values of the characteristic temperature T_{max} of steps with the same activation energy on the logarithm of the flux within a wide range of variation was observed for neutron irradiation [6] and for irradiation by helium ions [7]. The value T_{max} of the peak of the liberation of helium from B_4C at step III, was extrapolated to 10^{22} neutrons/cm^2 (Fig. 2), is 550 ± 100°C. In practice, this means that, with increasing flux, a relatively larger amount of helium will be liberated at a lower temperature of annealing or irradiation. Actually, almost all the helium formed is liberated from boron carbide irradiated up to a flux of $\sim 10^{22}$ neutrons/cm^2 when it is annealed at up to 1050°C, and, in the process of irradiation at 600°C, up to 30% of the total amount of helium is liberated [2].

The observed displacement of the stages of annealing with increasing flux [6, 7] is explained primarily by the "static" effect of an increase in the concentration of radiation defects, which are created in the lattice during irradiation and accompany the migration of atoms or complexes of helium when the samples are heated. A consequence of the increase in neutron flux density (threefold) at the same values of the flux and temperature of irradiation was the appreciable increase in gas liberation from boron carbide during irradiation (up to 80-90%) and the sharp decrease in swelling [2]. This means that an increased concentration of "dynamic" radiation defects in the material is responsible for an increase in the radiation component of the diffusion coefficient and leads to a shift of the main peaks of gas evolution of helium in the direction of lower temperatures. The more rapid passage of helium out to the surface (or into technological pores) promotes a decrease in the swelling of boron carbide.

LITERATURE CITED

1. V. P. Gol'tsev et al., At. Energ., 30, No. 3, 240 (1971).
2. V. P. Gol'tsev and G. M. Guseva, Problems of Atomic Science and Technology. Fuel and Construction Materials Series [in Russian], No. 3 (1975), p. 13.
3. I. Ya. Emel'yanov et al., At. Energ., 31, No. 3, 215 (1971).
4. A. G. Bespalov and L. V. Pavlinov, in: State and Prospects of Studies on the Design of Atomic Power Plants with Fast Neutron Reactors [in Russian], Vol. 2, FÉI, Obninsk (1975), p. 696.
5. A. C. Damesk and G. J. Dienes, Point Defects in Metals, Gordon (1964).
6. L. Keys and J. Moteff, J. Nucl. Mater., 34, 260 (1970).
7. V. S. Karasev et al., Problems of Atomic Science and Technology. Physics of Radiation Damages and Radiation Material Science Series [in Russian], No. 2(13) (1980), p. 82.

MULTIGROUP SYSTEM OF CONSTANTS FOR CALCULATING HIGH-ENERGY NEUTRON TRANSPORT

M. Yu. Vyrskii, A. A. Dubinin, A. I. Ilyushkin,
V. E. Kolesov, A. S. Krivtsov, I. I. Longe,
V. P. Mashkovich, and V. K. Sakharov

UDC 621.039.57.12

In order to calculate neutron transport in reactors and shielding, the system of constants in ARAMAKO-2F [1], OBRAZ [2], ARAMAK-F [3] and others, based mainly on the collection of group constants in BNAB-26 [4] or on the later versions BNAB-70 [5] and BNAB-78 [5], are widely used. These systems satisfy the basic requirements of the constants necessary for designing the reactor and shielding. However, the insufficiently detailed resolution in the fast-neutron energy range, use of the fission spectrum in obtaining the group cross sections, and absence of data on a number of processes that are important at neutron energies exceeding 10 MeV make it difficult to use the systems of constants indicated above for solving problems with high-energy neutron sources.

Table 1 presents the maximum allowable errors in nuclear data, permitting reliable calculation of the blanket and shielding of a thermonuclear reactor [6]. Here, the range of error in the corresponding group cross sections with different group separations, arising when the standard averaging spectrum (fission spectrum of ^{235}U for $E > 2.5$ MeV and $1/E$ for $E < 2.5$ MeV) is replaced by its inverse, is also indicated. The energy distributions indicated encompass practically all possible types of spectra encountered in real shields. The data in Table 1 show that the systems of constants listed above do not yield the required accuracy in solving problems of calculating the fields of radiation in thermonuclear reactors.

In this paper, we attempt to create a system of group constants for the fast-neutron energy range ($E > 0.8$ MeV) with a sufficient number of groups. The criterion of sufficiency was the independence (with an error not exceeding 3%) of the group values of the total cross section for interaction of neutrons from the shape of the intragroup spectrum.

Microscopic group constants were calculated using the SPURT program [7] based on the compilation of neutron data in ENDL [8]. The widely used 26-group separation of the neutron energy scale [4], supplemented in the high-energy range by two groups, 10.5-14.0 and 14.0-18.0 MeV, was chosen as the base group structure. Subsequent group structures in the energy range above 0.8 MeV were obtained from the base structure by separating each energy interval uniformly according to lethargy into 2, 4, and 8 parts, which, in the energy range 0.8-18.0 MeV, gave 14, 28, and 56 groups, respectively. The total number of groups was 28 (base separation), 35, 49, and 77. In the energy range below 0.8 MeV (21 groups), we used data from the BNAB-70 and BNAB-78 compilation of group constants.

The group values of the total interaction cross section (σ_t^q), elastic (σ_{el}^q) and inelastic (σ_{in}^q) scattering cross sections, absorption cross section (σ_a^q), fission cross section (σ_f^q), and (n, γ)-reaction cross section ($\sigma_{n,\gamma}^q$), as well as the elastic and inelastic scattering matrices from group q into group p, $\{\sigma_{el,l}^{q\to p}\}$ and $\{\sigma_{in,l}^{q\to p}$ were calculated for the following elements and isotopes: H, D, ^{6}Li, ^{7}Li, Be, ^{10}B, ^{11}B, C, N, Na, Al, Si, Ca, K, Cr, Fe, Ti, Ni, Zr, Nb, Mo, W, Pb, ^{232}Th, ^{235}U, ^{238}U, ^{239}Pu.

Taking into account the errors in the group cross sections and apparatus for analyzing the sensitivity of the results of the calculation to the interaction cross section [9, 10], we estimated the error in the functionals of the radiation field.

Analysis of the data on group cross sections showed that the requirement formulated above for the group cross sections is satisfied with a 49-group separation. For most elements encountered in practice in designing radiation shields, the main cross sections, which determine the transport of fast neutrons (σ_t^q, σ_{el}^q, σ_{in}^q, σ_a^q), are described with an error of not more than 3%. Oxygen and carbon are an exception; for them, the largest differences in the cross sections mentioned in the separate groups reach 4-8%. The error in the cross sections for transition from group to group, especially in the elastic-moderating cross section, is much greater and can attain 15-30%, even in the energy range below the inelastic scattering threshold, where this error can be determined.

We investigated the errors in calculating the functionals of the neutron field starting from a calculation of the neutron transmission for source energy 14 MeV through one-dimensional shields made of different materials, using the 28, 35, and 49-group separation of the energy scale. We calculated neutron transport using the ROZ-11 program [11]. We determined the sensitivity of the results of the calculation to the interaction cross sections using the ZAKAT program [10].

Translated from Atomnaya Énergiya, Vol. 53, No. 2, pp. 113-114, August, 1982. Original article submitted September 7, 1981.

0038-531X/82/5302- 0572$07.50

TABLE 1. Required Accuracy of Nuclear Data and Error of Group Representation of Cross Sections for Thermonuclear Reactor Materials

Element or nuclide	Interaction cross section	Energy range, MeV	Required accuracy %, [6]	Error in the group representation of cross sections, %		
				28 group [1]	35 group *	49 group
H	σ_t	to 15.0	3 †	5—15	1—5	1,5
^{6}Li	$\sigma_{n,\alpha}(E)$	0.1-0.3	3	5—15	1,0—5,5	2,5
	$\sigma_{n,n'}(E)$	to 15.0	10	50	30	10
^{7}Li	$\sigma_{n,n'\alpha}(E)$	to 15.0	5	15—50	4—40	1—7,5
O	$\sigma_t(E)$	to 15.0	3	5—15	3—12	1,5—4,5
Fe	$\sigma_t(E)$	to 15.0	3†	3—17	1—5	0,5—2
	$\sigma_{nn'}(E)$	3—15.0	10	5—17	3—5	1—2
Nb	$\sigma_{nn'}(E,\theta)$	—	—	100	80	10—50
	$\sigma_{n,2n}(E)$	to 15.0	10	20—60	10—40	10—20

*Group separation examined in this paper.
†Requirements of the present work.

TABLE 2. Errors in Calculating the Total Intensity of the Equivalent Dose and Neutron Flux Density

Detected effect on the right boundary of the barrier	No. of groups in the calculation	Barrier material and its thickness		
		iron, 1.0 m	graphite, 2.0 m	lithium and stainless steel, 0.34 m*
Intensity of equivalent dose	28	0,9	4,1	1,3
	35	0,5	1,7	0,8
	49	0,3	1,2	0,45
Flux density of neutrons with energies above 46.5 keV	28	3,3	68,0	0,55
	35	1,3	41,0	0,36
	49	1,1	22,5	0,32

*Sphere with R = 0.34 m.

As an example, Table 2 gives the errors in the calculation of the total intensity of the equivalent dose and flux density of neutrons with energies above 46.5 keV behind different shields. It is evident that in the case of the 49-group separation of the energy scale, the errors in the functionals examined, related to the uncertainty in the averaging spectrum with energies above 0.8 MeV, decrease to acceptable values. The investigations of the sensitivity of the computational results to different interaction cross sections showed that the accuracy in representing the total and partial cross sections, transition cross sections from group to group, and the anisotropy parameters for scattering with 49-group separation of the energy scale is satisfactory.

The microscopic group constants for energies above 0.8 MeV are collected in BND-49, analogous in structure to BND-14 [12], entering into the expanded version of the ARAMAKO-2F system [12]. Information on the scattering anisotropy is presented in P_{12} (elastic-scattering approximation) and in P_6 (inelastic-scattering approximation). The boundary for the upper groups with $E > 0.8$ MeV for the 49-group separation is as follows (in MeV): 18.0; 16.9; 15.8; 14.8; 14.0; 13.0; 12.1; 11.3; 10.5; 9.31; 8.26; 7.33; 6.50; 5.76; 5.1; 4.51; 4.0; 3.56; 3.16; 2.81; 2.5; 2.17; 1.87; 1.62; 1.4; 1.22; 1.06; 0.92; 0.8. The 49-group system of constants is programmed in the FORTRAN IV language for the BESM-6 computer. Thus, the 49-group system of constants, created from the compilation of group constants in BNAB-70 and BNAB-78 and the compilation of estimated data in ENDL[8], greatly decreases the effect of changes in the shape of the intragroup spectrum on calculations of high-energy neutron transport.

LITERATURE CITED

1. N. O. Bazazyants et al., ARAMAKO-2F System of Constants for Calculations of Radiation Transfer in Reactors and Shielding. Handbook of the Institute of Applied Mathematics of the USSR Academy of Sciences, Moscow (1976).

2. V. F. Khokhlov and V. D. Tkachev, in: Abstracts of Reports at the All-Union Scientific Conference on Shielding of Ionizing Radiation from Nuclear Technical Installations, MIFI, Moscow (1974), p. 78.
3. V. A. Lobyntsev and I. G. Timofeev, "Preparation of group constants for calculations of nuclear reactors on BÉSM-6 computer," Preprint IAE-2926, Moscow (1977).
4. L. P. Abagyan et al., Group Constants for Calculation of Nuclear Reactors [in Russian], Atomizdat, Moscow (1964).
5. L. P. Abagyan et al., Group Constants for Calculation of Reactors and Shielding [in Russian], Energoizdat, Moscow (1981).
6. O. V. Bochkarev et al., in: Neutron Physics, Part 1 [in Russian], FÉI, Obninsk (1974), p. 30.
7. V. E. Kolesov and A. S. Krivtsov, in: Neutron Physics, Part 1 [in Russian], TsNIIatominform, Moscow (1976), p. 140.
8. R. Howerton et al., The Evaluated Nuclear Data Library (ENDL). Evaluation Techniques, Reaction Index and Description of Individual Evaluations, UCRL-50400, P. A. E. Lawrence Livermore Laboratory, Vol. 15, 1975-1978.
9. E. Oblow, ORNL-TM-4110 (1973).
10. V. V. Bolyatko et al., At. Energ., 50, No. 5, 328 (1981).
11. M. Yu. Vyrskii et al., in: Abstracts of Reports at the Second All-Union Scientific Conference on Shielding of Ionizing Radiation from Nuclear Technical Installations [in Russian], MIFI, Moscow (1978), p. 10.
12. M. Yu. Vyrskii et al., Preprint FÉI-904, Obninsk (1979).

DENSITY DISTRIBUTION OF THE FLUX OF DELAYED FISSION NEUTRONS IN WATER

E. G. Vertman

UDC 539.1.03:539.12.04

Activation analysis of geological material for uranium and thorium, based on the method of delayed neutrons, imposes especially stringent requirements on the recording units. In order to improve the sensitivity of the method, it is necessary to maximize the neutron recording efficiency and minimize the background. This can be achieved by a suitable choice of detectors and by using the optimum measurement geometry.

The domestic models of units for delayed neutron recording use mainly SNM-11 corona-discharge counters with boron-coated cathodes, which are characterized by high efficiency in recording thermal neutrons [1, 2]. Since the mean energy of delayed fission neutrons is equal to 0.49 MeV, the source and the counters are placed in a hydrogenous moderator (water, paraffin, or polyethylene) in order to transform these neutrons into thermal neutrons.

We investigated the density distribution of the flux of delayed fission neutrons from a point source in water in order to determine the optimum recording geometry. The measurements were performed in a tank whose diameter and height were equal to 0.6 m. The delayed neutron source was produced by neutron irradiation of a rod (diameter, 17 mm; length, 50 mm; mass, 192 g) made of metallic uranium, enriched to 90% ^{235}U. A californium source, characterized by a total neutron flux of 1.5×10^7 neutrons/sec, was placed in a special container with an aqueous moderator, and the uranium rod was placed up against the source.

Since the recording pulse frequency for neutrons from the californium source exceeded the recording pulse frequency for delayed neutrons by a factor of 5000, it was necessary to shield the tank containing the detector from background neutrons from the californium source. For this, the tank and the container were placed 5 m apart, and a screen made of borated polyethylene and sheet cadmium was placed between them. The background of the SNM-11 counter did not exceed 2 pulses per 100 sec. All the precursors of delayed neutrons are short-lived radionuclides with a half-life of 0.2 to 56 sec; therefore, the durations of irradiation, exposure, and recording in measurements were equal to 180, 7, and 100 sec, respectively.

Figure 1 shows the density distribution of the flux of delayed fission neutrons from a point source as a function $\varphi(R)$ of the distance between the source and the detector. The diagram also shows the density distribution curves for the neutron flux from a californium source in water. The measurements were performed in the same geometry by using an SNM-11 boron counter and an indium detector (disk with a diameter of 100 mm and a thickness of 0.2 mm). During measurements, the indium detector was placed between two SBT-10 beta-counters. The measurements were performed under the following conditions: the durations of irradiation, exposure, and recording were equal to 60, 10, and 60 sec, respectively.

Translated from Atomnaya Énergiya, Vol. 53, No. 2, pp. 116-117, August, 1982. Original article submitted September 30, 1981.

 0038-531X/82/5302- 0574$07.50

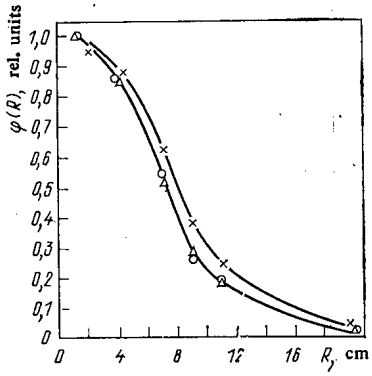

Fig. 1. Density distribution of the flux of delayed fission neutrons from a point ^{235}U source and of neutrons from a californium source in water. ○) Delayed neutrons (boron counter); X) neutrons from the californium source (boron counter); Δ) neutrons from the californium source (indium detector).

Comparison between the thermal neutron distributions recorded by means of the boron counter shows that the density of delayed neutrons decreases more rapidly than the density of neutrons from the californium counter for an increase in the distance between the source and the detector. This can be explained by the fact that the mean energy of delayed fission neutrons is one half as large as the mean energy of neutrons from the californium source.

The curve characterizing the distribution of delayed fission neutrons that have been slowed down to thermal energy (recorded by means of the boron counter) and the curve representing the distribution of neutrons from the californium source (recorded by means of the indium detector) virtually coincide, within the limits of experimental error. Comparison between the distributions of thermal and resonance neutrons in water around a californium source indicates that the distribution curve is shifted toward larger R values with a reduction in the energy of recorded neutrons. This agrees with the data obtained by Amaldi and Fermi [3].

Comparing the distributions of delayed fission neutrons and neutrons from the californium source, we reach the conclusion that, in determining the optimum geometry of units for delayed neutron recording, we can use the longer-lived californium source, which is also more convenient in measurements. In this, the error due to substitution of one neutron source for another does not exceed 10%.

LITERATURE CITED

1. E. G. Vertman, R. P. Meshcheryakov, and Yu. M. Stolbov, in: Nuclear Geophysical Methods in Geology [in Russian], Nauka, Novosibirsk (1975), p. 54.
2. E. G. Vertman, A. A. Vaishlya, and A. F. Sudyko, in: Abstracts of Reports to the Third Regional Scientific and Applied Science Conference: Young Scientists and Specialists in the Development of Productive Forces of the Tomsk Region [in Russian], Tomsk. Gos. Univ., Tomsk (1980), p. 187.
3. E. Amaldi and E. Fermi, Usp. Fiz. Nauk, 17, 343 (1937).

DETERMINATION OF THE CUMULATIVE YIELDS OF SHORT-LIVED PRODUCTS OF THERMAL-NEUTRON ^{239}Pu FISSION BY MEANS OF THE γ-SPECTROMETRIC METHOD UNDER CYLIC CONDITIONS

A. G. Golovanov, A. N. Gudkov, V. V. Kazantsev, V. V. Kovalenko,
A. B. Koldobskii, V. M. Kolobashkin, S. I. Lifanov, and A. I. Slyusarenko

UDC 539.173.8

Analysis of the experimental data on the yields of short-lived ($T_{1/2} < 50$ sec) fission products (FP) resulting from thermal-neutron ^{239}Pu fission [1] shows their obvious inadequacy for solving practical problems and for checking the efficiency of the calculation methods used to predict the yield values not determined by experiment. We have measured the cumulative yields of a number of short-lived FP resulting from ^{239}Pu fission by the thermal neutrons described in [2, 3], using the method of cyclic γ-spectrometric analysis of the radiation of unseparated FP mixtures.

A specimen of ^{239}Pu, hermetically sealed in a polyethylene capsule, was irradiated in an IRT-2000 reactor in a thermal-neutron flux with a density of $\sim 10^{10}$ neutrons/(cm^2·sec). The arrangement and conditions of the cyclic experiments were optimized according to the method described in [4] with regard to measurements of the 174.92-keV γ line, which appears with the decay of ^{139}Xe. This nucleus was chosen as a reference because, from among the ^{239}Pu FP that have been identified in experiments, it was only for ^{139}Xe that the cumulative yield was measured repeatedly earlier, using two different methods [1]. This made it possible to reduce to a certain extent the effect of the systematic errors incurred in using the reference value of the cumulative ^{139}Xe yield, equal to (3.078 $\pm$ 0.151)% according to [1]. In accordance with [5], the absolute quantum yield of the 174.92-keV γ line was assumed to be equal to 0.147 $\pm$ 0.014. The measurement results are given in Table 1. Our data are in good agreement with the theoretical data [1] and also with the measured [8, 9] values of cumulative ^{138}I yields, equal to (1.25 $\pm$ 0.13) and (0.86 $\pm$ 0.05)%, respectively.

TABLE 1. Cumulative Yields of Short-Lived Products of Thermal-Neutron ^{239}Pu Fission

Nuclide	Half-life, sec	Energy of measured γ-line, keV	Absolute quantum yield of γ line, %	Cumulative yield, %
^{99}Nb	15	137,2	87,5±8,9 [5]	3,7±0,6
^{100}Zr	7,1	504,3	24,1±2,0 [5]	5,5±1,4
^{101}Nb	7,1	157,7	16,7±1,6 [5]	6,3±1,1
^{102}Nb	4,5	296,4	36,7±3,9 [5]	1,9±1,3
^{136m}I	48	381,3	93,7 [6]	1,3±0,2
^{138}I	6,46	588,87	97,66 [7]	1,1±0,2
^{143}Ba	12	211,5	17,6±2,5 [5]	3,4±0,8
^{144}La	42,4	397,3	90,9±6,1 [5]	4,0±0,6

LITERATURE CITED

1. M. Meek et al., Rept.NEDO-12154-2 (1977).
2. A. N. Gudkov et al., Vopr. At. Nauki Tekh. Ser. Yad. Konstanty, No. 3(42), 49 (1981).
3. A. N. Gudkov et al., in: Experimental Methods of Nuclear Physics [in Russian], Vol. 8, Atomizdat, Moscow (1981), p. 38.
4. A. N. Gudkov et al., in: Experimental Methods of Nuclear Physics [in Russian], Vol. 9, Atomizdat, Moscow (1981), p. 9.
5. A. N. Gudkov et al., Vopr. At. Nauki Tekh., Ser. Yad. Konstanty, No. 3(42), 47 (1981).
6. V. Reus et al., Rept. GSI, Darmstadt, N 79-2 (1979).
7. J. Blachot et al., Atom. Data and Nucl. Data Tables, 20, No. 3, 262 (1977).
8. R. Brissot et al., Nucl. Phys., A282, 109 (1977).

Translated from Atomnaya Énergiya, Vol. 53, No. 2, p. 117, August, 1982. Original article submitted November 18, 1981.

0038-531X/82/5302- 0576$07.50

MEASUREMENT TECHNIQUES
Izmeritel'naya Tekhnika
Vol. 25, 1982 (12 issues) $400

MECHANICS OF COMPOSITE MATERIALS
Mekhanika Kompozitnykh Materialov
Vol. 18, 1982 (6 issues) $330

METAL SCIENCE AND HEAT TREATMENT
Metallovedenie i Termicheskaya Obrabotka Metallov
Vol. 24, 1982 (12 issues) $420

METALLURGIST
Metallurg
Vol. 26, 1982 (12 issues) $435

PROBLEMS OF INFORMATION TRANSMISSION
Problemy Peredachi Informatsii
Vol. 18, 1982 (4 issues) $320

PROGRAMMING AND COMPUTER SOFTWARE
Programmirovanie
Vol. 8, 1982 (6 issues) $135

PROTECTION OF METALS
Zashchita Metallov
Vol. 18, 1982 (6 issues) $380

RADIOPHYSICS AND QUANTUM ELECTRONICS
Izvestiya Vysshikh Uchebnykh Zavedenii, Radiofizika
Vol. 25, 1982 (12 issues) $400

REFRACTORIES
Ogneupory
Vol. 23, 1982 (12 issues) $380

SIBERIAN MATHEMATICAL JOURNAL
Sibirskii Matematicheskii Zhurnal
Vol. 23, 1982 (6 issues) $495

SOIL MECHANICS AND FOUNDATION ENGINEERING
Osnovaniya, Fundamenty i Mekhanika Gruntov
Vol. 19, 1982 (6 issues) $380

SOLAR SYSTEM RESEARCH
Astronomicheskii Vestnik
Vol. 16, 1982 (4 issues) $275

SOVIET APPLIED MECHANICS
Prikladnaya Mekhanika
Vol. 18, 1982 (12 issues) $400

SOVIET ATOMIC ENERGY
Atomnaya Énergiya
Vols. 52–53 (12 issues) $440

SOVIET JOURNAL OF GLASS PHYSICS AND CHEMISTRY
Fizika i Khimiya Stekla
Vol. 8, 1982 (6 issues) $175

SOVIET JOURNAL OF NONDESTRUCTIVE TESTING
Defektoskopiya
Vol. 18, 1982 (12 issues) $485

SOVIET MATERIALS SCIENCE
Fiziko-khimicheskaya Mekhanika Materialov
Vol. 18, 1982 (6 issues) $345

SOVIET MICROELECTRONICS
Mikroélektronika
Vol. 11, 1982 (6 issues) $195

SOVIET MINING SCIENCE
Fiziko-tekhnicheskie Problemy Razrabotki Poleznykh Iskopaemykh
Vol. 18, 1982 (6 issues) $420

SOVIET PHYSICS JOURNAL
Izvestiya Vysshikh Uchebnykh Zavedenii, Fizika
Vol. 25, 1982 (12 issues) $400

SOVIET POWDER METALLURGY AND METAL CERAMICS
Poroshkovaya Metallurgiya
Vol. 21, 1982 (12 issues) $435

STRENGTH OF MATERIALS
Problemy Prochnosti
Vol. 14, 1982 (12 issues) $495

THEORETICAL AND MATHEMATICAL PHYSICS
Teoreticheskaya i Matematicheskaya Fizika
Vols. 50–53, 1982 (12 issues) $380

UKRAINIAN MATHEMATICAL JOURNAL
Ukrainskii Matematicheskii Zhurnal
Vol. 34, 1982 (6 issues) $380

Send for Your Free Examination Copy

Plenum Publishing Corporation, 233 Spring St., New York, N.Y. 10013
In United Kingdom: 88/90 Middlesex St., London E1 7EZ, England
Prices slightly higher outside the U.S. Prices subject to change without notice.

RUSSIAN JOURNALS IN THE PHYSICAL AND MATHEMATICAL SCIENCES

AVAILABLE IN ENGLISH TRANSLATION

ALGEBRA AND LOGIC
Algebra i Logika
Vol. 21, 1982 (6 issues) $270

ASTROPHYSICS
Astrofizika
Vol. 18, 1982 (4 issues) $320

AUTOMATION AND REMOTE CONTROL
Avtomatika i Telemekhanika
Vol. 43, 1982 (24 issues) issues) $495

COMBUSTION, EXPLOSION, AND SHOCK WAVES
Fizika Goreniya i Vzryva
Vol. 18, 1982 (6 issues) $345

COSMIC RESEARCH
Kosmicheskie Issledovaniya
Vol. 20, 1982 (6 issues) $425

CYBERNETICS
Kibernetika
Vol. 18, 1982 (6 issues) $345

DIFFERENTIAL EQUATIONS
Differentsial'nye Uravneniya
Vol. 18, 1982 (12 issues) $395

DOKLADY BIOPHYSICS
Doklady Akademii Nauk SSSR
Vols. 262–267, 1982 (2 issues) $145

FLUID DYNAMICS
Izvestiya Akademii Nauk SSSR, Mekhanika Zhidkosti i Gaza
Vol. 17, 1982 (6 issues) $380

FUNCTIONAL ANALYSIS AND ITS APPLICATIONS
Funktsional'nyi Analiz i Ego Prilozheniya
Vol. 16, 1982 (4 issues) $320

GLASS AND CERAMICS
Steklo i Keramika
Vol. 39, 1982 (6 issues) $460

HIGH TEMPERATURE
Teplofizika Vysokikh Temperatur
Vol. 20, 1982 (6 issues) $400

HYDROTECHNICAL CONSTRUCTION
Gidrotekhnicheskoe Stroitel'stvo
Vol. 16, 1982 (12 issues) $305

INDUSTRIAL LABORATORY
Zavodskaya Laboratoriya
Vol. 48, 1982 (12 issues) $400

INSTRUMENTS AND EXPERIMENTAL TECHNIQUES
Pribory i Tekhnika Eksperimenta
Vol. 25, 1982 (12 issues) $460

JOURNAL OF APPLIED MECHANICS AND TECHNICAL PHYSICS
Zhurnal Prikladnoi Mekhaniki i Tekhnicheskoi Fiziki
Vol. 23, 1982 (6 issues) $420

JOURNAL OF APPLIED SPECTROSCOPY
Zhurnal Prikladnoi Spektroskopii
Vols. 36–37 (12 issues) $420

JOURNAL OF ENGINEERING PHYSICS
Inzhenerno-fizicheskii Zhurnal
Vols. 42–43, 1982 (12 issues) $420

JOURNAL OF SOVIET LASER RESEARCH
A translation of articles based on the best Soviet research in the field of lasers
Vol. 3, 1982 (4 issues) $95

JOURNAL OF SOVIET MATHEMATICS
A translation of Itogi Nauki i Tekhniki and *Zapiski Nauchnykh Seminarov Leningradskogo Otdeleniya Matematicheskogo Instituta im. V. A. Steklova AN SSSR*
Vols. 18–20, 1982 (18 issues) $680

LITHOLOGY AND MINERAL RESOURCES
Litologiya i Poleznye Iskopaemye
Vol. 17, 1982 (6 issues) $420

LITHUANIAN MATHEMATICAL JOURNAL
Litovskii Matematicheskii Sbornik
Vol. 22, 1982 (4 issues) $205

MAGNETOHYDRODYNAMICS
Magnitnaya Gidrodinamika
Vol. 18, 1982 (4 issues) $325

MATHEMATICAL NOTES
Matematicheskie Zametki
Vols. 31–32, 1982 (12 issues) $400

continued on inside back cover

Declassified and Approved For Release 2013/03/04 : CIA-RDP10-02196R000300010002-9